

Fluorescence Fluctuation Spectroscopy Applied to Living Plant Cells

Mark Hink

Proefschrift
ter verkrijging van de graad van doctor
op gezag van de rector magnificus
van Wageningen Universiteit,
prof. dr. ir. L. Speelman
in het openbaar te verdedigen
op woensdag 18 september 2002
des namiddags te half twee in de Aula.

Fluorescence Fluctuation Spectroscopy Applied to Living Plant Cells

Hink, Mark

Thesis Wageningen University, The Netherlands
With references – with summary in Dutch

ISBN 90-5808-702-6

Contents

	Scope	1
Chapter 1	Introduction to fluorescence fluctuation spectroscopy	5
Chapter 2	Dynamics of green fluorescent protein alone and fused with a single chain Fv protein	23
Chapter 3	Dynamics of fluorescent phospholipids in micelles: Characterization with fluorescence correlation spectroscopy and time-resolved fluorescence anisotropy	33
Chapter 4	Fluorescence correlation microscopy in living plant cells	49
Chapter 5	Fluorescence fluctuation analysis of fluorescent proteins in living plant cells: A study using FRET- and dual-color fluorescence cross-correlation microscopy	69
Chapter 6	Fluorescence fluctuation analysis of AtSERK1 oligomerization	89
Chapter 7	Summarizing discussion	105
	References	111
	Samenvatting	123
	List of abbreviations	127
	Dankwoord	129
	Curriculum vitae	131
	List of publications	133

Scope

One of the major goals in biological research is to understand how a living cell processes information in response to external stimuli leading ultimately to processes like proliferation, differentiation and apoptosis. To increase our understanding about the complexity of the signal transduction network in living cells, experimental data on the spatial-temporal organization of the signalling molecules is required. Major advances have been made in the field of molecular biology and genetics in the last decade. In recent years a concerted research effort has led to the complete genomic sequence of several organisms. Currently, much research has been devoted to the identification of functional proteins. However, the next challenge is not only to identify and characterize these proteins but also to monitor their function and interactions *in vivo*. In this respect, many unanswered questions are left. Microspectroscopic techniques, which rely on fluorescence for detection, are a valuable tool to answer part of these questions. Not only are the methods sensitive, selective and non-invasive, but also they can be used for the study of living cells. Moreover, some of these techniques provide quantitative information on dynamic processes like molecular interactions at the single-molecule level with very high spatial and temporal resolution. In the last decade intracellular research has been changed dramatically by the introduction of green fluorescent protein (GFP). To visualize proteins within living cells GFP is fused genetically to the protein of interest and, after transfection, the fusion product is expressed. Using GFP expression inside cells, intracellular introduction of purified, labeled protein through invasive techniques such as microinjection or electroporation is not required anymore. GFP is a protein of 28 kDa isolated from the jellyfish *Aequorea victoria*. The high molecular brightness, well protected fluorophore and relative inertness for aspecific interactions with cellular structures makes it an excellent fluorescent marker to study the behaviour of proteins at the single-molecule detection level. Moreover, point mutations of the wild type GFP have resulted in mutants with different spectral characteristics; the enhanced blue (EBFP), cyan (ECFP), green (EGFP) and yellow fluorescent proteins (EYFP). Recently, red-shifted fluorescent proteins (DsRed, HcRed) from coral species have been put forward but their use has been limited so far due to complex photophysics and self-aggregation. This variety of proteins with different colours now allows monitoring multiple proteins, each labeled with a different fluorophore, simultaneously inside the living cell. Co-localization studies provide an indication on molecular interaction between proteins *in vivo*. The process of intermolecular interaction can be visualised at even higher spatial and temporal resolution using several microspectroscopic techniques. Most methods are based on the principle of fluorescence resonance energy transfer (FRET) involving the non-radiative energy transfer from a donor to an acceptor molecule. FRET will only take place when both fluorophores are within several nanometer distance of each other. FRET can be visualized by confocal or spectral imaging or by

fluorescence lifetime imaging microscopy (FLIM). Other methods to visualize interactions are based on the analysis of fluorescence intensity fluctuations. Two such techniques are fluorescence correlation spectroscopy (FCS) and photon counting histogram analysis (PCH). Both methods retrieve information from the fluctuations in the fluorescence intensity observed in a small volume element. FCS enables us to analyse the time-dependent decay of the fluctuations, retrieving parameters such as the local concentration and diffusion coefficient of fluorescent molecules and rate constants of fast reversible reactions. With PCH one focuses on the analysis of the distribution of fluctuating intensity amplitudes, which is used to resolve mixtures of fluorescent particles having different molecular brightness. So far, these techniques have been used successfully in a widespread field of applications, characterizing molecular dynamics *in vitro*. However, the use of fluctuation spectroscopy to monitor the dynamics of molecules within the living cell has been limited so far.

The major goal of the study described in this thesis is to further develop fluorescence fluctuation techniques, FCS and PCH, in order to obtain quantitative information on the dynamic properties of biomolecules in living plant cells. In order to reach these objectives the behaviour of fluorescently labeled molecules was first studied in model biochemical systems. Then these techniques were applied to systems of higher complexity: living cells. The specific outline of this thesis is as follows:

Chapter 1 describes the principles, instrumentation and applications of FCS and PCH. The potential of FCS to monitor molecular interactions is demonstrated in **chapter 2**. Single-chain antibodies raised against lipopolysaccharides in the outer cell wall of Gram-negative bacteria were fused to EGFP. By exploiting the ability to distinguish between fluorescent particles having different diffusion coefficients, FCS was used to investigate the binding of these fusion proteins to the outer cell wall of these bacteria. In **chapter 3** various micelles, acting as membrane mimetic systems, were characterized. After FCS analysis both the diffusion rate and hydrodynamic radius of the micelles, loaded with a fluorescent phospholipid molecule, were recovered. The accuracy of these results has been confirmed by dynamic light scattering experiments. The introduction of the relatively large phospholipid molecule induced an increase in micellar size. Lateral diffusion within the micelle has been checked by time resolved fluorescence anisotropy measurements. This type of study was continued in **chapter 4**, which reports on the diffusion behaviour of fluorescent phospholipid molecules in the membranes of living plant cells. This chapter includes an extensive description of potential artifacts, which may complicate intracellular fluorescence correlation microscopy (FCM) experiments as illustrated by measurements in cowpea and tobacco plant cells. First, the autofluorescence has been characterized. FCM analysis of microinjected fluorophores in the cytoplasm and nucleus allows testing the applicability of these probes *in vivo*. To check for the presence of membrane inhomogeneities or non-specific interactions with cellular structures, the fluctuation data were analysed according to models describing restricted,

anomalous diffusion, deviating from normal Brownian motion. In **chapter 5** a detailed study is presented describing the photophysical properties of ECFP, EGFP and EYFP to test their applicability in fluctuation spectroscopy. In order to monitor molecular interactions via fluctuation analysis, the potential of FRET-FCM has been tested *in vitro* and *in vivo* using fusion proteins with ECFP and EYFP. As an additional method to examine molecular interactions, FCM has been extended to dual-color fluorescence cross-correlation microscopy (FCCM). **Chapter 6** reports on the mobility and oligomerization of *Arabidopsis thaliana* somatic embryogenesis receptor kinase (AtSERK1) in the plasma membrane of cowpea protoplasts. PCH analysis revealed the aggregation state of the AtSERK1 proteins fused to ECFP and EYFP. In **chapter 7** the research topics described in this thesis are summarized and discussed. Implications and future developments of fluorescence fluctuation techniques for intracellular studies are discussed.

1

Introduction to Fluorescence Fluctuation Spectroscopy

Fluorescence fluctuation spectroscopy comprises a series of microspectroscopic techniques capable to retrieve information about physical parameters of fluorescent molecules with high spatial and temporal resolution. Using these techniques small spontaneous variations of the fluorescence intensity in a microscopic volume are analysed in which the system is essentially not perturbed. The sensitivity and selectivity allow measurements at the single-molecule detection level. For this reason fluctuation spectroscopy is a promising method to study the behavior of biomolecules in the living cell, at physiologically relevant concentrations. Two of these techniques, fluorescence correlation spectroscopy (FCS) and photon counting histogram analysis (PCH) have been used to monitor physical parameters like local particle concentration, molecular brightness, diffusion behavior and internal dynamics of fluorescent molecules. This chapter describes the principles, applications and instrumental setup for both techniques.

Introduction

The concept of fluctuation spectroscopy has been introduced in the beginning of the 20th century. An early application was reported by Svedberg and Inouye (1911) who studied the number fluctuations of small gold colloidal particles in a fixed volume of the ultra-microscope using light scattering.

In macroscopic systems, which are at equilibrium, the concentration of molecules does not change with time. Dynamic processes, like diffusion of molecules into and out of the observation volume will take place but, due to the large number of molecules present, the number fluctuations tend to cancel out each other. Therefore, the relative changes caused by the various processes are of negligible magnitude. However, if the number of molecules in the observation volume is small, the processes do not average out and relative fluctuations in concentration or other parameters can become significant. Since dynamic processes cause the fluctuations in the system it was recognized that analysis of these fluctuations could provide a powerful way of investigating these processes.

To be able to monitor the number fluctuations, Svedberg and Inouye (1911) restricted the number of observed molecules by putting a small slit in the detection path hereby limiting the size of the observation volume. The experimental data they obtained were analysed according to the theoretical models developed by von Smoluchowski (1914). The detected number of particles was plotted in a histogram, reflecting the frequency of finding N particles in the observation volume. The data fitted well to the predicted Poissonian distribution, which describes the probability p to find N particles in a small open observation volume containing an average of \bar{N} particles:

$$p(N) = \frac{\bar{N}^N \exp(-\bar{N})}{N!} \quad (\text{Eq. 1.1})$$

This Poissonian behaviour will only be observed when the particles are independent, which is only realized in ideal solutions. Non-ideal solutions lead to deviations from the Poisson distribution as have been demonstrated by other experiments (Svedberg and Inouye, 1911). Von Smoluchowski used the normalized concentration autocorrelation function $G(\tau)$ to express the typical time course of the number fluctuations. It calculates the similarity between a signal and a copy of this signal, shifted by a time lag τ :

$$G(\tau) \equiv \langle N(t) N(t + \tau) \rangle - \langle N \rangle^2 = \langle \delta N(t) \delta N(t + \tau) \rangle \quad (\text{Eq. 1.2})$$

where brackets denote the time average and $\delta N(t)$ describes the deviation in particle number from the average particle number at time t . The time zero value of the normalized

autocorrelation function $G(0)$ represents the inverse number of particles in the detection volume.

In the following years different techniques have been developed using the concept of number fluctuations, by exploiting the characteristics of light scattering (Berne and Pecora, 1975) and electrical conductance (Feher and Weissman, 1973). Another method of detection is fluorescence, which has the advantage that it can be characterized by a large number of parameters such as intensity, wavelength, lifetime and polarization. Moreover, the combination of high sensitivity with specificity makes the use of fluorescence in fluctuation analysis attractive. Hence, in the early nineteen seventies fluorescence correlation spectroscopy (FCS) was introduced (Magde et al., 1972 & 1974; Elson and Magde, 1974; Ehrenberg and Rigler, 1974) which laid the foundations for a whole series of methods that are collectively referred to as fluorescence fluctuation spectroscopy. Although the first experiments suffered from low signal-to-noise ratios (SNR), technical improvements greatly increased the sensitivity and pushed the detection limit to the single molecule level (Eigen et al., 1994; Rigler, 1995).

A typical experiment is shown in figure 1.1. A focused laser beam continuously illuminates a fixed region within the sample. Although fluorescent particles throughout the excitation volume are excited, only the fluorescence from particles present in a limited observation volume (< 1 femtoliter) is detected. Every time a fluorescent molecule enters the observation volume a burst of fluorescence photons is detected. When diffusion is the only dynamic process resulting in intensity fluctuations, the duration of this burst reflects the time a particle needed to diffuse across the observation volume. Autocorrelation of the intensity trace results in the autocorrelation curve which can be analysed to yield the average number of particles N in the observation volume and the average diffusion time τ_{dif} . The amplitude of the emission bursts contains information about the molecular brightness of the particles, since bright particles will on average give rise to larger fluorescence bursts than dimmer molecules. The frequency of fluorescence intensities can be plotted in a histogram of fluorescence intensities. Analysis of this photon distribution yields the molecular brightness η and the number of the particles. The brightness can be defined as the number of detected fluorescence photons per molecule per second.

The temporal behaviour of the fluctuations is best described by the autocorrelation analysis, retrieved from FCS experiments. The amplitudes of the fluctuations can be characterized by the photon distribution, analysed by photon counting histogram analysis (PCH). In the next sections these techniques will be described in more detail.

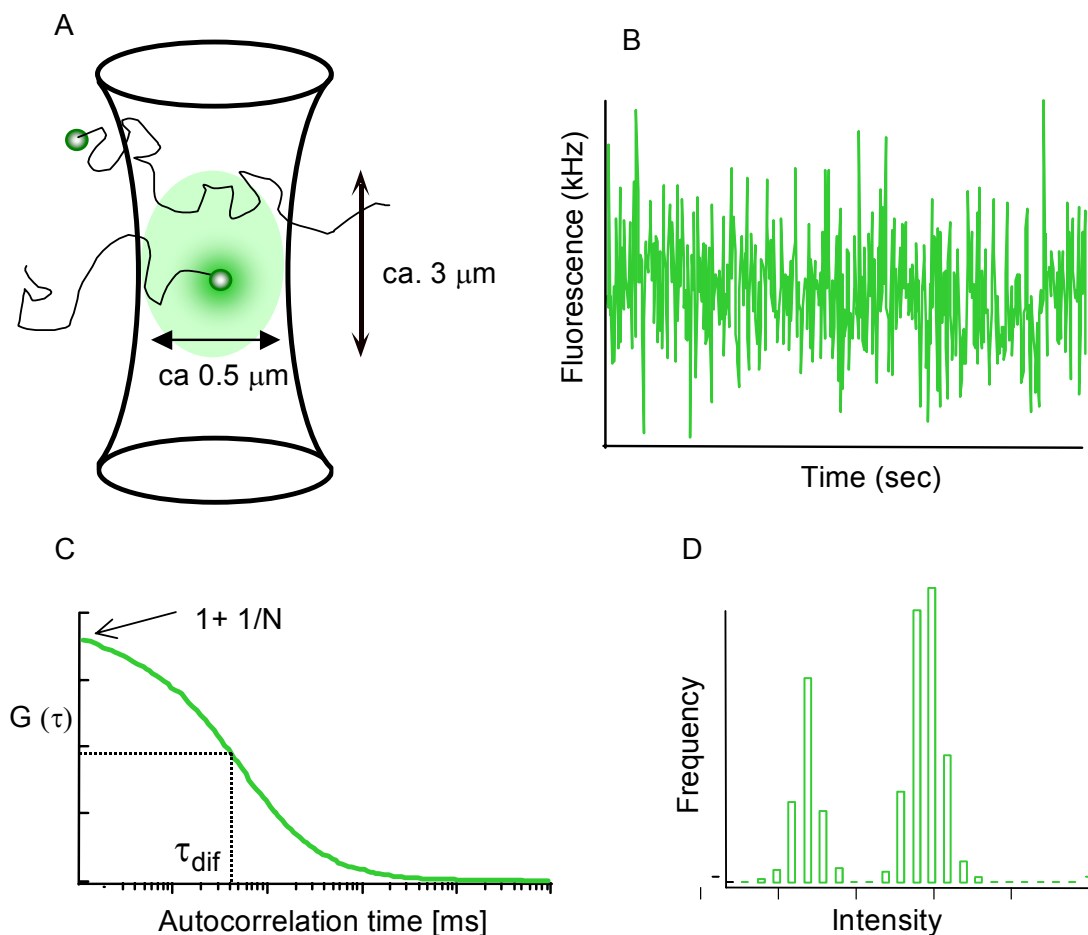


Figure 1.1: Principle of fluorescence fluctuation spectroscopy. (A) A focused laser beam continuously illuminates the sample. (B) When single fluorescent particles enter the observation volume, a burst of fluorescent photons will be detected. The duration of the burst reflects the time that the particle resides within the observation volume and the intensity of the burst corresponds to the molecular brightness of the particle. (C) Autocorrelation of the intensity trace results in the autocorrelation curve which can be analysed to yield the average number of particles N in the observation volume and the diffusion time τ_{dif} . (D) Plotting the frequency of fluorescence intensities results in the photon count distribution. Analysis yields the number and molecular brightness η of the particles.

Fluorescence correlation spectroscopy

Fluorescence Correlation Spectroscopy (FCS) was introduced (Magde et al., 1972 & 1974; Elson and Magde, 1974) as a method for measuring molecular diffusion and reaction kinetics. In the classical relaxation techniques used before, it was required to perturb the equilibrium state of the system by pressure or temperature jumps, after which the relaxation to equilibrium was observed. However, FCS does not require any perturbations, since it monitors small

spontaneous deviations from thermal equilibrium in an open system. These deviations are reflected by variations of the fluorescence intensity.

Theoretical and experimental studies soon established that with FCS one could measure not only translational diffusion but also aggregation, concentration, chemical rate constants and rotational dynamics can be measured (Elson and Magde, 1974; Ehrenberg and Rigler, 1974; Magde et al., 1974; Aragon and Pecora, 1975 & 1976). However, the first measurements suffered from poor signal-to-noise ratios (SNR), due to high background intensities mainly caused by Raman scattering of water and Rayleigh scattered laser light. It was until the integration of confocal detection optics that the observation volume could be reduced to subfemtoliter volume elements thereby significantly reducing the background emission (Qian and Elson, 1991; Rigler et al., 1993). Moreover, the introduction of highly efficient photon detectors, improved (faster) correlators, high-quality objectives, microscopic optics and emission filters greatly increased the sensitivity of FCS and subsequently decreased the detection limit to the single-molecule level (Eigen and Rigler, 1994; Rigler, 1995).

Theory

In the following section a brief derivation of the autocorrelation function will be described. More extensive descriptions, dealing with the basics of FCS have been published by Elson and Magde (1974) and Thompson (1991).

When fluorescence fluctuations arise only from changes in the local concentration δC within the observation volume V , the deviation of the signal $\delta F_i(t)$ from the average fluorescence intensity ($\delta F_i(t) \equiv F(t) - \langle F(t) \rangle$) can be described as

$$\delta F_i(t) = \kappa_i \int_V \frac{\text{PSF}_{\text{EX}}(\bar{r})}{I_0} \text{PSF}_{\text{DET}}(\bar{r}) \delta(\sigma_i q_i C_i(\bar{r}, t)) dV \quad (\text{Eq. 1.3})$$

with overall detection efficiency κ_i , The fluctuating term that describes the dynamics on single particle scale, $\delta(\sigma_i q_i C_i(\bar{r}, t))$, includes fluctuations of the molecular absorption cross section, $\delta\sigma_i$, the fluorescence quantum yield, δq_i , or in the simplest case just temporal changes of the local particle concentration, $\delta C_i(\bar{r}, t)$, due to Brownian motion. The spatial intensity distribution of the excitation light in the microscope is described by a point spread function (PSF_{EX}) (Qian and Elson, 1991). The detection point spread function, PSF_{DET} , describes the collection efficiency function. The spatial profile of the observation volume $W(\bar{r})$ is given by the convolution of PSF_{EX} and PSF_{DET} . It has been shown that $W(\bar{r})$ can be well approximated by a three-dimensional Gaussian which decays to $I_0 \cdot e^{-2}$ at ω_{xy} in lateral and at ω_z in axial direction (Rigler et al., 1993).

$$W(\vec{r}) = e^{-2\frac{x^2+y^2}{\omega_{xy}^2}} \cdot e^{-\frac{z^2}{\omega_z^2}} \quad (\text{Eq. 1.4})$$

The excitation intensity amplitude I_0 can be combined with the factors κ , σ and q into the molecular brightness parameter, $\eta_{0,i}$, which describes the count rate per detected molecule per second. Now the temporal fluorescence fluctuation can be written as:

$$\delta F(t) = \int_V W(\vec{r}) \delta(\eta C(\vec{r}, t)) dV \quad (\text{Eq. 1.5})$$

The normalized fluorescence fluctuation autocorrelation function $G_{ii}(\tau)$ for $\delta F_i(t)$ is defined as:

$$G_{ij}(\tau) = 1 + \frac{\langle \delta F_i(t) \cdot \delta F_j(t + \tau) \rangle}{\langle F_i \rangle \cdot \langle F_j \rangle} \quad \text{with } i = j \quad \text{for autocorrelation} \quad (\text{Eq. 1.6})$$

Equation 1.5 can be substituted into equation 1.6 where after the fluctuation term $\delta(\eta_i C_i(\vec{r}, t)) = (C_i \delta \eta_i + \eta_i \delta C_i)$ is simplified by assuming that the molecular brightness does not change in the observation time:

$$G_{ii}(\tau) = 1 + \frac{\iint W_i(\vec{r}) W_i(\vec{r}') \langle \delta C(\vec{r}, 0) \delta C(\vec{r}', \tau) \rangle dV dV'}{(\langle C \rangle \int W(\vec{r}) dV)^2} \quad (\text{Eq. 1.7})$$

When the particle diffuses freely in 3D with diffusion coefficient D_{tran} , the number density function is given by:

$$\langle \delta C_i(\vec{r}, 0) \delta C_i(\vec{r}', t) \rangle = \langle C_i \rangle (4\pi D_{\text{tran},i} \tau)^{-3/2} \exp\left(\frac{-(\vec{r} - \vec{r}')^2}{4D_{\text{tran},i} \tau}\right) \quad (\text{Eq. 1.8})$$

The lateral diffusion time τ_{dif} describes the time a particle stays in the observation volume, which is related to the diffusion coefficient by:

$$\tau_{\text{dif}} = \frac{\omega_{xy}^2}{4D_{\text{tran}}} \quad (\text{Eq. 1.9})$$

By inserting equations 1.8 and 1.9 into equation 1.7 and calculating the size of a 3D Gaussian shaped observation volume $V_{\text{eff}} = \pi^{3/2} \cdot \omega_{xy}^2 \cdot \omega_z^2$ results in the autocorrelation curve describing j independent species of freely diffusing molecules:

$$G(\tau) = 1 + \frac{1}{V_{\text{eff}} \langle C \rangle} \cdot \sum_j \frac{1}{\left(1 + \frac{\tau}{\tau_{\text{dif},j}}\right) \sqrt{1 + \left(\frac{\omega_{xy}}{\omega_z}\right)^2 \frac{\tau}{\tau_{\text{dif},j}}}} = 1 + \frac{1}{\langle N \rangle} \cdot \sum_j \frac{1}{\left(1 + \frac{\tau}{\tau_{\text{dif},j}}\right) \sqrt{1 + \left(\frac{\omega_{xy}}{\omega_z}\right)^2 \frac{\tau}{\tau_{\text{dif},j}}}} \quad (\text{Eq. 1.10})$$

The amplitude of the correlation function represents the average number of molecules found in the observation volume.

$$G(0) = 1 + \frac{1}{\langle N \rangle} \quad (\text{Eq. 1.11})$$

It was assumed that the fluorescent brightness of a molecule is not changed during the movement through the observation volume. However, an additional process commonly observed in the autocorrelation analysis is intersystem crossing, the reversible transition from the dye from the first excited singlet state to the relatively long-lived first excited triplet state. No fluorescent photons are emitted during the relaxation time to the ground state and the dye appears to be dark for a short interval. It has been shown that intra- and intermolecular reactions that induce intensity fluctuations on a time-scale much faster than mobility related fluctuations, thereby not altering the diffusion behaviour, could be taken into account by multiplying the motional term with one describing the reaction kinetics (Widengren and Rigler, 1998; Palmer and Thompson, 1987):

$$G_{\text{total}}(\tau) = G_{\text{motion}}(\tau) \cdot G_{\text{kinetics}}(\tau) \quad (\text{Eq. 1.12})$$

The correlation curves for a single species displaying intersystem crossing to the triplet state exhibit an additional shoulder on the microsecond timescale and are described by (Widengren et al., 1995):

$$G(\tau) = 1 + \frac{1}{\langle N \rangle} \cdot \frac{1 - T + T e^{-\tau/\tau_t}}{(1 - T)} \cdot \frac{1}{\left(1 + \frac{\tau}{\tau_{\text{dif},j}}\right) \sqrt{1 + \left(\frac{\omega_{xy}}{\omega_z}\right)^2 \frac{\tau}{\tau_{\text{dif},j}}}} \quad (\text{Eq. 1.13})$$

where T is the fraction of molecules in the triplet state and τ_T the corresponding triplet relaxation time. If the observed system consists of multiple species with differences in molecular brightness η , the autocorrelation curve has to be adjusted by taking into account the molecular fraction Y and molecular brightness η of each species:

$$G(\tau) = 1 + \frac{1}{\langle N \rangle} \cdot \frac{1 - T + T e^{-\tau/\tau_T}}{(1 - T)} \sum_j \Phi_j \cdot \frac{1}{\left(1 + \frac{\tau}{\tau_{\text{dif},j}}\right) \sqrt{1 + \left(\frac{\omega_{xy}}{\omega_z}\right)^2} \frac{\tau}{\tau_{\text{dif},j}}} \quad \text{with } \Phi_j = \frac{(\eta_j Y_j^2)}{(\sum_j \eta_j Y_j)^2} \quad (\text{Eq. 1.14})$$

In Eq. 1.14 it is assumed that all species have the same triplet characteristics.

Applications

Besides measurements of local concentrations or diffusion times, FCS is capable of observing a whole range of other dynamic processes. A comprehensive review (Hess et al., 2002) and a book (Elson and Rigler, 2001) dedicated to this technique clearly demonstrates the versatile applications which include measurements of molecules in solution observing translational (Magde et al., 1974) and rotational (Aragon and Pecora, 1976) diffusion, intersystem crossing (Widengren et al., 1995), chemical reactions (LaClair, 1997) conformational dynamics (Bonnet et al., 1998), protonation dynamics (Haupts et al., 1998) and photobleaching (Eggeling et al., 1998). Special studies have been addressed to investigate the implementation of two-photon excitation sources (Berland et al., 1995; Schwille et al., 1999b), the flickering dynamics of the variants of green fluorescent protein (Haupts et al., 1998; Schwille et al., 2000; Heikal et al., 2000), the hybridisation of DNA and RNA sequences (Walter et al., 1996; Oehlenschläger et al., 1996) and the interaction between various proteins (Rauer et al., 1996; van Craenenbroeck and Engelborghs, 1999).

In recent years there is an increasing number of publications concerning FCS in living cells (for a review, see Schwille, 2001a). The first publications reported on the mobility of microinjected fluorospheres (Berland et al., 1995; Brock et al., 1998). Applications have been describing either binding of substrates to the cell membrane of living cells (Rigler et al., 1999; Pramanik et al., 1999; Boonen et al., 2000; Goedhart et al., 1999 and 2000; Henriksson et al., 2001) or the intracellular diffusion of biologically relevant molecules (Politz et al., 1998; Koopman et al., 1999; Brock et al., 2000; Cluzel et al., 2000). Intracellular measurements demonstrated that FCS allows distinguishing different kinds of movement: active transport, 3D diffusion or restricted anomalous diffusion (Köhler et al., 2000; Wachsmuth et al., 2000; Schwille et al., 1999a). Furthermore, it has been demonstrated that two-photon excitation can significantly improve the signal quality in turbid samples like plant cells or deep cell layers (Schwille et al., 1999b). From these reports it has become clear that processes like cellular

autofluorescence, photobleaching of the dye, cellular damage and reduced signal to noise ratios due to scattering and absorption can seriously interfere the fluorescence fluctuation measurements in the living cell. In chapter 4 these problems will be discussed in detail in relation with the intracellular experiments described in this thesis.

Dual-Color Fluorescence Cross-Correlation Spectroscopy

The application of FCS to study molecular interactions upon differences in diffusion times is limited by the fact that the diffusion time is relatively insensitive to the molecular weight. The diffusion coefficient of a spherical particle scales inversely to the hydrodynamic radius r_h of the particle according to the Stokes-Einstein relation (Edward, 1970)

$$r_h = \frac{k T}{6\pi \eta_v D_{\text{tran}}} \quad (\text{Eq. 1.15})$$

where η_v is the viscosity, T the absolute temperature and k the Boltzmann constant. Assuming that r_h of the particle is proportional to the cubic root of its molecular weight M , equation 1.9 can be rewritten as:

$$\tau_{\text{dif}} = \frac{3\pi \omega_{xy}^2 \eta_v}{2 k T} \sqrt[3]{M} \quad (\text{Eq. 1.16})$$

As is shown by equation 1.16, the observed diffusion time scales only to the cubic root of the molecular weight. Therefore, to study interaction between different molecules of almost equal size, as in the case of homo-dimerisation of proteins, FCS will encounter problems to separate free diffusing molecules from molecular complexes. Meseth et al. (1999) have examined the resolving power of FCS to distinguish particles of different size. In case of an unchanged molecular brightness, the diffusion times of two species have to differ at least by a factor of 1.6, which corresponds to a minimum four-fold mass difference, which is required to distinguish both species. Smaller mass differences may be retrieved from the autocorrelation traces but then detailed knowledge on the photophysical properties of the molecules is required. In most experimental systems and especially for measurements inside the living cell, these properties are hard to obtain. To overcome these limitations dual-colour fluorescence cross-correlation (FCCS) has been proposed (Eigen and Rigler, 1994) and developed (Schwille et al., 1997 & 2001b). In FCCS-studies each partner involved in interaction is labeled by a spectrally different fluorescent group, *e.g.* green and red emitting dyes. The interacting molecules can now be studied by monitoring the particles that carry both labels. Hereto the sample is illuminated by two different laser lines and the fluorescence is split into two different channels, enabling us monitoring both dyes simultaneously:

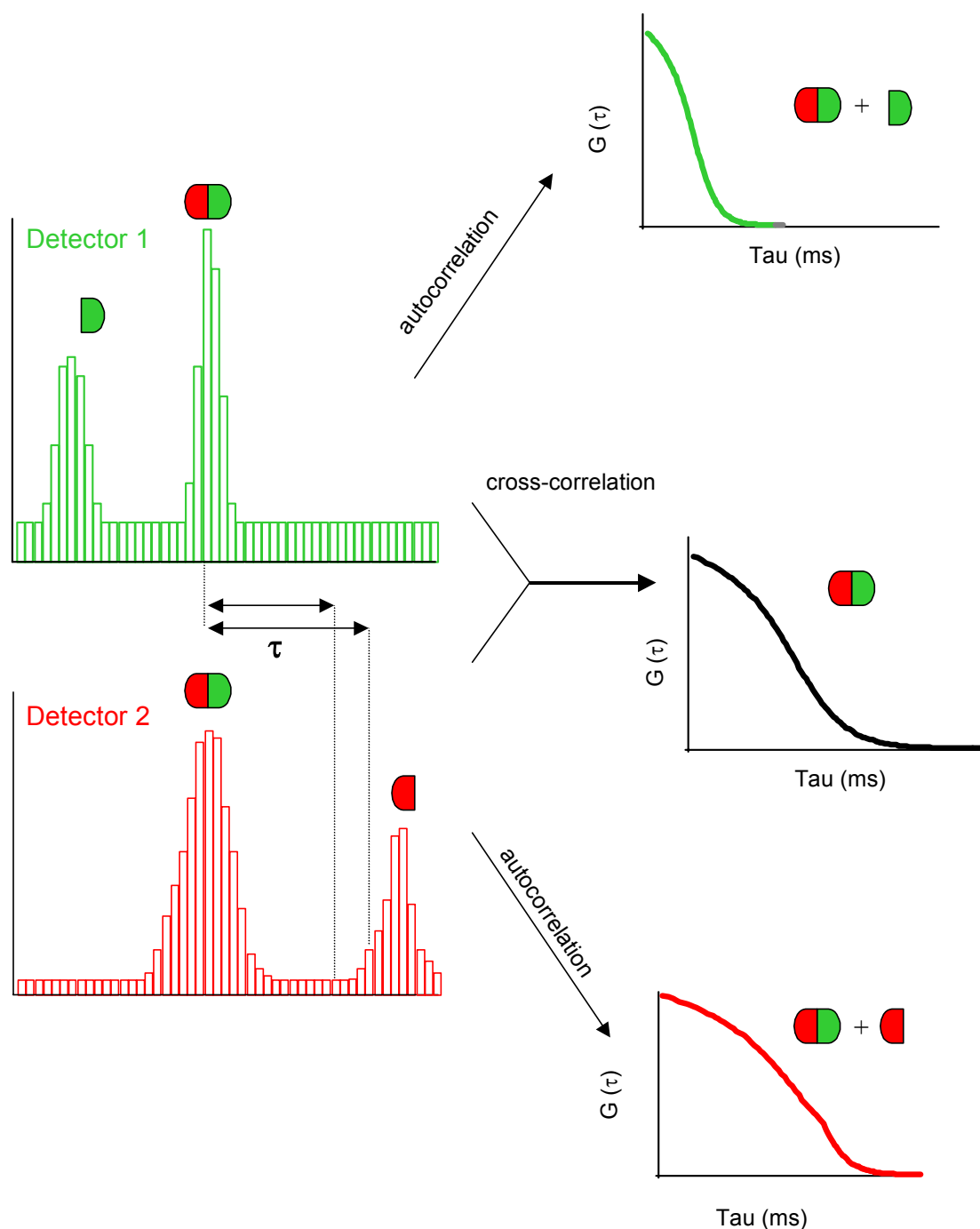


Figure 1.2: Principle of dual-colour fluorescence cross-correlation spectroscopy. Molecules labeled with two spectrally different dyes, *e.g.* green and red, are excited using two different laser lines. The fluorescence is split into two detection channels allows monitoring each dye individually. Free, non-interacting molecules will give rise to fluorescent photon bursts independent from the ones in the other channel. However, the presence of complexes of interacting molecules, carrying both dyes, will result in simultaneous fluorescent photon bursts in both channels. Cross-correlation of the signals from both detectors results in a curve that contains the dynamic information of the interacting species.

$$\begin{aligned}\delta F_R(t) &= \int W_R(\vec{r}) \eta_R (C_R(\vec{r}, t) + C_{RG}(\vec{r}, t)) dV \\ \delta F_G(t) &= \int W_G(\vec{r}) \eta_G (C_G(\vec{r}, t) + C_{RG}(\vec{r}, t)) dV\end{aligned}\quad (\text{Eq. 1.17})$$

The signal from both detectors is cross-correlated (see figure 1.2) according to equation 1.6 with $i \neq j$.

In the ideal case where the two detection volumes share the same observation volume and the dyes are fully spectrally separated the cross-correlation function $G_{RG}(\tau)$ follows

$$G_{RG}(\tau) = 1 + \frac{\langle C_{RG} \rangle}{V_{\text{eff}} (\langle C_R \rangle + \langle C_{RG} \rangle) (\langle C_G \rangle + \langle C_{RG} \rangle)} \frac{1}{\left(1 + \frac{\tau}{\tau_{\text{dif},RG}}\right) \sqrt{1 + \left(\frac{\omega_{xy}}{\omega_z}\right)^2} \frac{\tau}{\tau_{\text{dif},RG}}}} \quad (\text{Eq. 1.18})$$

The time-independent part, $G(0)$ is not equal to $1 + 1/N_{GR}$ here, but is also related to the number of singly labeled molecules, emitting in only one of the two channels. The retrieved diffusion time $\tau_{\text{dif},RG}$ now represents the weighted diffusion time of the doubly labeled molecules, N_{RG} . However, in practice, deviations from the ideal situation will result in a difference in size of the observation volumes. Therefore, the effective observation volume and diffusion time for the doubly labeled particles have to be corrected:

$$V_{\text{eff}} = \pi^{3/2} (\omega_{xy,R}^2 + \omega_{xy,G}^2) (\omega_{z,R}^2 + \omega_{z,G}^2) \quad (\text{Eq. 1.19})$$

$$\tau_{\text{dif},RG} = \frac{\omega_{xy,R}^2 + \omega_{xy,G}^2}{4 D_{RG} \cdot 2} \quad (\text{Eq. 1.20})$$

In practice, however, it is difficult to spectrally separate the two different dyes completely. In this case, some emission of the green dye will be detected in the red detector (this is called cross-talk). The emission of the red dye in the green channel can be omitted. To correct for the cross-talk the following expression must be used:

$$G(0) = 1 + \frac{N_G \left(\frac{\eta_{RGG}}{\eta_{RRR}} \right) + N_{GR} \left(1 + \frac{\eta_{RGG}}{\eta_{RRR}} \right)}{(N_G + N_{GR}) \left(N_R + N_G \left(\frac{\eta_{RGG}}{\eta_{RRR}} \right) + N_{GR} \left(1 + \frac{\eta_{RGG}}{\eta_{RRR}} \right) \right)} \quad (\text{Eq. 1.21})$$

N_g and N_r are the number of free, singly labeled molecules and $\eta_{\text{em,dye,ex}}$ are the molecular brightness values for the dyes at various emission and excitation wavelengths. In the ideal

case the time-dependent part of G represents only the fluctuation characteristics of the doubly labeled molecule. In practice, however, the cross-talk of the green dye will appear in the cross-correlation curve as an additional (false-positive) species.

In the last few years an increasing number of applications of dual-colour FCCS have been reported: Varying from enzyme kinetics (Kettling et al., 1998; Koltermann et al., 1998, Rarbach et al., 2001), nucleotide hybridisation (Schwille et al., 1997; Rigler et al., 1999; Földes-Papp et al., 2001a-c), protein-DNA interactions (Rippe et al., 2000) to the application of two-photon excitation (Heintze et al., 2000). So far, no intracellular applications of dual-colour FCCS have been described in the literature.

Photon Counting Histogram Analysis

Although FCS provides a sensitive method to investigate molecular dynamics it has limitations. Firstly, many of the studied processes involve the presence and/or interaction of two or more different, emitting species. As have been pointed out above, in order to separate multiple species by FCS, significant differences in molecular weight are required. Secondly, FCS is not capable of accurately evaluating cases in which species have different molecular brightness, as is the case commonly found in aggregation studies. In response to these shortcomings of the autocorrelation approach a number of other fluctuation techniques have been developed that separate species based on their molecular brightness rather than molecular weight. Initial methods make use of higher moments of photon count number distributions (Qian and Elson, 1990a,b; Chen et al., 2000). This approach may be considered as a simplified version of the higher order FCS (Palmer and Thompson, 1987 & 1989; Van den Broek et al., 1999), since the moments calculated and used in analysis have the same physical meaning as the amplitudes of the corresponding higher order correlation functions. Other statistical methods report on the analysis of rare events (Van Craenenbroeck et al., 1999 & 2001) or single molecule transits (Fries et al., 1998; Eggeling et al., 2001). Subsequently two research groups independently reported theoretical models capable of directly fitting photon count number distributions to resolve species of different molecular brightness. These methods were given two equivalent names: photon counting histogram (PCH) (Chen et al., 1999) and fluorescence intensity distribution analysis (FIDA) (Kask et al., 1999). Recent developments of the latter method resulted in techniques as two-dimensional FIDA (Kask et al., 2000), fluorescence intensity multiple distribution analysis (FIMDA) (Palo et al., 2000) and fluorescence intensity and lifetime distribution analysis (FILDA) which yield additional molecular information besides molecular brightness.

In the following section a brief overview of the PCH theory is given. A more detailed description of the principles can be found in Chen et al. (1999) and Müller et al. (2001). The

PCH retrieves the amplitude distribution of the intensity fluctuations (Mandel, 1958), yielding the number of particles and the molecular brightness of each species present in the sample. To describe the PCH of a freely diffusing species first a single particle diffusing within a small box of volume V_0 , that encloses the observation volume, is considered. A scaled point spread function $\overline{\text{PSF}}$ is defined so that its volume, $V_{\text{PSF}} = \int \overline{\text{PSF}}(\vec{r}) d\vec{r}$, equals the observation volume in FCS measurements. According to Mandel's formula (Mandel, 1958) the detected intensity fluctuations lead to the following expression for the photon count distribution:

$$p^{(1)}(k; V_0, \eta) = \int \text{Poi}(k, \eta \overline{\text{PSF}}(\vec{r})) p(\vec{r}) d\vec{r} \quad (\text{Eq. 1.22})$$

where $\text{Poi}(k, \eta \overline{\text{PSF}}(\vec{r}))$ is the Poisson distribution of detecting k photon counts, which depends on the reference volume V_0 and the molecular brightness. Equation 1.22 describes the probability that in a single particle system k photoelectrons counts are detected within the sampling time. In order to capture the intensity fluctuations by $\overline{\text{PSF}}$ the sampling times are chosen shorter than the fluctuation time scale. Inserting the description of the 3D Gaussian shaped PSF (Eq. 1.4) into equation 1.22 yields:

$$p_{\text{3dG}}^{(1)}(k; V_0, \eta) = \frac{1}{V_0} \frac{\pi \omega_{xy}^2 \omega_z}{2k!} \int_0^\infty \gamma(k, \eta e^{-4x^2}) dx \quad \text{for } k > 0 \quad (\text{Eq. 1.23})$$

where γ is the incomplete gamma function. If we consider N ($N > 0$) independent identical particles diffusing inside a box of volume V_0 , $p^{(N)}(k; V_0, \eta)$ is given by N consecutive convolutions of the single particle PCH function $p^{(1)}(k; V_0, \eta)$ (Eq. 1.22). However, the assumption of a closed system in which molecules diffuse inside a box does not describe the experimental situation since in most experimental systems a small open observation volume is in contact with a large reservoir. The distribution of particles in the observation volume is given by the Poisson distribution $p(N)$, as has been described in Eq. 1.1. Now the PCH for an open system can be expressed as:

$$\Pi(k; \overline{N}_{\text{PSF}}, \eta) \equiv \hat{p}(k; V_0, \overline{N}, \eta) = \langle p^{(N)}(k; V_0, \eta) \rangle_N = \sum_{N=0}^{\infty} p^{(N)}(k; V_0, \eta) \cdot p(N) \quad (\text{Eq. 1.24})$$

Since the choice of the reference volume V_0 is irrelevant, the photon count distribution can be referenced to the volume of the PSF, as has been used in FCS. This is described by $\Pi(k;$

$\bar{N}_{\text{PSF}}, \eta)$. In the case of two independent species, each present with N_i particles of molecular brightness η_i , the two individual photon counting histograms have to be convoluted:

$$\Pi(k; \bar{N}_1, \bar{N}_2, \eta_1, \eta_2) = \Pi(k; \bar{N}_1, \eta_1) \otimes \Pi(k; \bar{N}_2, \eta_2) \quad (\text{Eq. 1.25})$$

For more than two species all ‘single species’ photon counting distributions are convoluted successively to yield the photon count distribution of the mixture.

Three sources of fluctuation determine the shape of the photon counting histogram. The first one is generated in the detector. Due to the quantum nature of the photon detection process, the so-called shot noise is added to the measured intensity, thereby changing the photon counts (Saleh, 1978). Hence, a constant fluorescence intensity would not result in a single discrete number of photon counts, but will give rise to a Poisson distribution of photon counts (see Eq. 1.22). Secondly, the inhomogeneity of the point-spread function will give rise to intensity fluctuations since the particles are moving inside the $\bar{\text{PSF}}$ (see Eq. 1.22). Finally, the number fluctuations of molecules in the open observation volume follow Poissonian statistics (Eq. 1.1). All these intensity fluctuations result in a photon count distribution that follows super-Poissonian statistics (Teich and Saleh, 1988) and therefore the photon count distribution deviates from a Poissonian distribution. This deviation, which contains the fluctuation information, is clearly visible at the tail (at the highest photon counts) when the photon counting histogram values are plotted on a logarithmic scale. Chen et al. (1999) showed that the histogram approached a Poisson distribution when the concentration of the fluorophore was increased. Since the relative strength of the number fluctuations is inversely related to the square root of the average particle number, the fluctuations will vanish at high concentrations resulting in a decreased signal statistics. The resolving power of PCH to separate two species by differences in molecular brightness was studied by Müller et al. (2000). So far, PCH has been applied to monitor hormone receptors (Margeat et al., 2001), the formation of oligomer-polymer complexes (van Rompaey et al., 2000), the properties of luminescent nanoparticles (Akcakir et al., 2000) and, recently, the characteristics of EGFP in living HeLa cells (Chen et al., 2002).

Experimental considerations

Instrumental setup

Fluctuation measurements were performed on two commercially available instruments: The first generation ConfoCor (Carl Zeiss & Evotec Biosystems, Germany) is a single channel system based on a Zeiss Axiovert 135 inverted microscope with standard confocal epi-fluorescence microscope optics. An air-cooled Argon ion laser (488 and 514 nm) and a Helium-Neon laser (543 nm) were fibre-coupled to the back of the microscope where a

manually controlled mirror allows switching between the two excitation sources. Inserting neutral density filters in front of the laser output attenuated the intensity of the excitation light. Excitation dichroic and emission filters mounted in filter sliders were employed to select the proper excitation wavelength and separate the fluorescence from excitation light. A water immersion C-Apochromat 40x objective lens (N.A. 1.2) (Carl Zeiss, Germany) focused the excitation light to a diffraction-limited spot and collected the fluorescence. The objective contains an adjustable ring to correct for slight differences in refractive index (*e.g.* caused by variations in cover glass thickness). Refractive index mismatches between immersion liquid, sample support and sample can lead to a severe distortion of the observation volume. This will result in a deviation from the 3D Gaussian volume element, which is assumed in the FCS fitting models. The high numerical aperture of the objective ensures a high collection efficiency, which is required to achieve high signal to noise ratios. Samples were stored in 8 well Labtek chambered cover glasses (Naglenunc, USA) or 96-well plates (Whatman, UK) with borosilicate bottom. To limit the size of the observation volume a size adjustable and motor-controlled pinhole was placed in the image plane of the detection path. The diameter of the pinhole, which can drastically affect the SNR, is optimized to a value where a maximal count rate per molecule was observed. This diameter setting depends on excitation and emission wavelengths, magnification and numerical aperture of the objective and the degree of overfilling of the back aperture of the objective (Rigler et al., 1993; Qian and Elson, 1991). An oversized pinhole diameter leads to a non-Gaussian observation volume, which can be avoided by underfilling although this results in a larger excitation volume and thus greater number of observed (and background) molecules. The optimal pinhole setting is a trade off between increasing the SNR and minimizing the artifacts by underfilling the objective back aperture. The SPCM-AQ avalanche photodiode (APD) (Perkin Elmer, USA) detector is placed directly behind the pinhole. Avalanche photodiodes have high detection efficiencies above 450 nm (450 nm: 25%, 650 nm: 70%). However, APD's are unable to detect photons in a time interval (dead time) of approximately 35 ns after the previous event (Overbeck et al., 1998). Hence fluctuation processes that display themselves on a time scale shorter than 35 ns cannot be resolved. Widengren et al. (1995) increased the time-resolution of their system by applying cross-correlation to the signal that has been split by a 50% mirror into two separate detectors. For FCS analysis the detector is coupled to a fast digital ALV5000E correlator card (ALV, Germany) that calculates the real-time autocorrelation function. Access 1.0.12 software (Carl Zeiss & Evotec Biosystems, Germany) controls the system and allows evaluating single autocorrelation curves to a multi-component 3D Brownian motion model fit including triplet kinetics (Eq. 1.13). In case of PCH analysis, the detector is coupled to a dual channel 32 bits, PCI photon counting card (ISS, USA). Alba FCS 2.55 software (ISS, USA) controls the data acquisition and allows to analyse a user defined section of the raw data trace via auto- or cross-correlation or PCH. The card, created according to a prototype designed by Eid et al. (2000) can acquire the raw data in two different modes, time and photon mode.

Time mode saves the number of photoelectrons detected within a fixed time interval (i.e. bin), determined by the frequency of the clock. The photon mode, on the other hand, determines the number of clock cycles between two successive photon events. The latter method is more efficient when the average photon rate, typically 50 kHz in our experiments, is less than the clock frequency, which has been set to 24 MHz. The microscope was equipped with a 50 W mercury lamp and a back-illuminated TEK 512x512D CCD camera (Princeton, Netherlands) to collect widefield (fluorescence) images of cell. A microinjection system, consisting of an Eppendorf Microinjector 5242 and Micromanipulator 5170 (injection settings: $P_1 = 4000$ hPa, $P_{inj} = 100$ hPa, $P_{backpressure} = 60$ hPa and $t_{injection} = 0.2$ sec) (Eppendorf, Netherlands) was attached to the side of the microscope.

The second microscope to acquire fluorescence fluctuation data is the ConfoCor2 (Carl Zeiss, Germany), a dual channel system based on a Zeiss Axiovert 100M inverted microscope (Fig. 1.3). The system has been described in detail by Jankowski and Janka (2000). In brief, the microscope is equipped with two modules: At the baseport a LSM510 laser-scanning module is mounted which allows collecting confocal images.

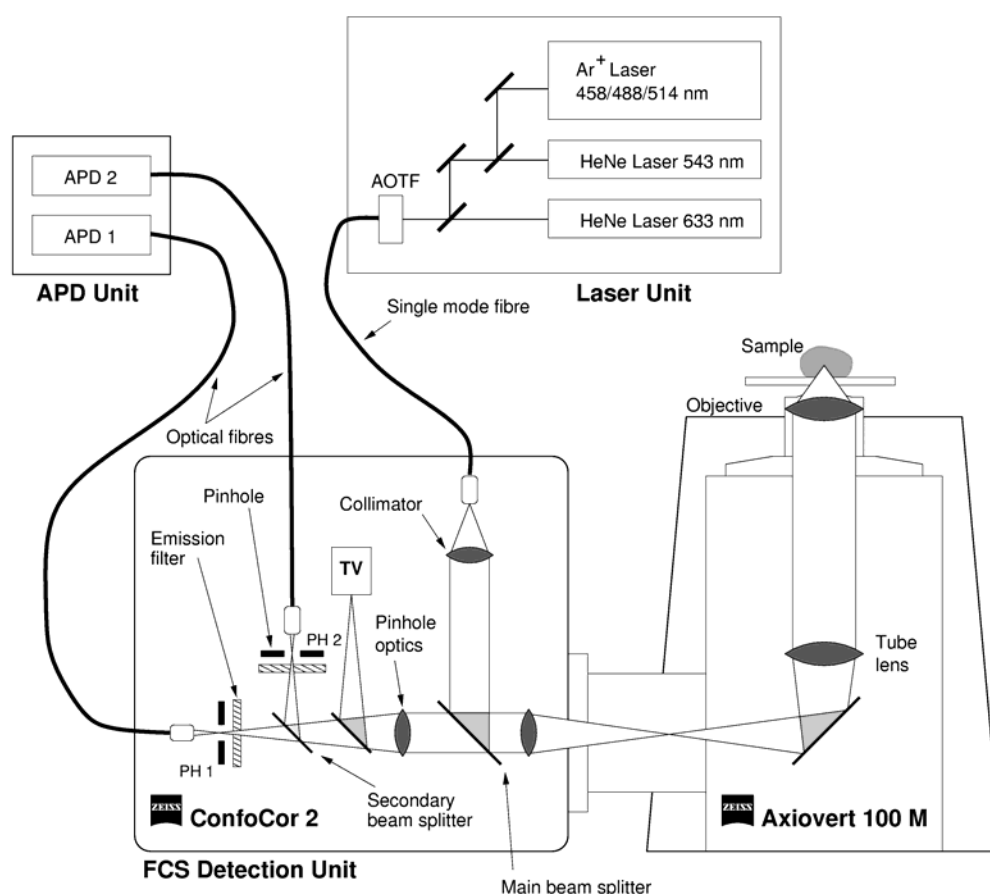


Figure 1.3: Schematic set-up of the beampath of ConfoCor2. Not shown here is the laser-scanning module (LSM510) that has been mounted to the baseport of the Axiovert microscope, allowing collecting confocal images. The figure has been reproduced from Jankowski and Janka (2000).

The ConfoCor2 module is connected to the sideport of the microscope and a manual controlled mirror in the base of the microscope allows switching between the two modules. Five laser lines supplied by three laser units, consisting of an air-cooled argon ion (458, 488 and 514 nm) and two helium neon lasers (543 and 633 nm) are focused by a telescope set-up into an optical fibre. An acousto-optic tuneable filter is used to control the transmission of each laser individually. The collimator lens creates a parallel beam that is reflected by one of the eight fixed dichroic mirror in the main beam splitter wheel and focused by a Zeiss water immersion C-Apochromat 40x objective lens (N.A. 1.2). This objective is highly corrected for chromatic aberrations, which is essential to have a perfect overlap between the two observation volumes used in dual-colour FCCS experiments (Schwille et al., 1997). Fluorescence from the sample passes the main dichroic filter and can be spectrally divided by the secondary beam splitter (wheel consisting of 8 fixed filters). After passing the emission filter (wheel consisting of 8 fixed filters) and the motor controlled, size-adjustable pinhole, the light enters the fibre light guide to either one of two SPCM-AQ APD detectors (Perkin Elmer, USA). The total system is controlled by AIM 2.8 software (EMBL Heidelberg, Germany). The data are autocorrelated in real time by a software correlator and multiple fits can be analysed according to multicomponent 3D Brownian motion models including triplet kinetics (Eq. 1.13). Moreover, the raw data can be stored in photon-delay mode.

Data acquisition

The systems were calibrated by optimising the position of the pinhole(s) and the correction ring of the objective lens, using a concentrated dye solution. Optimal settings were reached where the highest molecular brightness η (kHz/molecule) has been observed. The dimensions of the confocal volume element is represented as the structure parameter (sp)

$$sp = \frac{\omega_z}{\omega_{xy}} \quad (\text{Eq. 1.26})$$

and were obtained by fitting the autocorrelation curves of fluorophores with a known diffusion coefficient to equation 1.13. The retrieved structure parameter is allowed to vary between 4-10 for ConfoCor and 2-8 for ConfoCor2 (Carl Zeiss ConfoCor-manuals) to validate the assumption of a well-defined, 3D Gaussian shaped observation volume in the fitting models. In case of cross-correlation experiments the system was calibrated using 70 kDa aminodextrins (Molecular Probes, The Netherlands) labeled with the two dyes of interest or purified fusion proteins (see Chapter 5 for more details).

Data analysis

The software packages controlling the microscopes have only limited capabilities of fitting the correlation curves. Therefore an in-house software package was developed in collaboration with the Department of Systems Analysis (Belarussian State University, Minsk, Belarus). This software package, entitled Correlator Data Processor (version 1.3) (Windows 95/98/NT 4.0), consists of three modules: a user-interface, database and analysis part that can be developed independently. Intensity and correlation data acquired by ConfoCor or ConfoCor2 is imported into the measurement database. A data-editor allows selecting, removing or changing the bin width of certain sections of the raw data trace, after which a 'corrected' autocorrelation curve can be calculated. This opens the possibility to analyse small sections of the measured data trace in the case that the complete trace is disturbed by artefacts like intensity drifts (Chen et al., 2002) or the presence of high intensity bursts for example due to the presence of highly labeled particles (van Craenenbroeck et al., 1999) or aggregated fluorescent particles. The correlation curves are loaded into the analysis module that simulates or fits data according to one of the standard models describing 2D-, 3D- or anomalous diffusion. Moreover, a model-editor is included to create user-defined fitting models. Regularly used model and parameter settings can be stored in templates to accelerate the fitting handlings. The fit parameters are obtained by a global fitting procedure, based on the Marquardt-Levenberg non-linear method of least squares (Marquardt, 1963). In global analysis, several correlation functions are combined in a set and simultaneously fitted with certain parameters linked over the set, ensuring more reliable parameter recovery and thus a more consistent representation of the physical processes under investigation. Additionally, the quality of the fit and performance of the optimisation method can be improved by fixing the parameters that are known *a priori* from independent experiments and by generating appropriate initial guesses for parameters, for example, by the phase plane method (Novikov et al., 1998), adopted for the analysis of correlation functions. The goodness of fit is judged by criteria as χ^2 and visual inspection of the residuals between experimental and fitted curves. An error estimation of the recovered parameters is performed by the exhaustive search method (Beechem et al., 1992) resulting in the 67% confidence limits.

Acknowledgments

We thank Eugene Novikov (Institut Curie, Paris, France), Anatoli Digris and Victor Skakun (Dept. of Systems Analysis, Belarussian State University, Belarus) for the development of the Correlator Data Processor software package. The fluorescence microscopes were made available by an investment grant awarded by The Netherlands Organization for Scientific Research (NWO).

2

Dynamics of Green Fluorescent Protein Alone and Fused with a Single Chain Fv Protein

**Mark A. Hink, Remko A. Griep, Jan Willem Borst, Arie van Hoek,
Michel H.M. Eppink, Arjen Schots and Antonie J.W.G. Visser**

The green fluorescent protein (GFP) and its spectral variants are widely used in cell biology and biochemistry to fluorescently label endogenous proteins so that their distribution and dynamics can be followed in living cells. However, structural and dynamical information about fusion proteins itself is not available. Therefore, the dynamical properties of enhanced GFP (abbreviated as GFP here) and its fusion to a single chain antibody (scFv-GFP) have been studied. The single chain antibody was raised against the lipopolysaccharide of the outer cell wall of Gram-negative bacteria. Fluorescence correlation spectroscopy (FCS) has been used to monitor diffusion properties and to check the functionality of the scFv-GFP in a binding assay. The rotational motion of scFv-GFP, investigated with time-resolved fluorescence anisotropy, is too short to account for globular rotation of the whole protein. This result can be explained by assuming a fast hinge motion between the two fused proteins, which was supported by a modelled structure of scFv-GFP.

Published in edited form in the *Journal of Biological Chemistry* **275**, 17556–17560 (2000)

Introduction

The green fluorescent protein (GFP) isolated from the jellyfish *Aequorea victoria* has received widespread utilization as a natural fluorescent marker for gene expression and localization of gene products (Heim et al., 1994, 1995 & 1996; Chalfie et al., 1994; Delagrave et al., 1995). GFP is a protein consisting of 238 amino acids with a molecular mass of 27 kDa and has the shape of a cylinder with length $L = 4.2$ nm and diameter $d = 2.4$ nm. The chemical structure of the hexapeptide chromophore has been elucidated (Cody et al., 1993). The intrinsic fluorophore is a *p*-hydroxybenzylidene-imidazolidine derivative formed by a covalent modification of the sequence Ser65 (or Thr65), Tyr66 and Gly67 in the hexapeptide. The crystal structure of GFP has been solved at 1.9 Å and 2.1 Å resolution and showed the hexapeptide as part of a central helix inside a 11-stranded β -barrel (Ormö et al., 1996; Yang et al., 1996; Brecj et al., 1997). Mutagenesis, changing the local environment surrounding the chromophore group has resulted in GFP variants with altered spectral characteristics (Tsien, 1998). Enhanced GFP (EGFP) is a double mutant of the wt-GFP (F64L/S65T) and one of the most frequently used mutants in GFP research nowadays due to the red shifted absorption maximum at 488 nm and a higher molar extinction coefficient.

Although fusion proteins with GFP are used in numerous experiments, the number of studies on the structural behaviour of the GFP-moiety in fusion proteins has been limited. In order to understand why the functionality of proteins fused with GFP is often preserved, we have studied the motional properties of a particular GFP-fusion protein. We have selected the GFP linked to a single chain Fv fragment (scFv-GFP). Coupling the variable domains of the heavy and light chain of an antibody by a flexible peptide linker allowed expressing variable antibody fragments (Fv) in single chain molecules (scFv). Random combination of both variable domains has generated large combinatorial libraries, consisting of over 10^{10} different antibodies. In combination with the display of these scFv fragments on the tips of phages a powerful system to select specific monoclonal antibodies has been created (McCafferty et al., 1990). However, the screening of these libraries is still laborious. The monoclonal single chain fragment used in this study has been raised against the lipopolysaccharides (LPS) present in the outer cell wall of *Ralstonia solanacearum*. This organism can infect over 450 different plant species including many important crops (Hayward, 1991). To detect the presence of the bacteria already at the beginning stages of a disease outbreak, sensitive and fast techniques should be developed. Hence, fluorescence is a promising method to use. Fluorescence correlation spectroscopy (FCS) allows measuring the diffusion rate of fluorescent molecules. In this way FCS is able to monitor the binding of scFv-GFP to the *Ralstonia* bacteria, separating the relatively fast diffusing scFv-GFP from the large and slower diffusing complex. The rotational motion of the scFv-GFP has been studied with time-resolved fluorescence anisotropy. In order to have additional support for the observed rapid rotation of scFv-GFP a putative structural model has been built.

Results and Discussion

Diffusion and binding of scFv-GFP

To access whether or not the genetic function of GFP to a single chain Fv alters the binding properties, the affinity for LPS of scFv alone and scFv fused to EGFP to lipopolysaccharide has been determined by surface plasmon resonance measurements (Kretschmann et al., 1968). The measured affinities (in terms of dissociation constants) of 0.92 ± 0.12 nM for scFv alone and 1.00 ± 0.09 nM for the scFv-GFP fusion protein can be considered as identical because the difference in binding affinity falls within experimental error.

FCS experiments were performed to study the binding of scFv-GFP to the outer membrane of Gram-negative bacteria, rich in LPS. Binding of the fusion protein to the bacteria will result in a large fluorescent complex, which diffuses at a much longer timescale than the relatively small, free scFv-GFP proteins. In figure 2.1A a typical autocorrelation curve for scFv-GFP yielding a diffusion time of 256 ± 5 μ s is presented. In the presence of *Ralstonia solanacearum* bacteria the autocorrelation curves were best fitted according to a single component model with a characteristic diffusion time of 45 ± 21 ms (dotted line), indicating the presence of large and slowly diffusing complexes. The diffusion time had a similar value as that of the non-labeled autofluorescent bacteria (38 ± 18 ms) (dashed line), which was expected since binding of the relatively small scFv-GFP would hardly increase the radii of the bacterial cells. The absence of a second fast diffusing component in the fit, i.e. free diffusing scFv-GFP, could be explained by the multivalency of the bacteria since the outer cell membrane is covered by an almost infinite number of binding spots. Therefore it is possible that all unbound scFv-GFP is depleted from the solution. Another reason for the apparent absence of fast diffusing species could be the fact that the contribution of each fluorescent species to the autocorrelation curve scales with the squared value of the molecular brightness (Eq. 1.14). Hence, bacteria having multiple scFv-GFP proteins bound to their membranes would dominate in the autocorrelation curve, thereby suppressing the contribution of the less bright species. Measurements in the supernatant after spinning down the bacteria yielded only fluorescence intensity traces at the background level resulting in very noisy autocorrelation curves. It can therefore be assumed that almost all scFv-GFP has been depleted from solution due to the binding to the LPS in the bacterial membrane. On average the immunolabeled cells (Fig. 2.1C) gave rise to forty times more intense fluorescent bursts than the autofluorescent bacterial cells (Fig. 2.1B) and in this way both cell types could be distinguished from each other. In a control experiment, Gram-positive bacteria (*Clostridium histolyticum*) or *Spodoptera frugiperda* (Sf21) insect cells were added to a scFv-GFP solution. In both cases the diffusion time was approximately 260 μ s and no high intensity peaks in the fluorescent intensity traces were found, indicating that no immunolabeled cells were present (Fig. 2.1A, dotted line).

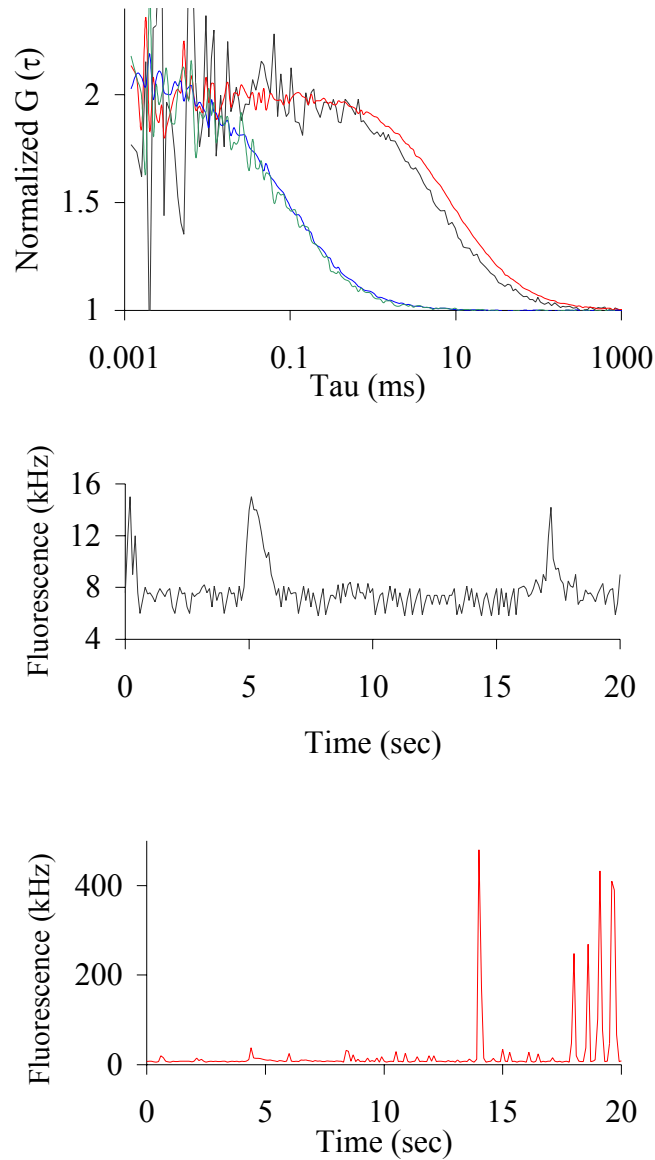


Figure 2.1: Binding of scFv-GFP to Gram-negative bacteria monitored with FCS. (A) The autocorrelation curves for scFv-GFP (green line), autofluorescent *Ralstonia solanacearum* bacteria (black line). Gram-positive (blue line) and Gram-negative bacteria (red line) were incubated with scFv-GFP to monitor binding. All curves were scaled to 2.0 (equivalent to one molecule in the detection volume) for clarity. Panels B and C show the fluorescence-intensity traces of autofluorescent and immunolabeled bacteria, respectively.

From the FCS-experiments on scFv-GFP alone, a translational diffusion coefficient (D_{tran}) of $6.05 \pm 0.24 \text{ m}^2 \cdot \text{s}^{-1}$ was calculated, which corresponds to a particle with an apparent hydrodynamic radius of 3.54 nm. The translational diffusion coefficient of free EGFP is $D_{\text{tran}} = 9.0 \pm 0.2 \cdot 10^{-11} \text{ m}^2 \cdot \text{s}^{-1}$ similar to the value found for wildtype GFP (Terry et al., 1995 Swaminathan et al., 1997) and EGFP (Wachsmuth et al., 2000). R_h turns out to be 2.42 nm (Table 2.1). The experiments described above indicate the potential of FCS as a tool to develop medium- or high-throughput screening technology.

Table 2.1: Translational diffusion-times and -coefficients (τ_{dif} , D_{tran}) and hydrodynamic radii (R_h) of green fluorescent protein and its fusion product to a single chain antibody (scFv-GFP). The standard deviation mentioned at each parameter is obtained from 10 experiments (5 experiments for 2 different protein preparations). D_{tran} and R_h are calculated from equations 1.9 and 1.15, respectively.

Sample	τ_{dif} (μs)	D_{tran} ($\text{m}^2 \text{s}^{-1}$). 10^{11}	R_h (nm)
GFP	167 ± 4	9.03 ± 0.22	2.42 ± 0.05
scFv-GFP	254 ± 10	6.05 ± 0.24	3.54 ± 0.14

Pharmaceutical companies have recognized this potential leading currently to high-throughput screening facilities, which combine FCS with other modalities of fluorescence (i.e. FIMDA, FILDA and spectral analysis) (Auer al., 1998; Rudiger et al., 2001; Meyer-Almes, 2001). In case of large combinatorial antibody libraries, one could think of developing a method to quickly isolate monoclonal antibodies against an antigen of interest.

Time-resolved fluorescence and rotation

Time-resolved polarized fluorescence of EGFP also results in an average hydrodynamic radius and indicates that the chromophoric group rotates together with the protein. Three fluorescence lifetimes were needed to give an optimal fit.

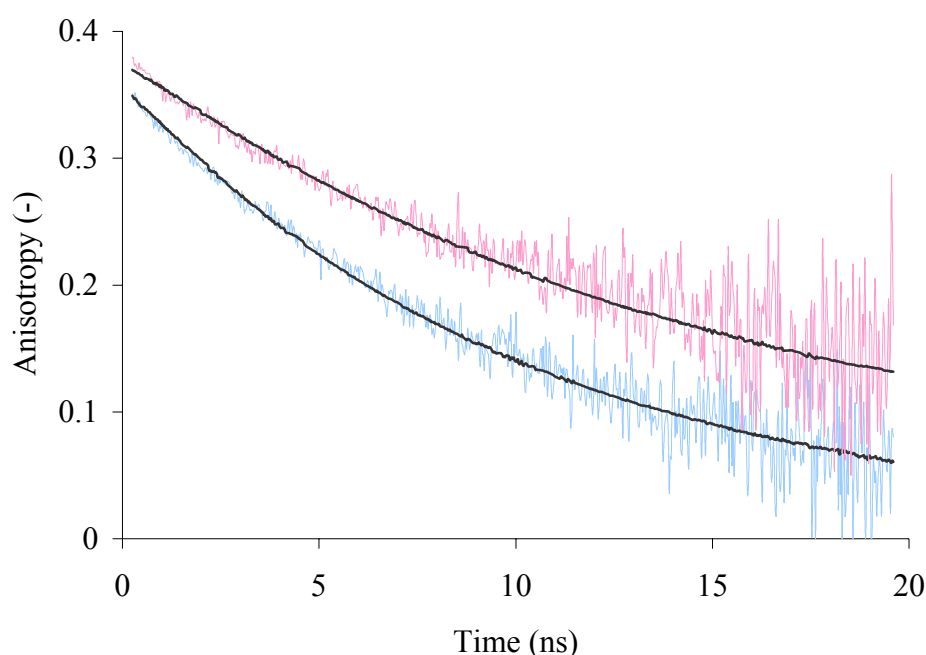


Figure 2.2: Fluorescence anisotropy decay curves of EGFP (blue) and scFv-GFP (red). The experimental curves were fitted with a single correlation time of 10.8 ns for EGFP and of 15.8 ns for scFv-GFP (solid black lines). Full results of analysis are collected in Table 2.2.

Table 2.2: Fluorescence decay parameters (α_i, τ_i) and anisotropy decay parameters ($\beta, \phi, D_{\text{rot}}, R_h$) of green fluorescent protein (GFP) and scFv-GFP. Values in parentheses below lifetimes and correlation time are the limiting values obtained after an exhaustive error search (at the 67% confidence limit) in a global analysis of two separate experiments. Pre-exponential factors are the average of two determinations and are accurate to the given digit.

Sample	Fluorescence						Anisotropy		
	α_1 (-)	τ_1 (ns)	α_2 (-)	τ_2 (ns)	α_3 (-)	τ_3 (ns)	β (-)	ϕ (ns)	R_h (nm)
GFP	0.23	0.51 (0.43-0.58)	0.70	2.57 (2.48-2.65)	0.07	4.9 (4.6-5.4)	0.37	10.6 (10.2-11.0)	2.21 (2.18-2.23)
scFv-GFP	0.21	0.53 (0.45-0.60)	0.73	2.53 (2.40-2.61)	0.06	4.1 (3.5-5.0)	0.38	15.8 (14.9-16.5)	2.52 (2.47-2.56)

These lifetime components and pre-exponential factors are collected in table 2.2. The main fluorescence lifetime is 2.6 ns, in fair agreement with values obtained previously (Losseau et al., 1996), but lifetimes of 0.50 and 4.9 ns are also present. The heterogeneity of the fluorescence decay is consistent with the reaction scheme proposed previously from subpicosecond time-resolved fluorescence spectroscopy (Chattoraj et al., 1996). This scheme has taken into account equilibria between different ground- and excited states, proton transfer- and photoconversion processes. These multiple states and the interconversion between them would lead to an inherent non-exponential decay as observed. The fluorescence anisotropy decay analysis of GFP yields a single rotational correlation time ϕ of 10.6 ns (Table 2.2 and Fig. 2.2). The fluorophore is rigidly bound in the protein matrix and rotates together with the whole protein. This observation is in full agreement with the 3-dimensional structures in which the fluorophore is rigidly incorporated in the central helix (Ormö et al., 1996; Yang et al., 1996; Brecj et al., 1997). The rigidity of the binding site seems a general property of fluorophores involved in bioluminescence: there is no internal motion of other light emitting antenna fluorophores as well (Visser et al., 1997; Lee et al., 1991). The hydrodynamic radius R_h , calculated from the obtained rotational correlation time (Eq. 2.1) is 2.21 nm (Table 2.2) and in good agreement with the fluorescence correlation experiment.

The fluorescence decay of scFv-GFP contains the same lifetime components as those arising from GFP alone (Table 2.2). However, the fluorescence anisotropy decays more rapidly than can be expected for a fusion-product, which is about twice the size of a single GFP-molecule (Fig. 2.2). The reason for this observation should be sought in the flexibility of the peptide region linking the two proteins. The transport properties of macromolecules with segmental flexibility have been theoretically investigated via simulations of the fluorescence anisotropy decay for two rigid proteins connected by a flexible hinge (Harvey et al., 1979 & 1980). It was shown that segmental flexibility is detected by fluorescence anisotropy provided that the orientation of the emission transition dipole is such that it reports on the bending motion.

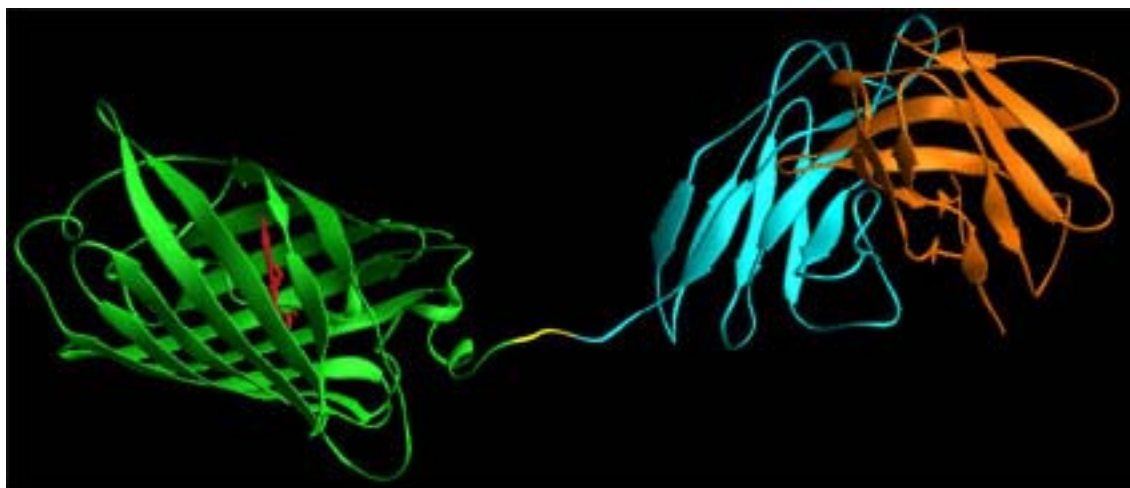


Figure 2.3: Ribbon drawing of the C α -backbone of the scFv-GFP model. The GFP is shown at the left side, the variable light domain in the middle interacts with the variable heavy domain at the right side. The linker residues in between the GFP and antibody moieties allows flexible movement. This schematic ribbon diagram was generated with RIBBONS (Carson, 1991).

On the other hand, the dipole can also be wrongly oriented so that the anisotropy decay is like that of a rigid body and no flexibility will be observed. Another important outcome of these simulations is that the extent of bending cannot be inferred from a two-exponential fit to the anisotropy decay. Apparently in our case of scFv-GFP the emission transition dipole of GFP has a favorable geometry for sampling the flexibility of the hinge between two relatively rigid molecules. Also in line with the simulations (Harvey and Cheung, 1980) is the fact that the fluorescence anisotropy decay is a single exponential.

Structural model

The C α -backbone of the scFv-GFP construct is presented in figure 2.3. The linkage between GFP and the variable fragment of the light chain consists of three alanine residues. Together with the three C-terminal amino acids of the light chain, a flexible connection between GFP and the single chain antibody is formed, well separating both proteins. This observation fully agrees with the data obtained with time-resolved fluorescence anisotropy, where a flexible hinge between two rigid fragments can explain the relatively short rotational correlation time. The structure also explains that the scFv-GFP construct easily recognizes its antigen. There is no spatial interference between the two proteins and the antigen-binding site is fully exposed.

Materials and Methods

To change the fluorescence excitation peak of wild type green fluorescent protein from 396 nm to 488 nm (Prasher et al., 1992), two amino acid changes (F64L & S65T) were introduced into the wild type GFP by PCR (Griep et al., 1998). The GFP gene was ligated in frame with the scFv using 3 alanine residues as linker. The produced GFPmut1 protein was isolated and purified as described by Griep et al. (1998). The purity of GFP and scFv-GFP was assessed by

SDS-polyacrylamide gel electrophoresis and western blotting. *Ralstonia solanacearum* bacteria were plated on growth factor agar and treated with NaN_3 before the measurement. *Spodoptera frugiperda* insect cells (Sf21) were grown in Grace's Insect medium (Sigma, The Netherlands) containing 10% Foetal Calf Serum and released from the culture flask bottom. Cell suspensions were diluted to a final concentration of 10^7 cells ml^{-1} using 0.1 M Tris-HCl buffer pH 7.8 containing 0.01% Tween-80 and incubated with scFv-GFP at room temperature for five minutes.

Fluorescence correlation spectroscopy

The fluorescence correlation spectroscopy measurements were performed with a ConfoCor system (Carl Zeiss & Evotec Biosystems, Germany), which has been described in detail in chapter 1. Here the sample was excited using the 488 nm Ar ion laser line and a fluorescein emission filter block allowed to separate the excitation light from the emission light. The pinhole, allowing confocal detection, was set at a diameter of 60 μm . The concentration of scFv-GFP amounted to 6.0 nM by diluting with 0.1 M Tris-HCl buffer pH 7.8. The system was calibrated by acquisition of autocorrelation curves of 50 nM rhodamine 6G during 20 seconds. The experimental curves were fitted according to the model describing Brownian diffusion and triplet kinetics (Eq. 1.13) using a structure parameter (Eq. 1.26) fixed in the fit to the value obtained from calibration measurements. Since it was noticed that the autocorrelation decay time of EGFP was distinctly shorter upon the use of relatively high laser power (Visser et al., 1999) and low pH (Haupts et al., 1998), the FCS data were acquired with a relatively small laser power density of ca. 20 kW.cm^{-2} and in buffered solutions at pH 7.8.

Biacore binding experiments

The surface plasmon resonance (Kretschmann et al., 1968) experiments were performed with the BIAcore 2000 system (Pharmacia, Sweden). Thereto, a streptavidin-coated sensorchip (Pharmacia, Sweden) was incubated with biotinylated lipopolysaccharide antigen until saturation was observed. The experiments were performed like described in Kamiuchi *et al.* (1998). In brief, the association kinetics were measured by flowing 10 μl purified scFv or scFv-GFP (both $0.2 \mu\text{g.ml}^{-1}$) at a rate of $10 \mu\text{l.min}^{-1}$. The dissociation kinetics was observed for five minutes by flowing buffer.

Structural model of scFv-GFP

In order to obtain a realistic impression of the structure of the scFv-GFP fusion product a putative homology model was constructed. Structural models of the variable domains of the heavy (V_H) and light (V_L) chains of anti-LPS were derived by homology modelling using the AbM software package (version 2.0, Oxford Molecular). The best templates for the V_L

domain were the V_L domains with PDB code 1BAF (Brünger et al., 1991) and 1BBD (Thormo et al., 1993) both with 47% sequence identity. The best template for the V_H domain of anti-LPS was the V_H domain with PDB code 1FVC (Eigenbrot et al., 1993) having 70% sequence identity. Both V_H and V_L domains of the homology models were together superimposed onto the V_H and V_L domains of 1BAF with the InsightII package (Release 97.0, Biosym Technologies, Inc.). The structure of GFP 1EMA (Ormö et al., 1996) was obtained from the Protein Data Bank and the Phe64Leu mutation was introduced with the homology module of InsightII. The N-terminus of the GFP molecule was coupled to the C-terminus of the V_L domain with a linker of three alanines using the InsightII software. The constructed scFv-GFP model was energy minimized with the conjugate gradient method of the XPLOR package (Brünger, 1992) using the parameter set as determined by Engh et al. (1991). For the chromophoric group a topology and parameter set were generated with the XPLO2D program (Kleywegt and Jones, 1998). The final model was obtained after 250 minimization cycles (gradient: 0.1 kcal/mol). The scFv-GFP model was stereochemical verified with PROCHECK (Laskowski et al., 1993) and the protein folding was assessed with PROSAIL (Sippl, 1993).

Time-resolved fluorescence

Time-resolved polarized fluorescence experiments were carried out using a picosecond laser system and time-correlated single photon counting as described in detail in chapter 3. The excitation wavelength was 480 nm (coumarin 150 dye as laser medium, pumped by a mode-locked Nd-YLF laser) and the fluorescence was selected by using a bandpass filter (K50) in conjunction with a GG495 cut off filter (both filters were from Schott, Mainz, Germany). The total fluorescence decay and the fluorescence anisotropy decay were analyzed using the global analysis program from Globals Unlimited, Inc. (Urbana, IL). The 67% confidence limits of fluorescence lifetimes and rotational correlation times were determined in a rigorous error analysis by linking two experiments on two different protein preparations. The hydrodynamical radius of the particles, r_h , could be calculated from the rotational correlation time, ϕ_R , via the Debye-Stokes-Einstein equation:

$$\phi_R = \frac{4\pi r_h^3 \eta_v}{3 k T} \quad (\text{Eq. 2.1})$$

where k denotes the Boltzmann constant, T the absolute temperature and η_v the viscosity of the medium. The hydrodynamic radius of the particle, r_h , could be determined from FCS experiments, since r_h is related to the observed diffusion coefficient via the Stokes-Einstein relation (Eqs. 1.9 and 1.15). The GFP concentration used was 200 nM adjusted with 0.1 M Tris-HCl buffer at pH 7.5. The same buffer was used to obtain a scFv-GFP concentration of 80 nM. The temperature of all experiments was 295 K.

Conclusion

The binding of a GFP labeled single chain antibody fragment (scFv-GFP) to its antigen, lipopolysaccharide, present in the outer cell membrane of *Ralstonia solanacearum* bacteria clearly demonstrates the ability of FCS to distinguish particles on basis of the difference in diffusion coefficient. This attractive property of FCS has opened the way for an enormous field of applications monitoring the interaction between small fluorescent ligands to its non-fluorescent counterparts at the nanomolar concentration level. Time-resolved fluorescence anisotropy revealed a characteristic rotational motion, which could be explained, by the intramolecular hinge motion in the scFv-GFP protein.

Acknowledgments

We thank Jan van der Wolf (IPO-DLO, Wageningen, The Netherlands) for supplying the bacterial cultures and Maurice Kunen (Department of Human Biology, Maastricht University, The Netherlands) for generous access to and assistance with the BIAcore experiments. This research was supported by an investment grant from The Netherlands Organization for Scientific Research (NWO) and by a grant from the Council of Earth and Life Sciences of NWO (ALW-NWO).

3

Dynamics of Fluorescent Phospholipids in Micelles: Characterization with Fluorescence Correlation Spectroscopy and Time-Resolved Fluorescence Anisotropy

Mark A. Hink, Arie van Hoek and Antonie J.W.G. Visser

The dynamic properties of two BODIPY labeled phospholipid molecules in micellar systems have been studied with fluorescence correlation spectroscopy (FCS) and time-resolved fluorescence anisotropy (TRFA). Phospholipid molecules labeled at the headgroup or at the acyl chain were mixed with different detergents and thus incorporated in micelles. FCS investigated the translational diffusion constant, aggregation number and hydrodynamic size of the micelles. The micelles were larger in size than reported in literature, which is due to the incorporation of the relatively large sized fluorescent probe. The micelles loaded with the head-labeled phospholipid had a significantly larger radius compared to the micelles loaded with a tail-labeled probe as was confirmed by dynamic light scattering experiments. TRFA experiments showed that the lateral diffusion of the probe is the main, rapid contributing process in micelles composed of detergents like Triton X-100, polyoxyethylene-9-laurylether (Thesit), cetyltrimethylammonium bromide (CTAB) and sodium dodecyl sulfate (SDS). However, micelles made from digitonin and deoxycholate had significantly different properties, which could be explained by more rigidly packed micelles. The calculated values for the wobbling motion, cone angle and order parameters indicated that the tail-labeled probe undergoes less restricted motion than the head-labeled probe.

Published in edited form in *Langmuir* **15**, 992-997 (1999) and in *Applied Fluorescence in Chemistry, Biology and Medicine*. W. Rettig, B. Strehmel, S. Schrader and H. Seifert (eds.), Springer Verlag, Berlin, 101 (1998).

Introduction

The plasma membrane has a crucial role in intracellular signal transduction processes. Membrane interactions involving proteins and lipid cofactors are continuously modulated enabling transmission of signals at the right moment and along the correct pathway. The physical structure of the lipid membranes strongly influences the dynamics of these processes. Therefore, experimental data on spatial-temporal organization of the plasma membrane are required.

Because of their sensitivity, microspectroscopic techniques such as fluorescence correlation spectroscopy (FCS) (Hess al., 2002) and time-resolved fluorescence anisotropy (TRFA) (Steiner, 1991) provide quantitative information on molecular interactions and dynamic events. Prior to applying these techniques to relatively complex cellular membrane systems one has to resort first to more simple model membranes, e.g. micelles. Although micelles do not mimic the exact biological bilayer, they have the advantage that they form a simple experimental system. In order to visualize the micelles for fluorescence-based methods, the micelles were loaded with amphiphilic fluorescent probes. The diffusion coefficient of single micelles, as measured by FCS, was related to the size and aggregation number of the loaded micelles.

TRFA provides complementary information on the intramicellar dynamics of the same micellar system as used in FCS. It turned out that the main depolarisation mechanism is not rotation of the micelle as a whole, but internal restricted motion and lateral diffusion within the micelle.

Principle of TRFA

Time-resolved fluorescence anisotropy measurements yield detailed information on the motional freedom of the probe molecules in their local environment. By measuring the time-dependent parallel and perpendicular polarized emission components, $I_{//}(t)$ and $I_{\perp}(t)$, relative to the polarization of the exciting beam, the fluorescence anisotropy $r(t)$ can be recovered:

$$r(t) = \frac{I_{//}(t) - I_{\perp}(t)}{I_{//}(t) + 2I_{\perp}(t)} \quad (\text{Eq. 3.1})$$

The fluorescence anisotropy decay of a fluorescent lipid in a micellar system was analysed according to a general diffusion model, abbreviated r_{g3} , in which the motion is described as diffusion in an anisotropic environment (Szabo, 1994; van der Meer et al., 1984; Pap et al., 1996). Here it is assumed that the orientation of the labeled phospholipid is Gaussian distributed over a given angular width, θ_g , around the micellar radius (Pap et al., 1996) (for this reason the model is referred to as the modified r_{g3} model). Although the r_{g3} model should be applied to analyse the anisotropy decay of cylindrically symmetrical probe molecules, it is

unlikely to introduce a serious error using this model for the analysis of the anisotropy decay of the (less symmetrical) fluorescent phospholipid probes. The fluorescence anisotropy decay curves of the fluorescent probes in micelles can be described by a product of three correlation functions (Eq. 3.2), corresponding to the internal motion of the probe, expressed by θ_g and D_{\perp} , the probe lateral diffusion described by the lateral correlation time ϕ_L and the overall rotation of the micelle with rotational correlation time ϕ_R (Pap et al., 1996):

$$r(t) = e^{-t/\phi_R} \cdot e^{-t/\phi_L} \cdot C(r_0, D_{\perp}, \theta_g, t) \quad (\text{Eq. 3.2})$$

where r_0 is the fundamental anisotropy. The fluorescence anisotropy decay analysis requires therefore 5 parameters, which are highly correlated. To simplify this analysis, some important assumptions have to be made. The micelles are expected to be spherical and to behave as isotropic rotors. The overall rotational correlation time, ϕ_R , can then be fitted according to equation 2.1. The hydrodynamic radius of the particle, r_h , could be determined from FCS experiments, since r_h is related to the observed diffusion coefficient via the Stokes-Einstein relation (Eqs. 1.9 and 1.15), assuming spherically shaped micelles. The calculated radius was then fixed in the analysis of the fluorescence anisotropy decay data. The fundamental anisotropy r_0 was obtained from the Maximum Entropy Method (MEM) analysis of the fluorescence anisotropy decay (Brochon, 1994) and was fixed as well. The lateral correlation time, ϕ_L , is related to the lateral diffusion constant, D_L , and the position of the fluorescent group along the micellar normal, r_p , according to:

$$\phi_L = \frac{r_p^2}{4 D_L} \quad (\text{Eq. 3.3})$$

Results and Discussion

Micellar diffusion

The micelles were visualized by loading one of the two selected fluorescent BODIPY-phospholipids. β -BODIPY₅₃₀₋₅₅₀-C₅-HPC consists of a phosphatidylcholine with a fluorescent BODIPY₅₃₀₋₅₅₀ group coupled to one of the fatty acyl chains. This probe will be referred to as the tail probe. In BODIPY₅₃₀₋₅₅₀-DHPE the BODIPY₅₃₀₋₅₅₀ group was coupled to the phosphoethanolamine head group (identified as the head probe). The amphiphilic fluorescent probes, displayed in figure 3.1 contain a charged phosphate group and hydrophobic (or lipophilic) acyl chains and therefore can easily be incorporated into micellar systems.

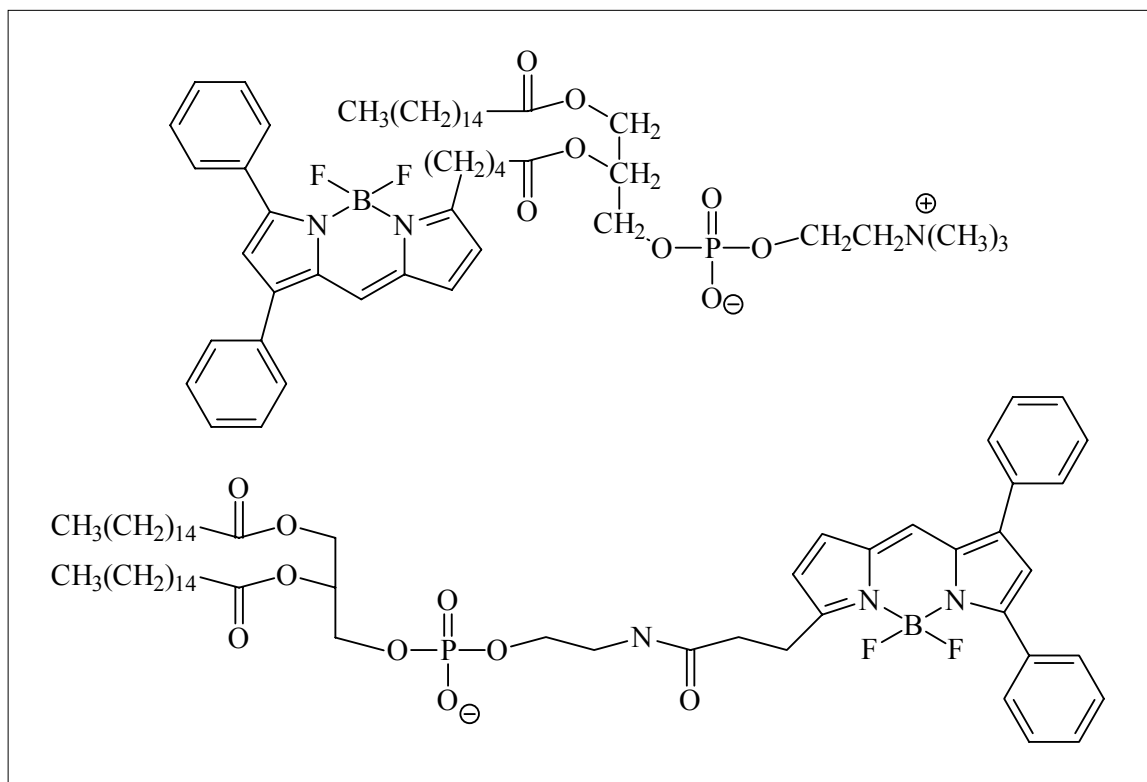


Figure 3.1: Molecular structures of the fluorescent phospholipids, β -BODIPY₅₃₀₋₅₅₀-C₅-HPC (upper structure) and BODIPY₅₃₀₋₅₅₀-DHPE (lower structure).

The fluorescence quantum yields of these probes are close to unity and are independent of pH and polarity of the local environment (Haugland, 1996). The fluorescent techniques used in this study will only detect the micelles, which have incorporated a fluorescent phospholipid. The autocorrelation curves, as obtained with FCS, were analysed according to an algorithm describing the 3D Brownian diffusion of one molecular species and a term for the triplet kinetics of the fluorophore (Eq. 1.13). At detergent concentrations below the critical micelle concentration (CMC), no micellar structures are formed. The diffusion time of the BODIPY-phospholipids at detergent concentrations below the CMC (both probes $\tau_{\text{dif}} = 71 \pm 4 \mu\text{s}$) was similar to that of the free lipid probe in buffer (both probes $\tau_{\text{dif}} = 70 \pm 4 \mu\text{s}$). The average diffusion time obtained for the loaded micelles ($\tau_{\text{dif}} > 150 \mu\text{s}$) was significantly larger than the one obtained for free lipid probes (Fig. 3.2A).

To validate if any free BODIPY-phospholipid molecules were present in the sample, the autocorrelation curves were fitted to a model including a second diffusing species fixed to the diffusion time observed of the free probe. The fit-quality using this model did not improve and no free probe molecules were observed. However, the presence of micelles loaded with a high number of probe molecules could give rise to a severe underestimation of the free diffusing probe molecules due to the difference in brightness: Significant differences in particle brightness can result in autocorrelation curves which are dominated by the

brightest species, where the fluctuations of dimmer species are less abundant or even not detectable (Eq. 1.14). However, it is unlikely that this effect masks the fluctuations of free probe in our experiments, since no fluorescent spikes are present in the intensity traces and the concentration of probe did not exceed $0.001 \cdot \text{CMC}$. Therefore it was concluded that the amphiphilic BODIPY-phospholipids were completely taken up in the micelles. Figure 3.2B shows the typical autocorrelation curves for fluorescent Thesit and Triton X-100 micelles. The differences in the translational diffusion times between both detergents are clearly reflecting their micellar sizes. Except for Tween 80, all micelles have a slower diffusion rate for the head-labeled phospholipid compared to the tail-labeled probe. The translational diffusion coefficient, hydrodynamic radius and aggregation number were calculated from the observed diffusion times according to equations 1.9, 1.15 and 3.4. As is presented in table 3.1, the micellar radii are in the nanometer range and are in the same order as the radii of the fluorescent probes. Except for the micelles made from the non-ionic detergents Triton X-100 and Thesit, the radii and aggregation numbers are larger than the literature values obtained with light scattering and sedimentation equilibrium experiments (Neugebauer, 1994; Maiti et al., 1995; Fendler, 1982; Robson and Dennis, 1977; Quitevis et al., 1993; Zana et al., 1997), although the relative size differences between the micelles were in agreement with literature.

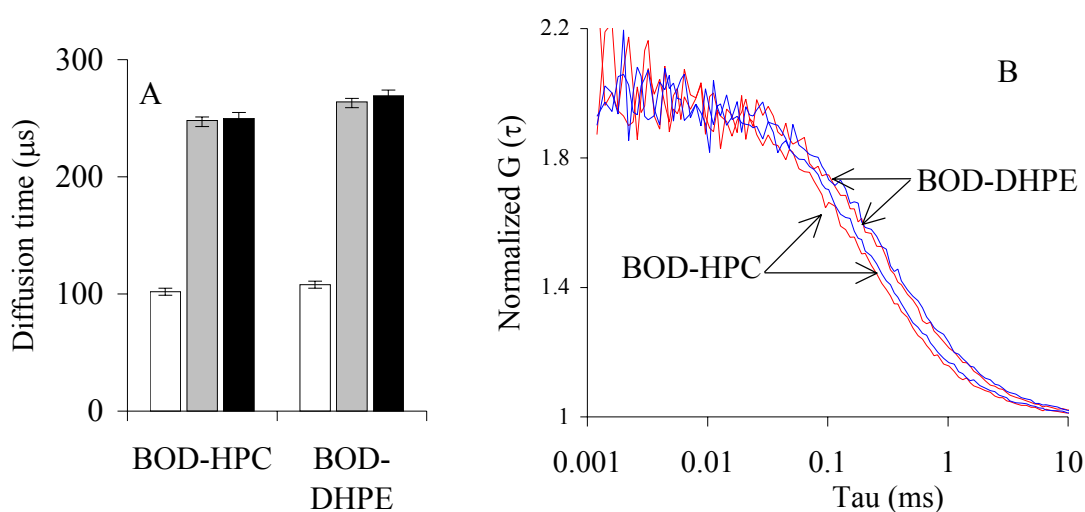


Figure 3.2: (A) Diffusion times of the two fluorescent phospholipids. The probes have been measured in PBS (white) and in 1 mM Triton X-100 using a probe concentration of 10 nM (grey) and 1 mM (black). Error bars indicate the variation between different measurements ($n=20$). (B) Normalized autocorrelation curves for Thesit (blue line) and Triton X-100 (red line) micelles in PBS, loaded with BODIPY-HPC or BODIPY-DHPE. The following diffusion times were obtained:

$\tau_{\text{dif}}(\text{Thesit, BODIPY-HPC}) = 233 \pm 3 \mu\text{s}$, $\tau_{\text{dif}}(\text{Thesit, BODIPY-DHPE}) = 323 \pm 4 \mu\text{s}$,
 $\tau_{\text{dif}}(\text{Triton, BODIPY-HPC}) = 208 \pm 4 \mu\text{s}$, $\tau_{\text{dif}}(\text{Triton, BODIPY-DHPE}) = 299 \pm 5 \mu\text{s}$.

Table 3.1: Translational diffusion constants, calculated rotational correlation times, aggregation numbers and hydrodynamic radii of several detergents at pH 7.0¹⁾ loaded with 10 nM of BODIPY-DHPE (first entry) or BODIPY-HPC (second entry), as determined with FCS. The overall micellar correlation time, ϕ_R , was calculated from FCS experiments. The micelles are assumed to have a spherical shape with a density of 1.05 g.cm^{-3} in a solution with a viscosity of 1.10^{-3} Pa.s . Standard errors are based on multiple measurements ($n=15$).

1) except the Digitonin solution which had pH 8.3.

Micelle	$D_{\text{tran}} \times 10^{11}$ [$\text{m}^2.\text{s}^{-1}$]	ϕ_R [ns]	Aggregation number	r_h [nm]
CTAB	5.3 ± 0.3	69	616 ± 69	4.5 ± 0.3
	6.6 ± 0.3	36	319 ± 41	3.7 ± 0.2
Deoxycholate	9.7 ± 0.7	11	73 ± 18	2.5 ± 0.2
	11 ± 1	8	50 ± 13	2.2 ± 0.2
Digitonin	3.4 ± 0.3	160	541 ± 65	7.1 ± 0.4
	5.0 ± 0.3	81	170 ± 32	4.8 ± 0.3
SDS	4.8 ± 0.3	94	900 ± 84	5.1 ± 0.2
	6.5 ± 0.4	37	357 ± 51	3.7 ± 0.2
Thesit	4.8 ± 0.3	90	400 ± 67	5.0 ± 0.2
	6.9 ± 0.4	31	136 ± 22	3.1 ± 0.2
Triton X-100	5.1 ± 0.4	77	315 ± 53	4.7 ± 0.2
	7.7 ± 0.4	22	92 ± 19	3.5 ± 0.3
Tween 80	5.0 ± 0.4	82	160 ± 41	4.8 ± 0.4
	4.3 ± 0.3	128	250 ± 68	5.6 ± 0.5

It should be noted that in our calculations the aggregates are assumed to have a spherical shape, which may be not accurate for all detergents. On the other hand, our aim is to compare the overall and internal dynamics of a series of micelles and the spherical shape as a first-order parameter approximation is therefore justified.

Dynamic light scattering

Additional dynamic light scattering experiments (DLS) were performed to verify if the difference between the experimental data and literature was caused by the incorporation of the relatively large probe molecules or possibly an artefact introduced in our experimental set-up. Table 3.2 summarizes the diffusion coefficients for unlabeled micelles, as determined with DLS. All coefficients correspond well to the ones calculated from literature. Addition of the fluorescent probe molecules to the micelles, in a ratio of approximately one fluorophore per micelle, resulted in a significant decrease of the diffusion coefficient.

Table 3.2: Diffusion constants ($\times 10^{11} \text{ m}^2 \cdot \text{s}^{-1}$) from micellar systems with or without BODIPY-DHPE (first entry) or BODIPY-HPC (second entry) as monitored with dynamic light scattering and fluorescence correlation spectroscopy. Literature values were calculated from available micellar radii or aggregation numbers assuming spherical shaped micelles with a density of $1.05 \text{ g} \cdot \text{cm}^{-3}$. Standard errors are based on multiple measurements ($n=15$).

	without fluorescent probe		with fluorescent probe	
	literature	DLS	DLS	FCS
CTAB	8.0	7.3 ± 0.4	5.2 ± 0.5 6.4 ± 0.4	5.3 ± 0.3 6.6 ± 0.3
Deoxycholate	21	--	-- --	9.7 ± 0.7 11 ± 1
Digitonin	4.2	4.3 ± 0.2	3.8 ± 0.5 5.6 ± 0.8	3.4 ± 0.3 5.0 ± 0.3
SDS	11	10.2 ± 0.4	4.9 ± 0.3 7.0 ± 0.5	4.8 ± 0.3 6.5 ± 0.4
Thesit	4.0	4.5 ± 0.3	4.6 ± 0.3 5.8 ± 0.6	4.8 ± 0.3 6.9 ± 0.4
Triton X-100	4.8	4.4 ± 0.3	5.0 ± 0.6 5.8 ± 0.8	5.1 ± 0.4 7.7 ± 0.4
Tween 80	4.2	4.5 ± 0.3	5.5 ± 0.5 3.9 ± 0.4	5.0 ± 0.4 4.3 ± 0.3

The diffusion coefficients of the loaded micelles, determined by DLS, were similar to the values obtained from FCS experiments. As have been noted above, the labeling position of the BODIPY group in the phospholipid molecule strongly affects the micellar characteristics: Thesit and Triton X-100 micelles loaded with the tail-labeled probe, BODIPY-HPC, moved faster through the detection volume than the micelles loaded with the head-labeled BODIPY-DHPE, as can also be seen from the diffusion constants presented in table 3.1. Except for Tween 80, the translational diffusion constants of BODIPY-DHPE-loaded micelles are roughly 30% smaller than those of the BODIPY-HPC-loaded aggregates. These differences are most likely caused by the different locations of the fluorescent groups: The BODIPY group of BODIPY-HPC is coupled to one of the hydrophobic acyl chains of the phospholipid and will therefore be located in the micellar core between the hydrophobic chains of the detergent molecules. In contrast, the large fluorescent headgroup of BODIPY-DHPE is expected to be positioned near the micellar interface, because the negatively charged phosphate group will prevent the fluorescent moiety to get solubilized in the hydrophobic

micellar core. BODIPY-DHPE will presumably require some more detergent molecules to 'solubilize' the BODIPY group, which is reflected in the larger aggregation number compared to BODIPY-HPC-loaded micelles. The hydrodynamic radii of the BODIPY-DHPE-loaded micelles are 1.1 to 1.6 times larger than those of the BODIPY-HPC-loaded micelles.

Both apparent anomalies, namely the larger micellar sizes of phospholipid-filled micelles as compared to non-filled ones and the size differences connected with the selected fluorescent probe lipid, are consequences of the fact that the dimensions of the fluorescent phospholipids are of non-negligible magnitude as compared to micellar dimensions. To prove this point we have carried out size determinations of single unilamellar vesicles (SUVs) of DOPC, which are much larger than the micelles used in this study and which are separately loaded with both fluorescent lipid probes. The hydrodynamic radii of BODIPY-HPC-loaded vesicles (36 ± 10 nm) and BODIPY-DHPE-loaded vesicles (38 ± 12 nm) were exactly the same within experimental error.

Time-resolved fluorescence and fluorescence anisotropy

Time-resolved fluorescence experiments revealed that the fluorescence intensity decayed in a non-exponential fashion. When the fluorescence decay was analysed in distributed fluorescence lifetimes, using the MEM approach, four peaks were observed at 0.054, 0.35, 2.5 and 5.6 ns. The lifetime distribution patterns for both types of fluorescent probe were similar and independent of the type of detergent (data not shown). This indicates that the depopulation mechanism of the excited state is independent of the local environment. These observations are supported by experiments (Haugland, 1996), which showed the low sensitivity of the BODIPY fluorescence quantum yield for the environment. The fluorescence lifetime distributions were also insensitive to a tenfold increase or decrease of the dye concentration. Hence the effect of excitation energy transfer between fluorescent probe molecules can be neglected, as was expected at the probe concentrations used. In figure 3.3 the fluorescence anisotropy decay curves for digitonin and Thesit micelles are presented. Both micelles were loaded with either BODIPY-HPC or BODIPY-DHPE. The smooth curves through the data points represent the optimised fits according to the modified r_{g3} model (Eq. 3.2) with the assumption that the orientation distribution of the fluorescent probe is Gaussian shaped around the micellar radius with angular width θ_g . It can be seen that the decay curve for the Thesit micelles loaded with BODIPY-DHPE (Fig. 3.3A) is similar to the curve for BODIPY-HPC-loaded Thesit micelles (Fig. 3.3B). However, the anisotropy decay of BODIPY-DHPE-loaded digitonin is considerably slower than for Thesit micelles and even much slower for digitonin micelles loaded with BODIPY-HPC. The dotted line in panel B represents a simulated curve for the case that only the rotational motion of the whole micelle ($\phi_R = 81$ ns) contributes to the anisotropy decay.

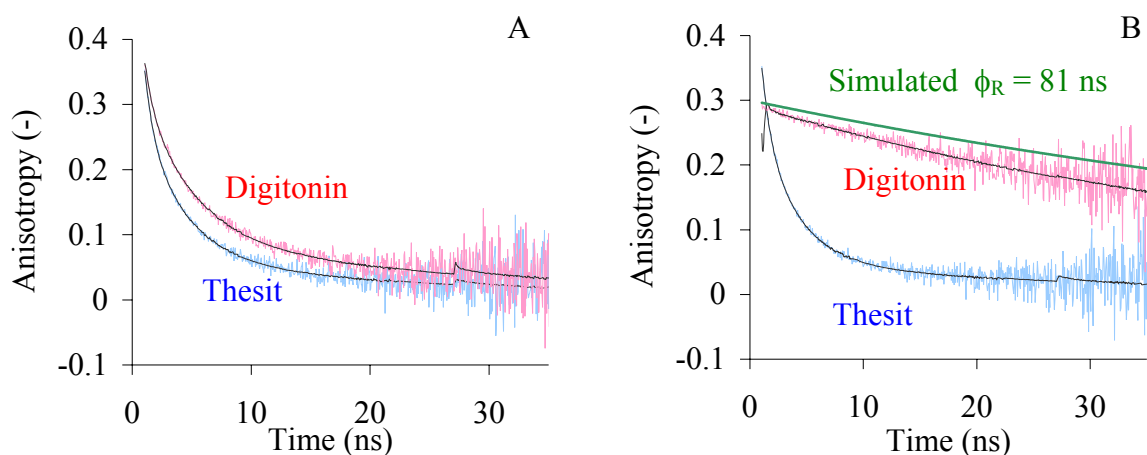


Figure 3.3: Experimental fluorescence anisotropy decay curves of digitonin and Thesit micelles loaded with BODIPY-DHPE (A) or BODIPY-HPC (B). The solid, smooth curve corresponds to the optimal fit with the r_{g3} modified model assuming a Gaussian orientation distribution. Also included in panel B is a simulated anisotropy decay curve (dashed) assuming that only micellar rotation ($\phi_R = 81$ ns) contributes to the anisotropy decay.

The experimental data for BODIPY-HPC loaded digitonin follows this simulated curve quite close, indicating that the contribution of other depolarisation processes is small. As will be discussed later, the molecular structure of the detergent molecules seems to have a strong effect on the motional freedom of the probes in the micelles. In table 3.3 all the recovered anisotropy parameters, as determined with the modified r_{g3} fit-model, are presented. The fundamental anisotropy was determined with MEM analysis and varied between 0.30 and 0.37, which is close to the maximum theoretical value of 0.4 for the case that the absorption and emission moments are oriented parallel. Analysis of the anisotropy decay data revealed that in most cases the contribution of the intramicellar, lateral diffusion of the probe was approximately five times larger than the contribution of the micellar rotation (data not shown). Hence, the uncertainty in the rotational correlation time ϕ_R is large. Therefore this value was calculated using the parameters obtained by FCS experiments and fixed in the TRFA-analysis. However, for digitonin and deoxycholate the contribution of the lateral diffusion was found to be much smaller ($\sim 8\%$). Analysis according to the modified r_{g3} fit-model showed that the uncertainty of the lateral correlation times in both detergents was large and even negative values showed up in the error of the analysis (Table 3.3). The lateral diffusion constants are small, indicating a severe restriction of the lateral movement. Since in these micelles the lateral and rotational diffusion processes occur in the same order of time and therefore these motions are not uncoupled, the modified r_{g3} model should not be applied to fit these experimental data.

Table 3.3: Anisotropy decay parameters obtained from the global analysis of micelles loaded with 100 nM BODIPY-DHPE (first entry) or BODIPY-HPC (second entry). The fundamental anisotropy, r_0 , was obtained from MEM analysis. The lateral diffusion constant D_L was calculated according to equation 3.5, assuming the position of the fluorescent group for BODIPY-DHPE and BODIPY-HPC at 0 and 1 nm, respectively under the micellar surface. The numbers between parentheses correspond to the errors as determined from a rigorous error analysis at a 67% confidence level, as described by Pap et al., 1996). χ^2 indicates the quality of the fit.

Micelle	ϕ_L [ns]	D_L [m^2s^{-1}]	D_{\perp} [μs^{-1}]	θ_g [rad]	r_0	P2	P4	χ^2
CTAB	20 (15-31)	$1.1 \cdot 10^{-10}$	53.6 (51.8-56.6)	0.59 (0.58-0.65)	0.33	0.60	0.18	1.27
	17 (12-28)	$2.5 \cdot 10^{-10}$	63.9 (61.8-66.7)	0.66 (0.60-0.73)	0.33	0.53	0.12	1.25
Deoxycholate	21 (13-73)	$1.2 \cdot 10^{-11}$	31.2 (27.0-33.7)	0.74 (0.54-0.83)	0.36	0.46	0.07	1.25
	29 (-18-85)	$7.4 \cdot 10^{-11}$	28.9 (23.4-32.8)	0.73 (0.49-0.83)	0.37	0.46	0.07	1.25
Digitonin	79 (69-105)	$4.4 \cdot 10^{-11}$	30.1 (1.0-384)	0.99 (0.94-0.99)	0.31	0.88	0.84	1.23
	154 (-80-230)	$1.6 \cdot 10^{-10}$	32.0 (3.0-500)	0.99 (0.97-0.99)	0.30	0.99	0.95	1.39
SDS	14 (8-27)	$4.9 \cdot 10^{-11}$	80.7 (78.5-85.6)	0.71 (0.63-0.81)	0.32	0.48	0.09	1.39
	14 (9-21)	$4.6 \cdot 10^{-10}$	89.4 (86.3-94.1)	0.79 (0.72-0.83)	0.32	0.40	0.05	1.35
Thesit	25 (14-37)	$5.1 \cdot 10^{-11}$	50.7 (48.6-54.2)	0.57 (0.52-0.65)	0.34	0.62	0.20	1.30
	22 (15-27)	$2.2 \cdot 10^{-10}$	57.3 (56.6-59.2)	0.65 (0.59-0.72)	0.34	0.55	0.13	1.25
Triton X-100	32 (22-47)	$8.2 \cdot 10^{-11}$	21.5 (20.6-23.6)	0.42 (0.35-0.51)	0.36	0.77	0.43	1.27
	19 (15-32)	$1.7 \cdot 10^{-10}$	21.4 (21.5-23.1)	0.43 (0.37-0.56)	0.36	0.76	0.39	1.17
Tween 80	21 (17-32)	$2.5 \cdot 10^{-10}$	31.6 (30.0-34.1)	0.49 (0.43-0.56)	0.34	0.70	0.30	1.32
	21 (15-33)	$2.7 \cdot 10^{-10}$	32.9 (32.2-35.0)	0.53 (0.46-0.61)	0.35	0.66	0.26	1.27

The angular range (θ_g) over which the probes are moving varies between 0.4 and 0.8 rad with relatively high uncertainties. Since the errors of θ_g at a 67% confidence level are within the error of the experiment, no differences are seen between the two different probes in micelles of deoxycholate, Triton X-100 and Tween 80. However, the tail-labeled probe in CTAB, digitonin, SDS and Thesit micelles possesses a significantly larger angle (around the micellar radius) than the head-labeled probe. Although the fluorescent BODIPY group is large, containing several aromatic rings, it seems that in the micellar core the probe can move more freely than near the micellar surface. This agrees with the thermodynamic theory (Benjamin, 1966) and spectroscopic experiments (Wagoner et al., 1967; Rosenholm et al., 1978) that showed that the core of micelles and the interior of lipid bilayers above the phase transition temperature behave as an organic fluid.

The local order around the phospholipid probe is described by the second-rank and fourth-rank order parameters $\langle P_2 \rangle$ and $\langle P_4 \rangle$ (Szabo, 1984; van der Meer et al., 1984; Pap et

al., 1996). These values are very high for the digitonin micelles, indicating a highly ordered local environment as was expected on the basis of the detergent structure discussed above. Although similar results were expected for deoxycholate, the local order seems to be lower than in the other micelles. Comparison of the local order between the two fluorescent probes showed that the order around the head-labeled probe is higher, again consistent with the model which describes the micellar core as a liquid hydrocarbon experiencing a relatively lower order than the interfacial environment around the ionic headgroup probe.

The wobbling diffusion constants D_{\perp} , representing the internal rotation of the probe, are listed in table 3.3. The wobbling motion of the probes in the negatively charged SDS micelles is significantly faster than in the positively charged CTAB micelles. It seems that the electrostatic repulsion between the negatively charged phosphate group of the fluorescent probe and the SDS detergent molecules will increase the distance between the headgroups, thereby creating space for less restricted wobbling motion. The wobbling motion in the non-ionic micelles is relatively slow compared to the two charged detergents. Quitevis *et al.* (1993) found similar results for the charged M540 probe in micelles made from various detergents. The latter authors proposed that in non-ionic micelles the charged headgroup of the fluorescent probe protrudes out of the micelle into the water region. Due to stronger interactions between the water molecules and the phosphate group, the fluorescent probe will be more motionally restricted. Large sized molecules are expected to be packed more densely, resulting in a lower wobbling rate. However, in our experiments no correlation between the micellar radius and the wobbling constant was found. The wobbling motion of the tail-labeled BODIPY-HPC is slightly faster than for BODIPY-DHPE. Probably the internal motion in the micellar core is less restricted than near the micellar interface. The rates are similar to the ones found for BODIPY-HPC and diphenylhexatriene-PC (DPH-PC) in DOPC vesicles (Hink and Visser, 1998; Pap et al., 1996) but are almost ten times smaller than the wobbling rates of the single chained M540 and octadecyl Rhodamine B in micelles (Quitevis et al., 1993) or porphyrins in micelles (Maiti et al., 1995).

These observations strongly suggest that the incorporation of a relatively large fluorescent phospholipid molecule perturbs the micellar structure: extra detergent molecules are required to 'solubilise' the fluorescent group, resulting in an increase of the hydrodynamic radius and aggregation number. The main conclusion from both FCS and DLS experiments is therefore that the probe has a significant effect on the self-assembly of the surfactant molecules resulting in distinctly larger particles. The restriction of the lateral motion of deoxycholate and digitonin can be explained by their molecular structures. Both detergent molecules are flat and rigid, consisting of several fused cyclic carbon rings. In contrast to the other detergents, deoxycholate and digitonin seems to be able to form rigid, cage-like structures in the micellar core which tightly accomodates the fluorophore. In this way the lateral mobility of the fluorescent probe is strongly limited.

The intramolecular lateral diffusion constants were calculated using equation 3.4 with the assumption that the fluorescent group of BODIPY-HPC is located 1 nm under the micellar surface and at the micellar interface for BODIPY-DHPE. The lateral diffusion constants for the head-labeled phospholipid are in the order of $10^{-10} \text{ m}^2\cdot\text{s}^{-1}$, and except for Tween 80, almost five times lower than for the tail-labeled probe. The intramolecular diffusion is in the same order as the lateral diffusion of BODIPY-HPC in vesicles (Hink and Visser, 1998) but much faster than rhodamine-labeled dipalmitoylphosphatidylethanolamine (DPPE-Rh) and N-4-nitrobenzo-2-oxa-1,3-diazolelaurate (NBD-C12) in black lipid membranes (BLM) (Fahey et al., 1977 & 1978). In BLM's the diffusion constants were in the order of $10^{-11} \text{ m}^2\cdot\text{s}^{-1}$ while whole vesicles have a $D_{\text{tran}} \approx 10^{-12} \text{ m}^2\cdot\text{s}^{-1}$. These observations can be explained by differences in packing, which is less tight in the curved micelles than in the lipid bilayers. In models for lateral diffusion, molecules move by exchanging positions or by migrating through gaps or interstitial sites in the membrane. Based on these jump-models the lateral diffusion will be faster when the surfactant molecules are more loosely packed.

Conclusion

Combination of fluorescence correlation spectroscopy and time-resolved fluorescence anisotropy provides detailed information on the dynamics of phospholipid probes in micelles, although the relatively large size of the fluorescent probes caused a disturbance of the relatively small micellar structures as has been confirmed by dynamic light scattering experiments. The relative size differences of the micelles and the motional properties of the fluorescent probes correspond well with literature values. Moreover, the experiments described in this chapter demonstrate the high concentration sensitivity of FCS compared to DLS. Additionally, FCS can retrieve information on molecular systems that is complementary to TRFA data due to the difference in temporal resolution. The time-window for TRFA is limited to the fluorescence lifetime of the dye (typically ps-ns), where FCS resolves processes ranging from the microsecond to seconds range.

Material and Methods

Probes and micelles

The fluorescent probes β -BODIPY₅₃₀₋₅₅₀-C5-HPC (2-(4,4-difluoro-5,7-diphenyl-4-bora-3a,4a-diaza-s-indacene-3-pentanoyl)-1-hexadecanoyl-*sn*-glycero-3-phosphocholine) and BODIPY₅₃₀₋₅₅₀-DHPE (N-(4,4-difluoro-5,7-diphenyl-4-bora-3a,4a-diaza-s-indacene-3-propionyl)-1,2-dihexadecanoyl-*sn*-glycero-3-phosphoethanolamine, triethylammonium salt) (Molecular Probes, The Netherlands) were dissolved in ethanol and stored at -20°C .

The detergents were dissolved in PBS (8.8 g.L⁻¹ NaCl, 0.2 g.L⁻¹ KCl, 1.45 g.L⁻¹ Na₂HPO₄·2H₂O and 0.5 g.L⁻¹ KH₂PO₄ in nanopure water): 5 mM CTAB (cetyltrimethylammonium bromide) (Serva, The Netherlands), 5 mM digitonin (Sigma, The Netherlands), 5 mM deoxycholate (Sigma, The Netherlands), 10 mM SDS (sodium dodecyl sulfate) (BDH, The Netherlands), 1 mM Triton X-100 (Merck, Germany), 1 mM Thesit (polyoxyethylene-9-lauryl ether) (Sigma, The Netherlands) and 1 mM Tween 80 (polyoxyethylene sorbitan mono-oleate) (Merck, Germany). All solutions were set at pH 7.0 using 1 M HCl, except for digitonin which was dissolved at pH 8.3. Subsequently, the fluorescent probe was added (maximal 3 volume %) to a concentration of 10 nM in FCS experiments and 100 nM in fluorescence anisotropy experiments. Under these conditions, the probability of having more than one dye molecule per micelle is smaller than 10⁻³. The samples were bath-sonified for 1 minute to guarantee that the probe is equally distributed among the available micelles and incubated for at least 10 minutes in the dark at 293 K before measurement.

Fluorescence correlation spectroscopy

FCS measurements were performed with a ConfoCor microscope (Carl Zeiss and Evotec, Germany) that has been described in detail in Chapter 1. The samples were excited by the 514 nm line from the air-cooled Argon ion laser which was filtered by a 515 ± 15 nm interference filter (Omega, USA) and reflected by a 515 dichroic filter (Omega, USA). The laser power was set with neutral density filters to less than 100 µW. The emission light was filtered using a 530-610 nm band-pass filter (Omega, USA) and passed the motor-controlled pinhole set at a diameter of 40 µm. The samples were measured during 20 seconds at 293 K. The number of detergent molecules in the micelle, *S*, can be estimated by equation 3.4 via Eq. 1.9 and Eq. 1.15 assuming a spherical shape of the micelle:

$$S = \frac{4\pi r_h \rho N_a}{3M} \quad (\text{Eq. 3.4})$$

with ρ the mean density of the micelle, N_a Avogadro's number and M the molecular mass of a single detergent molecule. It should be noted that equation 3.4 is a first-order approximation and that more elaborate equations should be used for other shapes.

Dynamic light scattering

Dynamic light scattering (DLS) measurements were carried out by an experimental set-up composed of a Lixel 150 mW multiline argon ion laser operating at 488 nm, a photomultiplier and a personal computer containing an ALV-5000 correlator card. Samples consisted of 50 mM detergent in PBS with 0, 0.1, 0.5 or 5 mM of the fluorescent phospholipids. To exclude the fluorescence photons originating from the probe molecules, a

475 \pm 15 nm bandpass filter (Omega, USA) was placed in front of the photomultiplier. Scattered intensities were recorded at a 90° scattering angle (θ) for 15 seconds per experiment, at 295 K. The diffusion constant D was obtained by fitting the experimental correlation curves, $g^{(1)}(\tau)$, according to:

$$g^{(1)}(\tau) = e^{-Dq^2\tau} \text{ with } q = (4\pi n_0/\lambda_{\text{ex}}) \sin(\theta/2) \quad (\text{Eq. 3.5})$$

with n_0 the refractive index of the sample, λ_{ex} the excitation wavelength and θ the scattering angle (Pecora, 1985).

Time-resolved fluorescence anisotropy

Time-resolved fluorescence anisotropy experiments were performed using the time-correlated single photon counting (TCSPC) technique (O'Connor et al., 1984). For excitation a synchronously pumped dye laser with laser dye Coumarine 460 was used (van Hoek et al., 1992). The pump laser is a 353 nm cw mode-locked Nd:YLF laser (Coherent model Antares 76-YLF with model 7600 mode locker). An electro-optic modulator set-up in a dual-pass configuration was used to reduce the frequency of the light pulses from 76 MHz to 594.5 kHz. In order to prevent pile-up distortion, the energy of the excitation pulses was reduced by a variable density filter such that a maximum photon frequency of 30 kHz ($\approx 5\%$ of 594 kHz) was obtained (Vos et al., 1987). Excitation pulses ($\lambda_{\text{ex}} = 512$ nm) were less than 4 ps full width at half maximum with energies up to 2.6 nanojoule. Quartz cuvettes (1 cm path length in excitation, 1 cm³ in volume) were placed in a thermostated holder (293 K). Fluorescence light was detected at an angle of 90° relative to the laser beam and passed through a combination of an OG 530 nm cut-off filter and a Balzers 550 band-pass filter ($\Delta\lambda = 12$ nm). All measurements consisted of a number of sequences of measuring 10 seconds parallel ($I_{\parallel}(t)$) and 10 seconds perpendicular ($I_{\perp}(t)$) polarized emission. 1024 channels were used per experimental decay with a time spacing of 50 ps per channel. The reference compound erythrosine B in nanopure water (with a known single lifetime of 80 picoseconds) served as reference compound to yield the dynamical instrumental response curve (Visser et al., 1998).

The fluorescence anisotropy decay curves were analysed with a global analysis program, obtained from Globals Unlimited Inc. (USA) (Beechem et al., 1991) and adapted using equation 2.2 as model function. The correlation times of the overall rotation of the micelles (ϕ_R), were calculated from the data obtained from FCS experiments, and the fundamental anisotropy (r_0) was obtained from data-analysis with the Maximum Entropy Method (MEM) (Brochon, 1994). The MEM software was obtained from Maximum Entropy Data Consultants Ltd. (UK).

Acknowledgments

We are grateful to Eward Pap (Avensis Hoechst, Germany) and Frank Vergeldt (Laboratory of Biophysics, Wageningen University, The Netherlands) for assistance in the fluorescence anisotropy decay analysis and Remko Fokkink and Martien Cohen Stuart (Laboratory for Physical Chemistry and Colloid Science, Wageningen University, The Netherlands) for generous access to the dynamic light scattering experiments. Peter Bremer and Reinhard Janka from Carl Zeiss, Inc., Jena, Germany are gratefully acknowledged for technical and financial support. This research was supported by an investment grant from The Netherlands Organization for Scientific Research (NWO) and by a grant from the Earth and Life Sciences Foundation of NWO (ALW-NWO).

4

Fluorescence Correlation Microscopy in Living Plant Cells

Mark A. Hink and Antonie J.W.G. Visser

Fluorescence correlation microscopy (FCM) is an attractive technique to monitor dynamical processes of single molecules in living cells. However, processes like cellular autofluorescence, light scattering and dye depletion can severely interfere with the intracellular measurements. In this chapter these potential artefacts are discussed and illustrated by FCM measurements in living plant cells. As an example the mobility of microinjected fluorophores and fluorescently labeled lipids has been studied in tobacco suspension cells and cowpea protoplasts. Cytoplasmic diffusion of rhodamine green and tetramethyl-rhodamine were restricted and indicate non-specific interaction of these dyes with subcellular structures. The diffusion of all fluorophores was restricted in cowpea protoplasts but not in tobacco cells. A model of two-dimensional Brownian motion with a single component could not describe the diffusion rate of the fluorescent lipids in the plasma membrane of tobacco suspension cells. Comparison with the results of an experimental model system, consisting of labeled giant unilamellar vesicles, suggests that the probes are diffusing anomalously or are localized in microdomains.

Introduction

Fluorescence correlation spectroscopy (FCS) is capable of studying dynamic processes of single, fluorescently marked molecules under equilibrium conditions. Using FCS the intensity fluctuations of the fluorescence observed in a small open confocal volume element are analysed. Dynamic processes which are accompanied by a temporal change of the fluorescence intensity can be studied: examples are translational diffusion of molecules moving through the observation volume, chemical reaction kinetics such as arising from association-dissociation of a biomolecular complex, conformational transitions in macromolecules or photophysical processes as the intersystem crossing to the (dark) triplet state. Fast correlation of the intensity fluctuations is used to evaluate the particle number (concentration), reaction dynamics and diffusion rates of molecules. FCS has been applied to a wide range of *in vitro* systems and the high sensitivity and selectivity render it a highly attractive technique for acquiring information in living cells as well. Moreover the confocal detection principle, introduced in FCS to reduce background fluorescence, also allows acquiring data at high spatial resolution, thus making it possible to distinguish the dynamics of fluorescent molecules in different subcellular compartments. Hence, fluorescence correlation microscopy (FCM), an extension of FCS optimised for live cell studies, has been proposed (Brock et al., 1998). The first publications concerning FCS in living cells (Berland et al., 1995; Brock et al., 1998) reported on the mobility of microinjected fluorospheres. Although these studies did not include experiments on true biomolecules it clearly demonstrated the high potential for intracellular FCM measurements. However, it has not been until recently that an increasing number of intracellular applications were reported (for a review, see Schwille, 2001a). Applications have been described on the binding of proinsulin C-peptide (Rigler et al., 1999; Henriksson et al., 2001), galanin (Pramanik et al., 1999) and kavain derivatives (Boonen et al., 2000) to the cell membrane of living cells. Koopman et al. (1999) measured the diffusion rate of fluorescent probes applied to monitor Ca^{2+} waves in *Xenopus* melanotropes upon stimulation. Goedhart et al. (1999, 2000) studied the binding and mobility of various Nod-factors to plant root hairs. The mobility of free enhanced GFP (EGFP) and its fusion protein to the EGF receptor, targeted to several cellular compartments has been studied by Brock et al. (2000) and Nomura et al. (2001). Harms et al. (2001a,b) studied the photophysical characteristics of membrane targeted EYFP and the aggregation of EYFP-fused Ca^{2+} channels in HEK293 cells. Studies on the cellular uptake of cell permeable peptides (Waizenegger et al., 2002) and microparticles (Yoshinda et al., 2001) open ways to investigate and optimise drug-delivery systems. Cluzel et al. (2000) related the concentration of a phosphorylated signalling protein, CheY-P, to the flagella motion in single bacteria. Politz et al. (1998) examined the mobility of oligo(dT) and oligo(dA) in the nucleus of rat myoblasts to monitor intranuclear hybridisation. FCM allows distinguishing between different kinds of movement: active transport, 3D diffusion or restricted anomalous diffusion as has been shown for EGFP in plastid tubules of tobacco plant cells (Köhler et al., 2000), for EGFP

in the nucleus of T1 and COS7 cells (Wachsmuth et al., 2000) and diI-C12 lipid molecules in the membrane of RBL cells (Schwille et al., 1999a). It has been demonstrated that two-photon excitation can significantly improve the signal quality in turbid samples like plant cells or deep cell layers (Schwille et al., 1999b).

Experimental Considerations for Intracellular FCS

Notwithstanding its attractiveness, cellular applications of FCS may suffer from artefacts like cellular autofluorescence, light absorption and scattering, cell damage and dye depletion due to photobleaching.

Autofluorescence

One of the most perturbing factors for single-molecule experiments such as FCS, is the presence of autofluorescent molecules. Endogenous molecules like NAD(P)H, flavins and flavoproteins fluoresce strongly in the blue and green spectral regions. In most animal cell types, the autofluorescence intensity decreases above 550 nm and the use of red-shifted fluorophores will therefore result in a reduced contribution of the background fluorescence to the autocorrelation curves. In plant cells, however, chlorophyll may be present which absorbs in a broad spectral range (400-550 nm) and fluoresces strongly above 610 nm. Hence, the optimal emission wavelengths for fluorescent probes used in plant cell studies lie between 550 and 610 nm. In addition, differences between subcellular locations, the metabolic state of a cell and the excitation intensity can strongly influence the brightness of the autofluorescent molecules (Brock et al., 1998).

Autofluorescence can contribute to the correlation curves in two different ways: First, a steady background arising from solvent and immobile fluorescent molecules will be present as a constant, non-correlating species, lowering the amplitude of the correlation curve according to:

$$G_{\text{cor}}(\tau) = G(\tau) \cdot \left(1 - \frac{F_{\text{background}}}{F_{\text{total}}} \right)^2 \quad (\text{Eq. 4.1})$$

where F_{total} is the total fluorescence intensity, including the signal from the uncorrelated background, $F_{\text{background}}$. Secondly, free autofluorescent molecules appear in the correlation curve as an additional, correlating component. In the latter case the molar fraction and relative molecular brightness of the autofluorescent molecules determine its relative contribution (Eq. 1.14). Moreover, even in the absence of autofluorescent molecules one has to consider the absorption of the fluorescence light by endogenous molecules, which may significantly reduce the signal to noise ratio (SNR). Methods to reduce the cellular background is the usage of total-internal reflection (TIR) excitation which significantly reduces the excitation volume

but has only a limited working distance (Starr and Thompson, 2001). In case of autofluorescent molecules with a significantly shorter fluorescence lifetime than that of the probe, a pulsed laser system combined with time-gated detection can reduce the background (Lamb et al., 2000). A third possibility is to treat the cells with a short intense laser pulse before the actual experiment starts, thereby photobleaching the autofluorescent molecules in a selected region. In case of spot-bleaching mobile molecules will diffuse from the surrounding area into the bleached region thereby replacing the destructed fluorophores causing a recovery of the observed fluorescence intensity. The immobile molecules are not replaced thus recovery may be not complete. The rate of ingrowth of the fluorescence intensity contains information about the mobility of the molecules and the fraction of immobile molecules. This principle is exploited by fluorescence recovery after photobleaching (FRAP) (Axelrod et al., 1976; Petersen and Elson, 1986) to retrieve diffusion coefficients of fluorescent molecules. However, the destructive nature of this technique, using an intense light pulse may induce non-relevant physiological reactions in the cell or even cell death.

Fluorescent molecules

Studying molecules with FCM requires that the molecule of interest is fluorescent. The intrinsic fluorescence of most biological abundant fluorophores like flavins, flavoproteins, nucleotides or tryptophan residues usually is not very strong. Although it is possible to study biological fluorophores by FCS (Visser et al., 2001; van den Berg et al., 2001; Wennmalm et al., 2001) the low molecular brightness, high photobleaching rate and high background at near-UV excitation wavelengths result in a low SNR that makes the use of such fluorophores in intracellular FCM measurements extremely difficult. Moreover, due to the high number of endogenous fluorophores it is not possible to selectively monitor or control a subset of molecules. Therefore some type of external label must be used. Nowadays a whole range of highly fluorescent molecules for intracellular research has become available which allow to specifically visualize subcellular compartments (nucleus, mitochondria, endoplasmatic reticulum etc.), monitor ion concentrations (e.g. pH, Ca^{2+} , etc.) or specifically label biomolecules, e.g. DNASTains, FLASH probes (Griffin et al., 1998). To fluorescently tag a specific molecule of interest one can covalently link a fluorophore via organic synthesis, like esterification to reactive amino and thiol groups (Haugland, 1996). During the last few years labeling strategies of proteins have been changed completely by the usage of fluorescent proteins (FP). The FP's are fused genetically to the protein of interest after which the fusion product is transfected and expressed inside the living cell. Nowadays a whole range of FP's with different spectral characteristics have become available with emission maxima ranging from the blue to the red (Clontech, 2002). Although the relatively large mass of the FP's (approx. 28 kDa) and the potential artifact of disturbing the physiological behaviour of the protein of interest in the fusion product, the FP's have the advantage of possessing a high

molecular brightness (Tsien, 1998), well protected fluorophore (Ormö et al., 1996; Wachter et al., 1998; Wall et al., 2000) and relative inertness to aspecific interactions with cellular structures (Dittrich et al., 2001). Therefore, FP's are excellent markers to visualize the behaviour of proteins. Moreover, the FP's are fused genetically to the protein of interest and after transfection the fusion product is expressed. This approach has the advantage that no labeling, purification and microinjection or electroporation is required. However, some FP's have complex photophysics and are sensitive to pH and the laser intensity (Haupts et al., 1998; Schwille et al., 2000, Heikal et al., 2000) that may complicate measurements at the single-molecule level.

The lower concentration limit of detectable probe is related not only to the probe concentration but scales to the squared value of the probe molecular brightness relative to background components (Eqs. 1.14 & 4.1). Hence, the fluorescent dye should possess a high molecular brightness. At concentrations below 10^{-9} M the average number of fluorescent molecules in the observation volume is smaller than 1 and longer measurement times are required to achieve a good SNR since one only monitors the background fluorescence in the time period between the arrival of subsequent molecules in the observation volume. Since fluctuation techniques analyse the relative fluorescence fluctuations an upper concentration exists above which the intensity fluctuations are too small compared to the average intensity (Eq. 1.6). Above this limit no information can be retrieved from fluctuation analysis since the high number of fluctuations tend to cancel out each other. As a result the normalized autocorrelation curve will be a straight line with an amplitude of one and the photon counting histogram approaches a Poisson distribution. In general, the number of fluorescent molecules in the observation volume should not exceed 100, corresponding to a concentration of ca. 1 μ M. Therefore, the cellular expression level of proteins fused to a FP should be controlled. A widely used promoter in plant research is the 35S-promoter which yields high levels of fluorescent protein that are useful for imaging or protein purification, but too high for fluctuation analysis. Therefore, proteins expressed under 35S can only be monitored during a limited time-window, relatively soon after transfection of the construct. An alternative possibility to manipulate the level of expressed protein is the use of inducible promoters like tetracycline or ethanol promoters or to photobleach a fraction of the proteins.

Photophysical effects resulting in a conversion of the fluorophore into a non-fluorescent or dim state can significantly reduce the SNR and may dominate the correlation curve, thereby masking other fluctuation processes like diffusion. A well known example is the intersystem crossing to the long-lived and "dark" triplet state (Widengren et al., 1995) but also photochemical reactions like cis-trans isomerisation as found for Cy5 and Merocyanine 540 (Widengren and Schwille, 2000; Widengren and Seidel, 2000) and chromophore protonation of fluorescein (Widengren et al., 1999) or FP's (Haupts et al., 1998; Schwille et al., 2000) can result in a significant fraction of fluorophores in a dark state.

Dye depletion

Since the subcellular compartments are rather small and the diffusion may be restricted, dye depletion due to photobleaching can create serious problems. Photobleaching, i.e. the irreversibly light-induced destruction of the fluorophore, takes place after the emission of approximately 100.000 photons (Eggeling et al., 1998). For *in vitro* systems the photobleached molecules will be replaced by fresh material diffusing from outside the confocal volume element. This is often not possible in living cells due to compartmentalisation of fluorescent molecules and therefore only a limited number of molecules are present. Photobleaching of the dye will give rise to artefacts in the correlation curves. Since the dye will be bleached during its passage through the detection volume, the apparent diffusion time will be too small (Widengren and Rigler, 1997). This problem is clearly present when particles with a small diffusion coefficient, due to their large size or environmental diffusion restrictions, are being monitored. The prolonged residence time in the excitation volume will result in a higher chance of being photobleached. Photodepletion itself is a correlated process giving rise to a contribution in the correlation curve. Moreover, the internal logic of an autocorrelator board may introduce staircase-like artefacts in the tail of the correlation curve.

Cellular damage, movement and light scattering

Intense light exposure can severely affect the physiological state of the cell resulting in cell damage, malfunctioning or stress reactions that may ultimately lead to cell death. To prevent these effects a careful selection of the optimal laser intensity and exposure time is required.

When intracellular dynamics are monitored over longer periods of time movement of intracellular structures or even the complete cell can occur, which may cause additional fluctuations in the correlation curve. Although a constant unidirectional movement with velocity v can be corrected for by a flow model

$$G(\tau) = 1 + \frac{1}{\langle N \rangle} \cdot \sum_j \frac{1}{\left(1 + \frac{\tau}{\tau_{\text{dif},j}}\right) \sqrt{1 + \left(\frac{\omega_{xy}}{\omega_z}\right)^2 \frac{\tau}{\tau_{\text{dif},j}}}} \cdot e^{\left(-\left(\frac{\tau \cdot v}{\omega_{xy}}\right) \cdot \frac{\tau}{\tau_{\text{dif},j}}\right)} \quad (\text{Eq. 4.2})$$

most cells or subcellular structures will move randomly therefore affecting the observed fluctuations in an uncontrolled way. To fix the living cells, the glass support can be coated with polylysine or the cells may be incubated with low melting point agarose.

Measurements in thick specimen or samples containing optically dense structures as organelles or plant cell walls are subject of low SNR due to scattering. Multiphoton excitation (Denk et al., 1990) can significantly improve these experiments (Williams et al., 1994). Moreover, the size of the excitation volume is, in contrast to one photon excitation, limited to

a small focal spot thereby significantly reducing the photobleaching of the dye above and below the focal plane (Schwille et al., 1999b). However, for many fluorophores two-photon excitation enhances the photobleaching rates, resulting in a reduced emission rate (Dittrich and Schwille, 2001).

Restricted diffusion

Due to compartmentilisation, inhomogeneous environments, interaction with subcellular structures, active transport, flow and obstruction by inert particles, the movement of the fluorescent molecules may be restricted and will not follow normal 3D Brownian motion. The autocorrelation curve of free moving fluorescent molecules diffusing along a planar surface (*i.e.* plasma membrane), which is oriented perpendicular to the optical axis is described by a 2-dimensional Brownian motion model:

$$G(\tau) = 1 + \frac{1}{N \cdot (1 + \tau/\tau_{\text{dif}})} \quad (\text{Eq. 4.3})$$

where N is the average number of fluorescent particles in the focal volume element and τ_{dif} represents the time for the particle to diffuse through the observation volume. In case of obstructed diffusion or anomalous (sub-)diffusion the time-dependence of the mean square displacement of the molecule is no longer linear, as for Brownian motion, but is confined leading to:

$$G(\tau) = 1 + \frac{1}{\langle N \rangle} \cdot \sum_j \frac{1}{\left(1 + \frac{\Gamma_j \tau^{\alpha_j}}{\omega_{xy}^2}\right)} \quad (\text{Eq. 4.4})$$

Here Γ represents the transport coefficient and α the temporal exponent that lies between 0 and 1. In case when the diffusion is described by $\alpha=1$ no sub-diffusion but Brownian diffusion takes place. For 3D anomalous diffusion we have:

$$G(\tau) = 1 + \frac{1}{\langle N \rangle} \cdot \sum_j \frac{1}{\left(1 + \frac{\Gamma_j \tau^{\alpha_j}}{\omega_{xy}^2}\right) \sqrt{1 + \left(\frac{\omega_{xy}}{\omega_z}\right)^2 \left(\frac{\Gamma_j \tau^{\alpha_j}}{\omega_{xy}^2}\right)}} \quad (\text{Eq. 4.5})$$

Gennerich and Schild (2000) derived modified FCS fitting models for experiments where the observed processes are restricted to small cellular compartments, which confine the effective observation volume. Standard FCS models will lead to erroneous results, since these

equations are based on the assumption that the boundaries of the observation volume are defined by confocal optics, rather than determined by cellular structures.

Signal to noise

FCM measurements in living cells will in general suffer from a significantly lower SNR compared to *in vitro* measurements. Since the SNR scales to the square root of the measurement time, T_m , (*i.e.* $T_m \gg$ delay time τ) (Kask et al., 1997), the quality of the acquired data can be improved by longer recording. However, as has been shown by Koppel (1974), the crucial parameter controlling the SNR is the molecular brightness η rather than the total fluorescence intensity. In order to acquire good-quality data the product $\eta \cdot \tau$ should be optimised. The maximal photon rate is found at the saturating intensity level. Increasing the excitation intensity further will lead to a reduced photon rate due to ground state depletion (Lakowicz, 1999). Considering all the effects discussed in previous sections it is clear that η may be enhanced by increasing the intensity of the excitation source but not to an unlimitedly high level. Therefore, the optimal setting will be a compromise between high molecular brightness of the dye and a low contribution of processes like photobleaching, cellular damage and autofluorescence.

FCM in plant cells

So far, most FCS studies have been performed *in vitro* but in recent years the number of applications of this technique inside living cells has grown significantly, leading to the first publications describing FCM experiments in plant cells (Schwille *et al.* 1999b; Köhler et al., 1999; Goedhart *et al.*, 2000; Goedhart *et al.*, 2001). To further study the potential of FCM in living plant cells, experiments have been carried out in two plant model systems: cowpea protoplasts and tobacco bright yellow suspension cells (BY2). Firstly, the autofluorescence of both lines has been characterized after which the diffusion behaviour of fluorescent lipid molecules and cytoplasmic fluorophores were studied.

Results and Discussion

Autofluorescence

Protoplasts isolated from cowpea leaves and suspension cells from tobacco (BY2) are widely used as model systems to study proteins *in planta*. The whole cell absorption spectra, displayed in figure 4.1A, shows a broad band ranging from 450-550 nm for the BY2 cells and continuing up to 600 nm for cowpea protoplasts. The latter contribution to the absorption spectrum is due to the presence of chloroplasts containing the autofluorescent chlorophyll. Tobacco BY2 suspension cells lack chloroplasts since they have been grown under dark conditions.

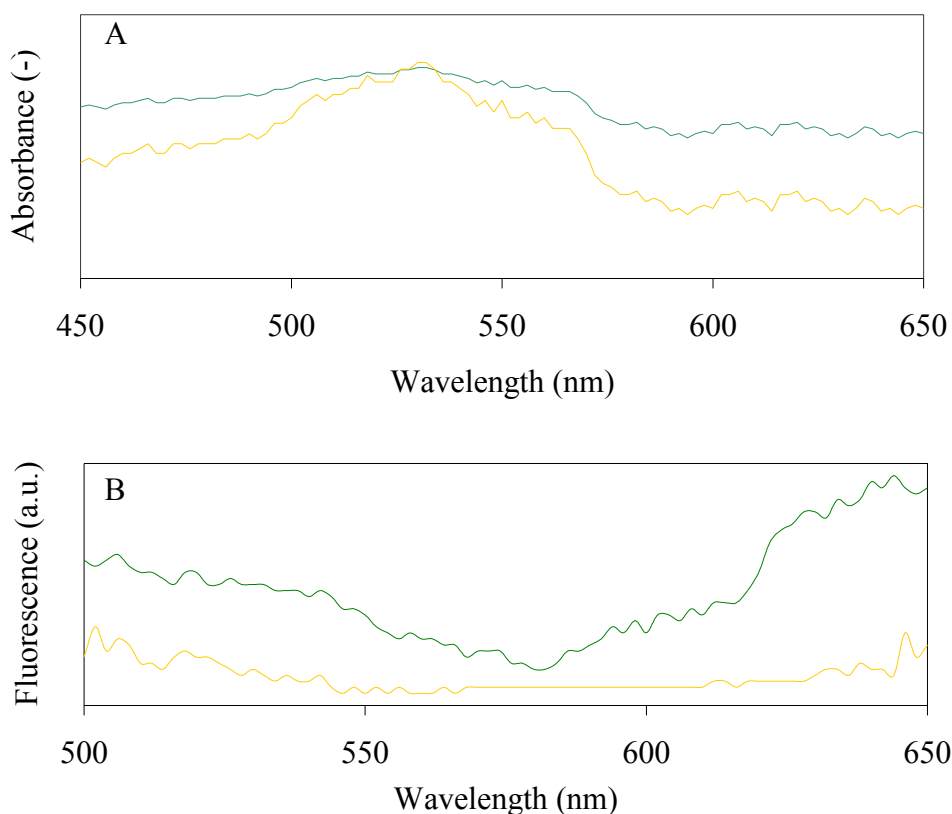


Figure 4.1: Autofluorescence characteristics of BY2 suspension cells (yellow) and cowpea protoplasts (green). (A) Whole cell absorbance spectra. (B) Emission spectra, using the Argon ion laser line of 488 nm for excitation.

Fluorescence spectral imaging microscopy (FSPIM) can be used to acquire a complete emission spectrum along a line in a microscopic object (Balaban et al., 1986) and thus allows yielding emission spectra of autofluorescent molecules inside (parts of) a living cell (Martínez-Zaguilán et al., 1994). The emission spectra for both plant cell types, presented in figure 4.1B, were acquired at an excitation wavelength of 488 nm. The autofluorescence spectra show broad-banded emission peaks without any fine structure. The autofluorescence intensity decreases going towards 600 nm, as is also shown by the FCM intensity traces at various excitation wavelengths. The molecular brightness, obtained by analysis of the autocorrelation curves, decreases as well when excited further in the red. However, above 620 nm a steep increase of intensity and brightness is found for the cowpea protoplasts that are due to the presence of chlorophyll in the chloroplasts. The latter emission peak is not present inside the BY2 cells, lacking chloroplasts.

Autofluorescence at different subcellular locations.

In Table 4.1 the molecular brightness values of the autofluorescent molecules at various subcellular locations have been summarized using the experimental set-up for detection of enhanced (EGFP). The laser intensity has been set at 2.5 kW.cm^{-2} in the focal plane, optimized for the detection of GFP in protoplasts (see Chapter 5 for a study of the photophysical characteristics of the FP's). The brightness values are low compared to the ones obtained for GFP and therefore the contribution of autofluorescence to the correlation curve can be neglected except for measurements performed in the cytoplasm of cowpea protoplasts, where many chloroplasts are located. To remove autofluorescent molecules from the observation volume, the sample can be pre-bleached before the FCM measurement is started. However, this approach turned out not very successful in the plant cells studied due to the high mobility of the autofluorescent molecules, which quickly replace the destroyed molecules in the pre-bleached area.

To check the cellular damage induced by the laser light, individual cells were exposed to various laser intensities at either 458, 488 and 514 nm and re-cultured for 8 hours, after which the cells were visually inspected and counted to check the growth rate. Below a laser intensity of 50 kW.cm^{-2} no effect was seen, but at 75 and 100 kW.cm^{-2} the growth rate was ca. 15% reduced and some morphological changes were present: an increased number of cells started to leak resulting from cell lysis and in some cells chlorophyll was released out of the chloroplasts. However, at the moderate light intensities used in the studies no damaging effect has been observed. The intensity and brightness of the autofluorescent molecules did not change within 5 hours.

Table 4.1: Molecular brightness of autofluorescence at various subcellular locations in tobacco suspension cells and cowpea protoplasts as determined from FCM-analysis (n=60). Purified GFP has been microinjected into the cytoplasm and measured in regions lacking chloroplasts. Samples were excited at 488 nm at 2.5 kW.cm^{-2} .

Location	Fluorescence intensity (kHz)		Molecular brightness (kHz/molecule)	
	cowpea	tobacco	cowpea	tobacco
nucleus	7 ± 1	5 ± 1	0.1 ± 0.0	0.1 ± 0.1
cytoplasm with chloroplasts	38 ± 16	-	1.0 ± 0.2	-
cytoplasm without chloroplasts	12 ± 2	6 ± 1	0.5 ± 0.2	0.7 ± 0.1
plasma membrane	6 ± 2	2 ± 1	0.3 ± 0.1	0.0 ± 0
vacuole	13 ± 2	10 ± 2	0.6 ± 0.2	0.5 ± 0.2
cytoplasmic EGFP	29 ± 5	18 ± 5	7.2 ± 0.4	6.3 ± 0.3

Diffusion of free fluorophores in cytoplasm and nucleus

To study the behaviour of free fluorophores in the nucleus and cytoplasm within the living cell, solutions of rhodamine-110 (R-110), rhodamine green (RGr), EGFP, tetramethylrhodamine (TMR) or Alexa-546 were microinjected into the cytoplasm. Microinjection in plant cells requires specialized skills and the percentage of successful injections without collapsing the cell, caused by the high internal pressure (turgor), was in our studies approximately 50% for the BY2 suspension cells and only 9% for the cowpea and BY2 protoplasts. Upon microinjection of the dyes into the cytoplasm, the nucleus became fluorescent as well due to the limited size of the fluorophores that could easily pass the nuclear membrane. To prevent the absorbance of fluorescence light by chlorophyll, FCM measurements in the cytoplasm and nucleus of cowpea protoplasts were performed in regions lacking chloroplasts. The retrieved autocorrelation curves are presented in figure 4.2. The concentration fluorescent dye used in fluctuation spectroscopy is typically 100 pM-1 μ M *in vitro*. However, by varying the concentration of microinjected dye, it was shown that at least 3 nM dye should be present in the cytoplasm of the cowpea protoplast to be detected. The diffusion of the fluorophores in PBS buffer (pH 7.8) could be fitted according to normal Brownian motion models. In plant cell cytoplasm the diffusion rate is slowed down by a factor of 2.4 compared to aqueous solution, similar to values obtained by others in mammalian cells (Politz et al., 1998; Schwille et al., 1999; Brock et al., 1999). The diffusion rates observed in the cytoplasm were smaller than those in aqueous solutions, which can be explained by the higher intracellular viscosity (Brock et al., 1998; Wachmuths et al., 2000). The diffusion behaviour of RGr and TMR in plant cells deviates from free diffusion and could only be fitted with a model for restricted, anomalous diffusion (Eq. 4.5) with $\alpha=0.72$ and $\alpha=0.61$ ($n=30$) respectively, or with a two-component diffusion model (Eq. 1.13) differing by almost two orders of magnitude in diffusion coefficient ($D_1=1.10^{-10}$, $\text{m}^2.\text{s}^{-1}$ (24%), $D_2=4.10^{-12}$ $\text{m}^2.\text{s}^{-1}$ (76%)). Dittrich et al. (2001) observed similar effects for Alexa-488, TMR, rhodamine B, RGr and Cy5 in human embryonic kidney cells. The authors explained this effect to non-specific interactions with (large) subcellular structures. This hypothesis is supported by our observations of initial bleaching in and the presence of high intensity peaks in the intensity traces using TMR, which are absent for cell measurements of the other dyes and for experiments in buffer solution. In BY2 cells the diffusion of all dyes, including RGr and TMR, within the nucleus can be described by a 3D Brownian motion model (Figure 4.2B) resulting in diffusion rates a factor of 3.1 smaller than observed in buffer ($D_{\text{tran}} \sim 10^{-10}$ $\text{m}^2.\text{s}^{-1}$). In the nucleus of cowpea protoplasts, however, all fluorophores display restricted diffusion with an average time exponent $\alpha=0.89$ ($n=30$). Wachsmuth et al. (2000) observed similar anomalous behaviour for EGFP in the nuclei of transfected AT-1 and COS-7 cells with $\alpha \approx 0.8$ for free EGFP and $\alpha \approx 0.7$ for the EGFP- β -galactosidase fusion protein.

However, not all their cells showed obstructed diffusion while other studies reported on normal Brownian diffusion with a nuclear viscosity greater than (Brock et al., 1999) or equal to that of water (Politz et al., 1998). Most likely, cells at different phases of the cell cycle are being monitored, which display variations in their nuclear organisation caused by the differences in chromosomal structure.

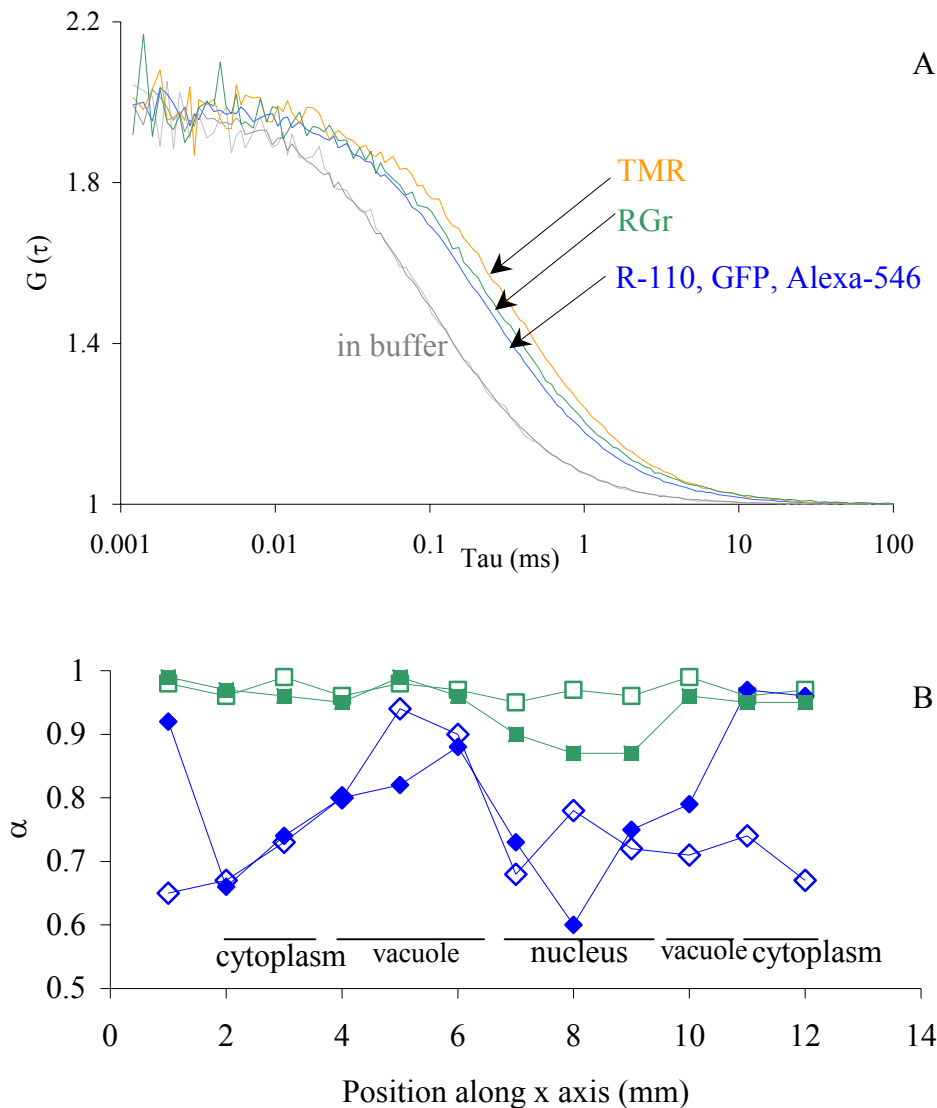


Figure 4.2: (A) Diffusion measurements of various fluorescent probes. Autocorrelation curves were acquired in PBS buffer solution (grey lines) and in the cytoplasm of cowpea protoplasts (black lines). Fluorophores, excited at 488 nm (R110, RGr and GFP) and 543 nm (TMR and Alexa-546) follow normal Brownian diffusion in buffer but in cytoplasm anomalous diffusion is observed for RGr and TMR. (B) Spatial distribution of the temporal exponent, α , retrieved from FCM analysis according to 3D anomalous diffusion models (Eq. 4.5). Rhodamine green (blue circles) or GFP (green squares) were microinjected into the cytoplasm of BY2 (open symbols) and cowpea protoplasts (filled symbols). The data were acquired by measurements along a line through the cell passing several intracellular compartments such as the cytoplasm, nucleus and vacuole.

Diffusion of amphiphilic molecules in the plant plasma membrane

The plasma membrane has a crucial role in processing information in response to external stimuli that is reflected by the fact that membrane interactions involving proteins and lipid cofactors are continuously modulated enabling transmission of signals at the right moment and along the correct pathway. The phase behaviour of the membrane strongly influences the dynamics of these processes. It is recognized that the plasma membrane is not homogeneous: microdomains are present, often called rafts, which differ in lipid composition and probably also in phase behaviour with the surrounding membrane (Edidin, 1997). The major difficulties in studying microdomains are their highly dynamic nature, requiring high temporal resolution, and the small domain size that is well below the resolution limit of optical microscopy. The immobile fraction observed in FRAP experiments may be associated with anomalous subdiffusion (Feder et al., 1996). Single particle tracking (SPT) (Saxton, 1997) allows monitoring molecular motion with a resolution down to tens of nanometers and has been applied to detect fluorophores on supported bilayers (Schmidt et al., 1996; Schütz et al., 1997). The results of these measurements suggest that the immobile fractions observed by FRAP are in fact due to restricted motion in inhomogeneities in the lipid bilayer. FCS has been applied to the study of membranes as well (Fahey et al., 1977 & 1978; Hink and Visser, 1998; Meyer et al., 1998), retrieving information on the diffusion rate of phospholipids in different environments. Studies by Korlach et al. (1999) and Schwille et al. (1999a) demonstrated in model systems of giant unilamellar vesicles (GUV's) and in the membrane of rat basophilic leukaemia cells that FCS is sensitive enough to probe the different lipid bilayer phases and the anomalous type of diffusion that has been observed when microdomains are present. To date studies on rafts have been performed in model membrane systems or in the plasma membrane of animal or human cells. In this chapter some data are presented concerning restricted diffusion in the plasma membrane of living plant cells.

To compare the experiments *in planta* and to validate our experimental set-up, GUV's were loaded with the amphiphilic probes, measured with FCS and the results analysed. The GUV's were prepared according to the method of Akashi *et al.* (1996) and consisted of 1,2-dilauroyl-*sn*-glycero-3-phosphocholine (DLPC) mixed with various amounts of cholesterol (0, 30 and 60%). GUV's without cholesterol did not show anomalous diffusion yielding $\alpha = 0.99 \pm 0.01$ ($n = 20$) with a transport coefficient of $\Gamma = 4.8 \pm 0.7 \cdot 10^{-12} \text{ m}^2 \cdot \text{s}^{-\alpha}$. These values, displayed in figure 4.3, are similar to the ones reported by others (Schwille et al., 1999a) and the transport coefficient approaching the value of 1, indicating that a Brownian motion model could accurately describe the experimental data. However, upon increasing the cholesterol content of the GUV's to 30%, α decreased to 0.88, 0.77 and 0.80 for BODIPY-HPC_{530/550}, octadecyl-rhodamine and DiOC₂(3) respectively with an transport coefficient of $\Gamma = 3.9 \pm 0.5 \cdot 10^{-12}$, $1.8 \pm 0.6 \cdot 10^{-12}$ and $1.6 \pm 0.5 \cdot 10^{-12} \text{ m}^2 \cdot \text{s}^{-\alpha}$, respectively.

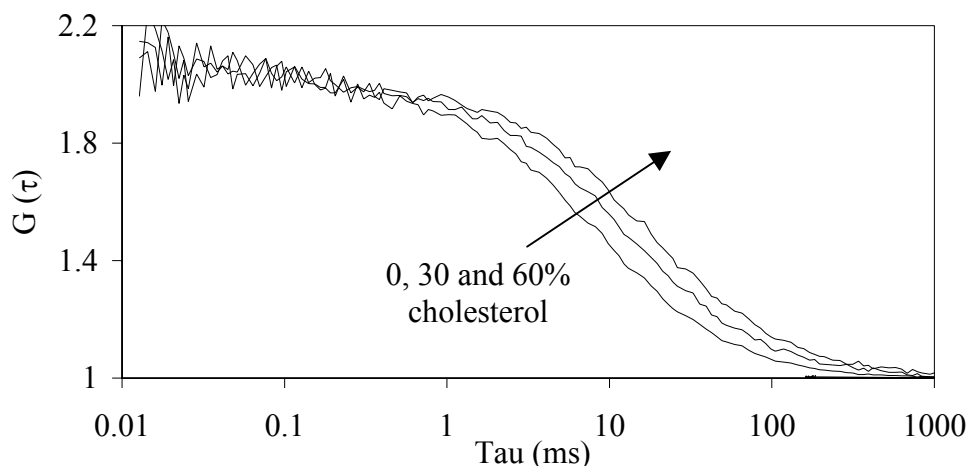


Figure 4.3: Diffusion characteristics of BODIPY-HPC_{530/550}, measured in the membrane of giant unilamellar vesicles in the binary mixture of DLPC and various amounts of cholesterol (molar fractions). The measured autocorrelation curves have been normalized and analysed according to the 2D anomalous diffusion model (Eq. 4.4).

The diffusion of BODIPY-HPC_{530/550} is the least restricted of the three probes, which is likely due to its preference for fluid phases caused by the large bulky moiety which has been coupled to the acyl chain (Huang *et al.*, 1988). Analysis of the experimental data according to a 2-component 2D Brownian diffusion model retrieves D_1 (76%) = $9.1 \pm 2.3 \cdot 10^{-13} \text{ m}^2 \cdot \text{s}^{-1}$ and D_2 (24%) = $6.8 \pm 1.9 \cdot 10^{-13} \text{ m}^2 \cdot \text{s}^{-1}$. This result indicates an increased confinement of the probe going from a purely fluid-ordered phase (0% cholesterol) to a lipid mixture with less fluid ordered phase (30% cholesterol). At 60% cholesterol the GUV's approach a purely fluid-ordered phase again (Silvus *et al.*, 1996) and the diffusion behaviour for all three probes can be fitted with a normal Brownian motion model again.

To study the behaviour of fluorescent lipid analogues in plant membranes the cowpea protoplasts and tobacco suspension cells were incubated in growth-medium (Nagata *et al.*, 1992) containing 1 nM of fluorescent lipid analogues for 10 minutes. To prevent absorption of the fluorescence by chlorophyll pigment, measurements in cowpea protoplasts were performed in membrane regions lacking chloroplasts. Figure 4.4A shows a confocal slice in the middle of a BY2 cell labeled with BODIPY_{530/550}-HPC. The fluorescence is located at the border of the cell. One should note that the observation volume of a confocal microscope, as has been used in the FCM experiments, has a radius of approximately 250 nm in radial and 1.2 μm in axial direction. Therefore, it is not possible to exclusively monitor the plasma membrane that has a height of approximately 5 nm. An intensity profiles along the x-axis showed two fluorescent peaks separated by approximately 25 μm , corresponding to the average diameter of the cell with a peak full width half maximum (FWHM) of 0.3 μm (Fig. 4.4B). The peaks were almost 20 times more intense than the interior of the cell and 50 times higher than background intensity. Starting from 20 minutes after incubation, an increased

fluorescence intensity was observed inside the cell, most likely due to the endocytosis of (fluorescently labeled) membrane fragments. Only for octadecyl-rhodamine B this effect has been observed already within 7 minutes after incubation. To prevent observing internalised lipid, experiments were executed until 5 minutes after incubation. To ensure that the fluorescent probe is membrane-localized and not distributed directly into the cytoplasm the intensity profile was compared to that of cytoplasmic labeled BY2 cells, via microinjection of EGFP. Besides broad intensity peaks at the border of these cells (FWHM 2.1 μm) other intense peaks are present, corresponding to cytoplasmic strands which cross the cell. The BY2-cells have been cultured during log-phase growth to prevent the presence of a cell wall which may non-specifically interact with the fluorescent probe and prevent the uptake of the probe to the plasma membrane. Shortly after cell division hardly any cell wall is present, but within several hours the cell wall starts to grow in size and thickness.

To validate that the monitored fluorescence was originating from the plasma membrane and not from the cell wall, suspension cells 3, 6 and 9 days after passage were incubated with the fluorescent lipid followed by addition of 0.1 M of NaCl to plasmolyse the plasma membrane from the cell wall. Confocal laser scanning images and FCS-measurements (the latter experiments with 100-fold lower concentration) showed that the cell wall was not fluorescent for cells of 3 days old while a significant fluorescent signal was present in cells of 6 and 9 days old.

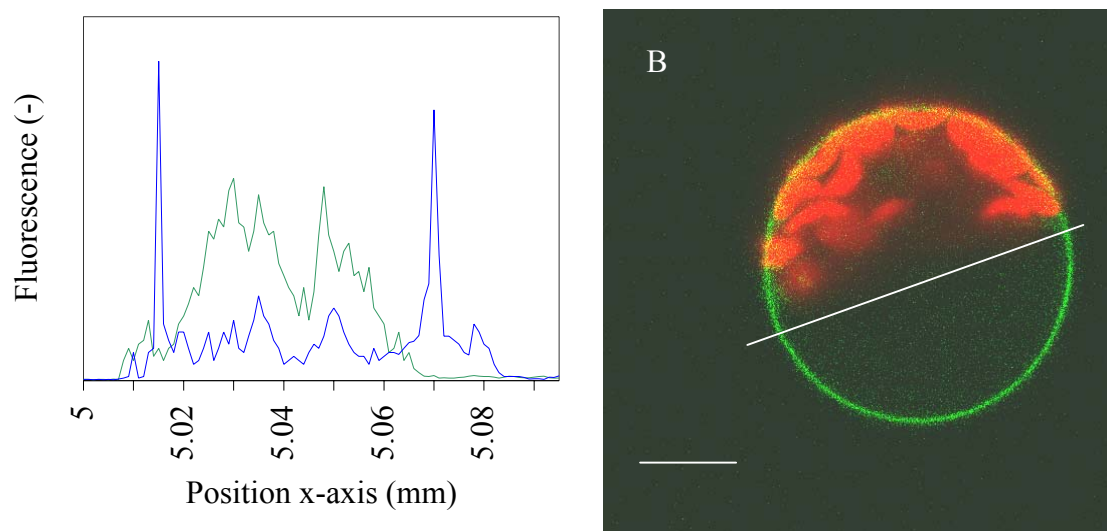


Figure 4.4: The fluorescence intensity-profile along the x-axis in the equatorial of a cowpea protoplast labeled with octadecyl-rhodamine B (blue line) and with EGFP (green line). (B) Confocal image of a tobacco suspension cell (36 hours after cell passage) after 5 minutes incubation with a 1 μM octadecyl-rhodamine B. Indicated is the line for the fluorescence profile, the bar denotes 10 μm . Clearly visible are the autofluorescent chloroplasts (red).

The curves could be fitted successfully with the anomalous diffusion model or the two-component 2D Brownian motion model. A one-component model, however, gave rise to a significant misfit as visualized by residuals between fitted and experimental curves (Fig. 4.5). The transport coefficient varied over the various probes from 8.6 to $21 \cdot 10^{-13} \text{ m}^2 \cdot \text{s}^\alpha$, with α ranging between 0.78 and 0.93 . Again, BODIPY-HPC_{530/550} displays the least restricted diffusion. To validate if the observed fluctuations were originating from the cell membrane and not from particles in the cytoplasm, the observation volume was focussed at several positions along the z-axis with $1 \text{ } \mu\text{m}$ interval to vary the fraction of observed cytoplasm. Cytoplasm localized fluctuations would decrease in amplitude if the observation volume was moving outward the cell. However, this effect has not been observed. The values for the measurements inside the cowpea protoplasts were similar to those of the BY2-cells. The translational diffusion is non-uniform and could only be fitted by models describing heterogeneous microenvironments. The reason for this deviation from Brownian diffusion is not clear yet. Molecular interactions between proteins and (probe) lipids or restricted diffusion in small heterogeneous membrane domains may originate these observations.

Conclusion

Intracellular experiments may be complicated by processes such as autofluorescence, cellular damage, light scattering and dye depletion and therefore special care must be taken in characterizing and selecting the most optimal conditions for FCM measurements *in vivo*. FCM was able to monitor differences in intracellular diffusion behaviour among different fluorophores: Cytoplasmic diffusion of rhodamine green and tetramethyl-rhodamine was restricted and indicate the non-specific interaction of these dyes with subcellular structures. All fluorophores diffuse according to normal Brownian motion in the nuclei of BY2 cells but in the nuclei of cowpea protoplast the motion is restricted. Additionally, the diffusion rate of fluorescent lipid analogues in the plasma membrane of tobacco suspension cells could only be analysed to a model describing anomalous diffusion, suggesting that the probes are diffusing anomalously or are localized in microdomains.

Table 4.2: Translational diffusion and transport constants of fluorescently labeled lipid analogues in cowpea protoplasts (n=20) as determined by FCS-analysis using a two-component 2D Brownian motion model and the 2D anomalous diffusion model.

Probe	Anomalous diffusion model		Brownian motion model	
	Γ ($10^{-13} \text{ m}^2 \cdot \text{s}^{-\alpha}$)	$\langle \alpha \rangle$	D_1 ($10^{-13} \text{ m}^2 \cdot \text{s}^{-1}$)	$\langle \% \rangle$
BODIPY-HPC _{530/550}	21 ± 5	$\langle 0.93 \rangle$	9.9 ± 0.5	$\langle 86 \rangle$
Octadecyl-rhodamine	8.9 ± 0.6	$\langle 0.80 \rangle$	6.1 ± 0.5	$\langle 76 \rangle$
DiOC ₂ (3)	9.6 ± 0.9	$\langle 0.78 \rangle$	7.1 ± 0.7	$\langle 78 \rangle$

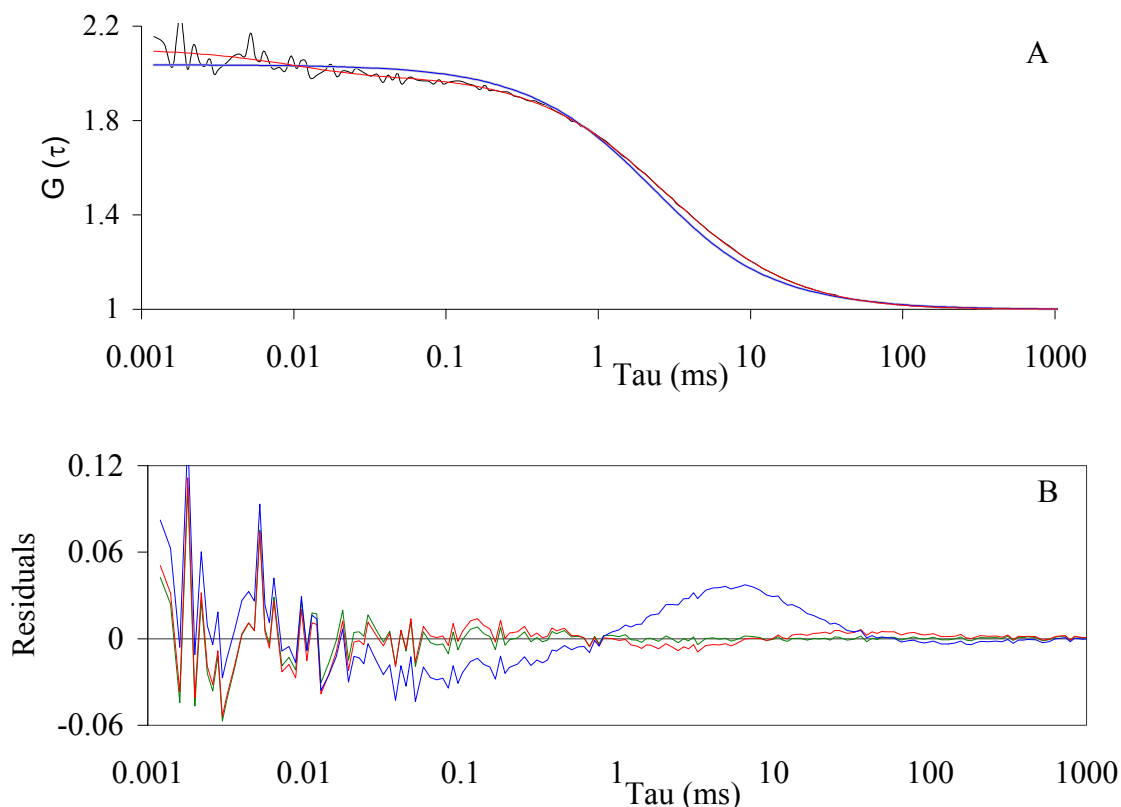


Figure 4.5: (A) Autocorrelation curve (black line) of cowpea protoplasts (36 hours after cell passage) after 10 minutes incubation with 1 nM octadecyl-rhodamine B in BY2 growth-medium. (B) The data were analysed according to the one- (blue line) and two- (red line) component 2D Brownian models or to the anomalous diffusion model (green line). Also indicated are the residuals between experimental and fitted values.

Material and Methods

Probes

Rhodamine-110, rhodamine green, tetramethyl rhodamine (TMR) and Alexa-546 were purchased from Molecular Probes (The Netherlands). To monitor the diffusion behaviour of lipid analogues in the plant plasma membrane the fluorescent probes contain a large hydrophobic (or lipophilic) part having the ability to be incorporated in membrane systems:

β -BODIPY₅₃₀₋₅₅₀-C5-HPC (2-(4-(4-difluoro-5,7-diphenyl-4-bora-3a,4a-diaza-s-indacene-3-pentanoyl)-1-hexadecanoyl-*sn*-glycero-3-phosphocholine), in which the fluorescent BODIPY group was coupled to one of the fatty acyl chains of phosphatidylcholine) and ODRB (octadecyl rhodamine B chloride, which consists of a fluorophore coupled to a long hydrophobic alkyl chain). All fluorescent probes were purchased from Molecular Probes Inc. (Netherlands), dissolved in ethanol and stored at -10°C. NBD-PE, rhodamine-101, rhodamine green and GFP were excited at 488 nm, BODIPY-HPC and ODRB were excited at 514 nm and TMR and Alexa-546 were excited at 543 nm. GFP was isolated and purified from transfected *E. coli* cells as have been described in Chapter 5.

Giant unilamellar vesicles

Giant unilamellar vesicles were prepared by the method of Akashi et al. (1996). Briefly, phospholipid mixtures were dissolved in chloroform: methanol 2:1 to make a lipid solution of 10 mg/ml. 120 ml solution was dried at 45°C with a rotary evaporator to form a lipid film in a 10 ml tube. The tube was placed *in vacuo* to remove traces of organic solvent. The film was subsequently dehydrated at 45°C with nitrogen for 20 minutes. A nitrogen purged solution of 0.1 M sucrose and 100 mM NaCl was gently added to the tube and incubated under argon at 37°C overnight.

Cell culture and handling

Suspension cells of tobacco BY2 (*Nicotiana tabacum* L. cv. Bright Yellow 2) were cultured at 22°C under gently shaking (13 rpm) in growth medium (4.3 g/l Murashige and Skoog Plant Salt Base, 255 mg/l KH_2PO_4 , 1 mg/l thiamin-HCl, 0.2 mg/l 2,4-dichlorophenoxyacetic acid, 30 g/l sucrose and 100g/l myo-inositol, pH 5.8) and weekly sub-cultured at 50 times dilution with fresh medium. Protoplasts were prepared from the cells cultured after 3 days of sub-culture by adding 10 ml enzyme solution consisting of 1% cellulase, 0.1% pectolyase and 0.4 M mannitol, pH 5.5. After 3 hours of incubation at 28°C in a rotating vessel at 60 rpm for two hours the cells were washed twice by centrifugation for 2 min at 850 rpm followed by addition of 10 ml solution containing 125 mM CaCl_2 , 154 mM NaCl, 5 mM KCl, 5 mM sucrose and 0.1% MES, pH 5.5. Cowpea mesophyll protoplasts were prepared by peeling off the lower epidermis of the primary leaves of ten-days old *Vigna unguiculata*, using forceps. Three leaves were floated on a 15 ml enzyme solution (0.1% cellulase, 0.05% pectinase, 10 mM CaCl_2 and 0.5 M mannitol, pH 5.5) for 3.5 hours at room temperature with gentle shaking. The cells were washed twice by adding 2 ml solution containing 10 mM CaCl_2 and 0.5 M mannitol followed by centrifugation for 5 min at 600 rpm.

Microinjection

Fluorescent probe was dissolved in 50 mM PBS (pH 7.8) to a final concentration of 1 μM and centrifuged at 80,000 rpm for 10 minutes to remove possible aggregates. Femtotips (Eppendorf, The Netherlands) with an opening diameter of $0.5 \pm 0.2 \mu\text{m}$, were loaded with approximately 10 μl green fluorescent protein solution using Microloader tips (Eppendorf, The Netherlands). The cells were injected under visual control using an Eppendorf Microinjector 5242 and Micromanipulator 5170 to control injection parameters ($P_1 = 4000$ hPa, $P_{\text{inj}} = 100$ hPa, $P_{\text{backpressure}} = 60$ hPa and $t_{\text{injection}} = 0.2$ sec). After injection FCS measurements were repeated twice at intervals of 5 minutes to check for leakage of the cell.

Fluorescence correlation spectroscopy

FCS measurements were performed with a ConfoCor microscope (Carl Zeiss and Evotec, Germany) that has been described in detail in Chapter 1. The samples were excited by the

488, 514 or 543 nm lines from air-cooled Argon ion and Helium-Neon lasers which were filtered by 488 ± 12 nm, 515 ± 15 nm or no interference filters, respectively (Omega, USA) and reflected by a dichroic filter (Omega, USA). The laser power was set with neutral density filters to less than 80 μ W. The emission light was filtered using either a 500-560, 530-610 or 560-610 nm band-pass filter (Omega, USA) and passed the motor-controlled pinhole set at a diameter of 40 μ m. The samples were measured during 20 seconds at 293 K.

Fluorescence spectral imaging microscopy

Fluorescence spectral imaging microscopy (FSPIM) (Goedhart et al., 2000) experiments were executed on a Leica DMR epifluorescence microscope equipped with a 250IS imaging spectrograph (Chromex) coupled to a CH250 CCD camera (Photometrics, The Netherlands) incorporating a back-illuminated SIT502 chip with 512x512 24 μ m square pixels. The excitation light source was a 100 W-mercury arc lamp coupled to an excitation filter wheel. Fluorescent spectral images were acquired using a 20x Plan Neofluar objective (NA 0.5), a 485 ± 15 nm bandpass excitation filter (Omega), a 505DCLP dichroic mirror (Omega) and a 505 longpass emission filter (Schott). Spectral images were acquired using a 150 groove/mm grating, set at a central wavelength of 500 nm and a slit width of 150 μ m corresponding to 7.5 μ m in the object plane. Typical exposure and CCD integration time was 3 seconds. The spectra were corrected for background fluorescence and camera bias by background subtraction using an extracellular region next to the cell from the same spectral image. The spectra were not corrected for the spectral instrument response yielding a slightly underestimated intensity in the blue edge of the spectra.

Acknowledgments

This research was supported by an investment grant from The Netherlands Organization for Scientific Research (NWO) and by a grant from the Earth and Life Sciences Foundation of NWO (ALW-NWO).

5

Fluorescence Fluctuation Analysis of Fluorescent Proteins in Living Plant Cells: A Study using FRET- and Dual Color Fluorescence Cross-Correlation Microscopy

Mark A. Hink, Jan W. Borst and Antonie J.W.G. Visser

Molecular interactions play a key role in the complex organisation of a living plant cell. Several elegant microspectroscopic techniques have been developed to study the interaction between proteins, thereby making use of the spectral variants of the green fluorescent protein to tag the protein of interest. The applicability of several variants of green fluorescent protein in fluctuation techniques, such as fluorescence correlation spectroscopy (FCS) and microscopy (FCM), has been tested both *in vitro* as in cowpea protoplasts. Additionally, the possibility to combine correlation microscopy with fluorescence resonance energy transfer (FRET) and dual color cross-correlation microscopy (FCCM) was studied using fusion constructs consisting of ECFP and EYFP, coupled by a linker of 8 or 25 alanine residues. Both fusion proteins resulted in a cross-correlated product in cowpea protoplasts, but the poor signal quality of sensitised EYFP fluorescence upon FRET prevented to develop a FCM-FRET assay based upon fluorescent protein labels.

Published in edited form in *Methods Enzymol.* **361**, in press.

Introduction

Several elegant biochemical methods have been developed to study protein-protein interactions. In general, such biochemical studies are carried out *in vitro* and have provided valuable information about the properties of the studied molecules. However, to what extent these properties reflect their behaviour in living cells is not clear. The complex organisation and the compartmentalisation of plant cells makes it probable that molecular behaviour in test tube and cell are not identical and therefore it is essential to study molecules in their natural environment. Several innovative microspectroscopic approaches provide such possibilities, since in addition to the high spatial resolution of microscopic techniques also information about the dynamical behaviour of molecules can be obtained *in vitro*. Fluorescence fluctuation techniques such as fluorescence correlation microscopy (FCM) and photon counting histogram analysis (PCH) allow to monitor the dynamics and brightness distribution of fluorescently labeled molecules at equilibrium conditions. In this chapter the applicability of several variants of green fluorescent protein (GFP) (Tsien et al., 1998) as fluorescent markers in fluctuation analysis were checked both in buffer solutions as in living plant cells. In addition, the possibility to combine correlation microscopy of fluorescent proteins (FP's) with fluorescence resonance energy transfer (FRET) and dual color cross-correlation (FCCM) was tested.

Fluorescent proteins

A prerequisite of studying molecules with fluorescence fluctuation spectroscopy techniques is that the molecule of interest is fluorescent. Since most natural molecules show only weak autofluorescence, labeling with an external fluorophore is essential. The labeled molecule can be introduced into the cell via uptake of esterase cleavable dyes, pH-shock methods, cell loading agents, electroporation or microinjection. However, plant cell walls form a large physical barrier for most techniques, resulting in an inefficient uptake. In the case of protein studies, it is therefore far more attractive to couple fluorescent tags by genetic approaches. Intrinsic fluorescent proteins like the green fluorescent protein (Tsien, 1998; Conn, 1998), identified in the jellyfish *Aequorea victoria*, are especially suitable for this purpose since they can be relatively easily fused to the gene of interest. The high molecular brightness, well protected fluorophore and relative inertness for aspecific interactions with cellular structures makes it an excellent fluorescent marker to study the behaviour of proteins at the single molecule level. Moreover, point mutations of the wildtype GFP resulted in mutants with different spectral characteristics: the enhanced blue (EBFP), cyan (ECFP), green (EGFP) and yellow fluorescent proteins (EYFP) (Clontech, 2002). Recently red-shifted fluorescent protein (DsRed) has been isolated (Matz et al., 1999; Fradkov et al., 2000) and optimized (HcRed) (Clontech, 2000). The range of available color variants now allows to specifically label

different types of protein that can be monitored simultaneously via microspectroscopic methods.

Fluorescence resonance energy transfer

A widely used technique to monitor molecular interactions in cell biology is fluorescence resonance energy transfer. FRET was first described by Förster (1948) as a photophysical process where energy is transferred non-radiatively from a donor molecule (D) to an acceptor molecule (A) via dipole-dipole interactions. Energy can be transferred in this way only over a limited distance and the efficiency of the energy transfer, E , scales with the sixth power of the distance R , separating donor from acceptor molecule.

$$E = \frac{1}{1 + \left(\frac{R}{R_0}\right)^6} \quad (\text{Eq. 5.1})$$

Therefore the FRET range is limited to 1-10 nm, making FRET a useful tool to measure distances far below the resolution limit of modern optical microscopes (Stryer and Haugland, 1967; Stryer, 1978), which is currently approximately 100 nm (Hell et al., 1997).

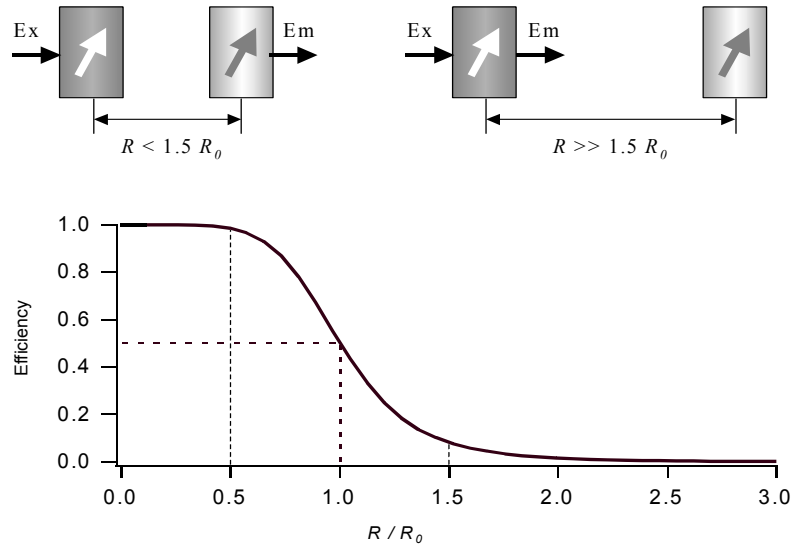


Figure 5.1: Fluorescence resonance energy transfer (FRET) can take place when there is a spectral overlap and the angle between the donor and acceptor transition moments is not 90° . Upon FRET the donor intensity decreases and the acceptor intensity increases. The efficiency of energy transfer, E , scales inversely with the sixth power of distance R between donor and acceptor molecule and depends on the Förster radius, R_0 , at which the FRET efficiency is 50% (approximately 5.0 nm for the ECFP-EYFP pair).

R_0 defines the distance between the acceptor and donor molecule where the FRET efficiency is 50%. R_0 is strongly dependent on the spectral properties of the DA pair like acceptor quantum yield, spectral overlap between the emission of the donor and excitation of the acceptor and the relative spatial orientation of their emission and excitation transition dipole moments respectively, as is illustrated in figure 5.1.

FRET is manifested in several ways: Upon FRET the fluorescence intensity of the donor (if this is a fluorescing molecule) decreases while the acceptor intensity increases. With digital imaging techniques it is possible to quantify the FRET efficiency by monitoring the changed ratio of donor and acceptor fluorescence (Gordon et al., 1998; Xia and Liu, 2001). The fluorescence lifetime of the donor molecule decreases upon energy transfer since an additional path for de-excitation of the first excited state is introduced. Fluorescence lifetime imaging microscopy (FLIM) exploits this phenomenon by observing the shortening of the donor fluorescence lifetime (Gadella, 1999; Bastiaens and Squire, 1999). Due to the energy transfer between molecules, acceptor-specific fluorescence intensity fluctuations may be 'sensitised', which can be monitored by FRET-FCM. In contrast to FCCM, which will be discussed in a next section, FRET-FCM requires a short distance between the donor and acceptor molecule. An advantage compared to FCCM is that one can monitor molecular interactions requiring only a single laser line to excite the donor and therefore no laborious alignment is required in order to optimise the overlap of the excitation volume elements. In the last few years several groups have reported on the use of FCS to monitor intramolecular dynamics by changes in the FRET-efficiency (Ha et al., 1999; Brasselet et al., 2000; Wallace et al., 2000; Kim et al., 2002). As mentioned before, upon FRET the donor intensity is decreased accompanied by increased acceptor fluorescence intensity. Changes in the FRET-efficiency therefore result in an anti-correlation where the relaxation time of the anti-correlation represents the time scale of the process that caused the change in FRET-efficiency. Besides the possibility to test the occurrence of FRET by FCS, Widengren et al. (2001) could also determine the FRET efficiency using two different concepts. Therefore, DNA duplexes were labeled with a donor (Alexa488) and acceptor molecule (Cy5). In the first approach, the characteristic cis-trans isomerisation in the Cy5 molecule is observed (Widengren and Schwille, 2000). The rate of isomerisation is only dependent on the acceptor fluctuations and is not affected by donor cross-talk, background, label densities or the concentration of the dyes. In the second approach, FRET efficiencies are determined from the detected acceptor fluorescence rate per molecule (η_A) according to (Widengren et al., 2001):

$$\eta_A = g \Phi_{FA} \sigma_D I_{exc} E \quad (\text{Eq. 5.2})$$

The molecular brightness of the acceptor (η_A) can be determined from PCH analysis or dividing the average fluorescence intensity by the number of molecules as determined from FCS-analysis. Now E can in principle be determined. However, for an accurate absolute determination of E the overall detection quantum efficiency, g , the fluorescence quantum yield of the acceptor dye, Φ_{FA} , and the excitation cross section of the donor, σ_D , have to be known.

All the effects described above can be inverted if the acceptor molecule is destroyed and several techniques using acceptor (or donor) photobleaching have been developed (Gadella et al., 1995, Siegel, et al., 2000).

Certain combinations of FP's have proven to be an efficient FRET pair (see for a review Tsien, 1998; Pollok and Heim, 1999 and Gadella et al., 1999). A good pair requires high spectral overlap and a minimized cross-talk caused by emission of the donor in the acceptor channel and direct excitation of the acceptor molecule at the wavelength used to excite the donor. The amount of cross-talk is low for the EBFP-EGFP or EBFP-EYFP pairs but the use of EBFP may be problematic due to the low, near-UV excitation wavelength required, which results in high autofluorescence levels, and its sensitivity to photobleaching. In addition the extinction coefficient of EBFP is relatively low. ECFP-EYFP is a widely used pair but has high cross-talk whereas the EGFP-DsRed pair suffers from the lower fluorescence quantum yield and the broad absorption bands of DsRed, causing significant amount of direct excitation of DsRed when exciting EGFP. Additionally, DsRed has the tendency to form tetramers which may lead to erroneous non-physiological results (Baird et al., 2000).

In the last decade major advances have been made in the field of single molecule detection by fluorescence (Xie and Trautman, 1998; Ambrose et al., 1999; Weiss, 1999). By analysis of single molecules it is possible to observe heterogeneities that are masked in ensemble measurements which has been exploited to detect and analyse FRET on single molecules (for a review see Ha, 2001; Dahan et al., 1999). As have been proposed by Haas and Steinberg (1984), FCS can be used to monitor intramolecular dynamics by changes in FRET efficiencies as well. The cross-correlation of donor and acceptor fluorescence should result in an anticorrelation where the relaxation time of this process reflects the intramolecular motion and the amplitude scales with the distances between donor and acceptor. Another approach is to correlate the ratio of the donor and acceptor fluorescence (Ha et al., 1999; Brasselet et al., 2000; Wallace et al., 2000). Widengren et al. (2001) could calculate the intramolecular FRET efficiency of doubly labeled double stranded DNA molecules by analysing the molecular brightness of the acceptor or by monitoring the specific cis-trans isomerisation fluctuations of the Cy5 acceptor dye. In the study presented in this chapter the applicability of intracellular FRET-FCS is tested by monitoring the molecular brightness of ECFP fused to EYFP.

Fluorescence cross-correlation microscopy

The application of FCS to study molecular interactions upon differences in diffusion times is limited by the fact that the diffusion coefficient scales only to the cubic root of the molecular weight. It has been shown that in case of an unchanged molecular brightness upon binding, a minimum four-fold mass difference is required to distinguish a complex from free diffusing molecules (Meseth et al., 1999). To overcome these limitations dual-color fluorescence cross-correlation spectroscopy (FCCS) has been proposed (Eigen et al., 1994) and developed (Schwille et al., 1997 & 2001b). In FCCS-studies both partners involved in interaction is labeled by a spectrally different fluorescent group, *e.g.* green and red emitting dyes. The interacting molecules can now be studied by monitoring the particles that carry both labels. Hereto the sample is illuminated by two different laser lines and the fluorescence is splitted into two different detection channels, allowing monitoring both dyes simultaneously. The close proximity of an acceptor to a donor molecule necessary to observe FRET is not required for fluorescence cross-correlation microscopy (FCCM) since the technique is not based upon interaction of the dyes but on the temporal coincidence of both dyes in the observation volume (Fig 1.2). Therefore a spectral overlap between both dyes is not required. Moreover, it is even not desirable since an emission overlap complicates the effective separation of the fluorescence of both dyes. So far, only *in vitro* studies have been reported on FCCS, monitoring processes such as enzyme kinetics (Kettling *et al.*, 1998; Koltermann *et al.*, 1998, Rarbach et al., 2001), nucleotide hybridisation (Schwille *et al.*, 1997; Rigler *et al.*, 1999; Földes-Papp *et al.*, 2001a-c), protein-DNA interactions (Rippe *et al.*, 2000) and the application of two-photon excitation (Heinze et al., 2000).

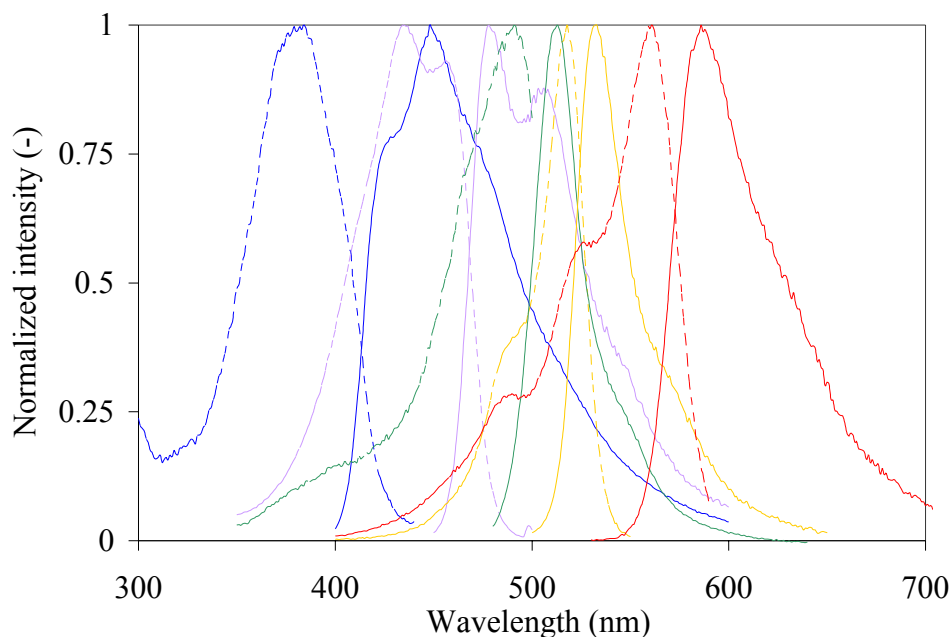


Figure 5.2: Corrected excitation (dashed) and emission spectra (solid) of (from left to right) EBFP, ECFP, EGFP, EYFP and DsRed.

Results and Discussion

Spectral characteristics of the fluorescent proteins

In figure 5.2 the corrected fluorescence excitation and emission spectra of EBFP (F64L, Y66H, Y145F), ECFP (F64L, S65T, Y66W, N146I, M153T, V163A), EGFP (F64L, S65T), EYFP (S65G, V68L, Q69K, S72A, T203Y) (also known as “Citrine”, denoted as EYFP in this thesis) and DsRed are displayed. The spectra were acquired at pH 7.5. The high spectral overlap between excitation and emission makes many FP-pairs good candidates for FRET studies. However, the long emission tails complicates the spectral separation of the dyes. EBFP-EGFP, ECFP-EYFP and EGFP-DsRed are the most commonly used FRET-pairs. However, the relatively low fluorescence quantum yield, the sensitivity to photobleaching and the high autofluorescence at the emission wavelengths of EBFP and DsRed, these FP’s were not suitable for single molecule experiments in plant cells and therefore omitted from further studies.

It has been shown that the chromophoric group of several FP’s can exist in a neutral, protonated, dim or non-fluorescent form and an anionic, deprotonated fluorescent form. Therefore the emission of EGFP and EYFP will be quenched progressively upon lowering the pH (Tsien et al., 1998; Patterson et al., 1997). The fluorescence intensity of EGFP or EYFP from the cell extracts of cowpea protoplasts is displayed in figure 5.3A.

Fitting the fluorescence intensity F to equation 5.3 (Kneen et al., 1998) with signal baseline B and gain G :

$$F = B + \frac{G}{1 + 10^{pK_a - pH}} \quad (\text{Eq. 5.3})$$

yielded pK_a values of 6.1 ± 0.1 (ECFP), 5.8 ± 0.3 (EGFP) and 5.9 ± 0.3 (EYFP-Citrine) respectively, similar to the values found *in vitro* by others: pK_a 5.9 (Llopis et al., 1998; Kneen et al., 1998; Haupts et al., 1998) and 6.1 (Miyawaki et al., 1999), respectively. These values indicate that in the cytoplasm, where the pH is approximately 7.0, more than 95% of these FP molecules are in the deprotonated, fluorescent form. However such FP’s could be quenched to a major extent in organelles having a acidic environment such as endosomes, lysosomes, mitochondria or Golgi compartments. The pH sensitivity of some FP’s can also be exploited to measure cellular pH but proper calibration is required.

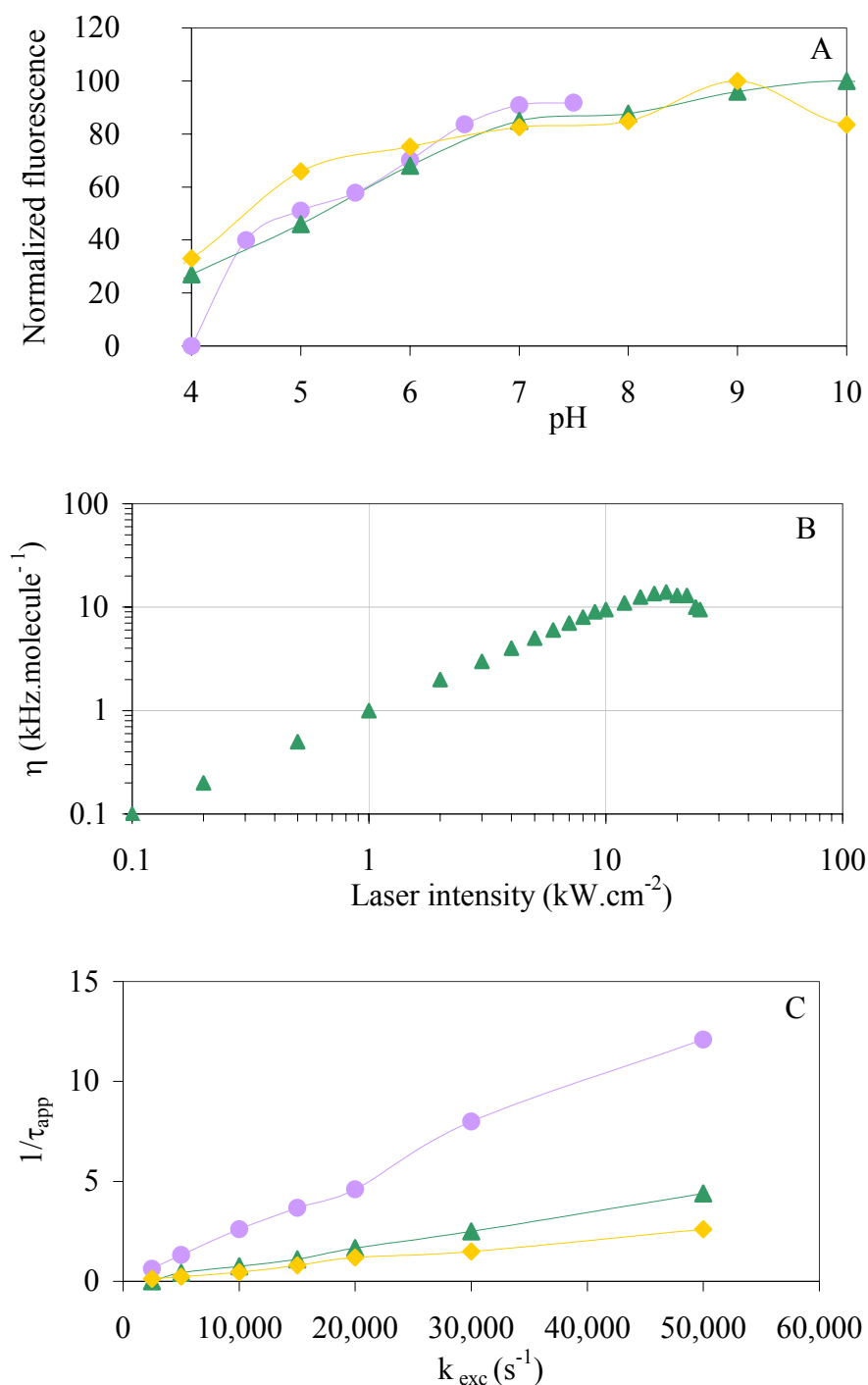


Figure 5.3: Fluorescence properties of ECFP (●), EGFP (▲) and EYFP (◆). (A) Fluorescence intensity of cell extracts from FP expressing cowpea protoplasts at different pH. The curves were normalized and fitted to equation 5.3, yielding a pK_a of 6.1 ± 0.1 (ECFP), 5.8 ± 0.3 (EGFP) and 5.9 ± 0.3 (EYFP), respectively. (B) Molecular brightness of 50 nM EGFP in PBS buffer, pH 7.5 measured at various laser intensities. (C) Photobleaching yield of 50 nM fluorescent protein in PBS buffer, pH 7.5 containing 10% sucrose as determined by fitting FCM curves to equation 5.4.

A disadvantage of using FP's in fluctuation analysis are the pronounced photophysical processes which have been described for EGFP, EYFP and DsRed, that may complicate single molecule measurements since the fluorophores may be transferred temporarily to non-

fluorescent states, thereby reducing the amount of emitted photons. As have been outlined above, protonation of the chromophoric group at pH values below 7.0 can result in a large fraction of fluorophores residing in a dark state. The dynamics of this process, that occurs on a tens of microsecond time scale, is superimposed on the diffusion fluctuation in the correlation curve (Haupts et al., 1998; Widengren et al., 1999; Schwille et al., 2000; Heikal et al., 2000). Additionally, a light-driven fluorescence flicker has been observed for EGFP (Haupts et al., 1998; Widengren et al., 1999), EYFP (Schwille et al., 2000; Heikal et al., 2000) and DsRed (Heikal et al., 2000). A third source of fluorescence flicker is the so-called blinking which has been observed in the second time range for immobilized individual EGFP proteins (Dickson et al., 1997). The on-off switching of the fluorescence has been attributed to photoconversions between the neutral, intermediate and anionic states of the chromophore. The latter process is not visualized in the experimental correlation curves presented here, due to the relatively short passage time of the fluorescent proteins through the observation volume with respect to the characteristic blinking time. In order to optimize the signal to noise ratio (SNR) the molecular brightness, η , defined as the counting rate per molecule, has been measured at various excitation intensities. At moderate laser intensities the molecular brightness scales linear to the excitation intensity until processes like photobleaching and ground state depletion cause a deviation (see figure 5.3B). At the saturation intensity, I_s , the maximum molecular brightness is achieved but nonlinear processes may introduce severe errors in the analysis of fluorescence data acquired at this intensity.

The photobleaching yield is an important quantity in single-molecule techniques since it is related to the total number of photons that can be detected until the moment of photo-induced destruction of the dye. To estimate the photostability of the FP's, FCM experiments were performed using an experimental setup with a slightly opened pinhole (\varnothing 60 μm). Moreover, the samples were solubilized in PBS buffer, pH 7.5 containing 5% sucrose to effectively increase the residence time of the molecules in the observation volume. Hence, it was possible to effectively separate diffusion and photobleaching kinetics from the relative fast protonation, triplet and dark state kinetics in the submicrosecond range. FCM curves were obtained at laser densities between 0.1 and 25 $\text{kW}\cdot\text{cm}^{-2}$ and fitted according to

$$G(\tau) = 1 + \frac{1}{\langle N \rangle} \cdot \sum_{i=1}^3 \frac{1 - T_i + T_i e^{\frac{-\tau}{\tau_i}}}{(1 - T_i)} \cdot \frac{1}{\left(1 + \frac{\tau}{\tau_{\text{dif},j}}\right) \sqrt{1 + \left(\frac{\omega_{xy}}{\omega_z}\right)^2} \frac{\tau}{\tau_{\text{dif},j}}} \quad (\text{Eq. 5.4})$$

and for diffusion in a two dimensional plane oriented perpendicular to the optical axis:

$$G(\tau) = 1 + \frac{1}{\langle N \rangle} \cdot \sum_{i=1}^3 \frac{1 - T_i + T_i e^{\frac{-\tau}{\tau_i}}}{(1 - T_i)} \cdot \frac{1}{\left(1 + \frac{\tau}{\tau_{\text{dif},j}}\right)} \quad (\text{Eq. 5.5})$$

Here τ_i denotes the kinetic lifetimes for protonation, triplet and dark state transitions and T_i their occupations. The photobleaching quantum yield (Φ_b) was characterized by monitoring the variation of the apparent diffusion time with excitation rate. The slope of the apparent diffusion rate vs. the excitation rate yields Φ_b resulting in values of 25 ± 4 , 0.8 ± 0.3 and $5 \pm 2 \cdot 10^{-5}$ for ECFP, EGFP and EYFP in solution, respectively (Fig. 5.3C). The values are within the same range as the results determined by Baird et al. (2000) and Harms et al. (2001). Table 5.1 summarizes the characteristics of the fluorescent proteins. Comparing the diffusion coefficients of the three FP's, no difference has been observed as was expected. To monitor the effect of the cellular environment on the photophysical properties of the fluorophores, cowpea protoplasts were transfected with constructs of non-targeted FP, which localizes in the cytoplasm and the nucleus. Constructs of FP fused to a membrane targeting sequence CAAX yielded intense, homogenously fluorescence in the plasma membranes and weakly fluorescent internal membranes. Measurements performed in the cytoplasm and in the plasma membrane were analysed according to equation 5.4 and 5.5, respectively. The diffusion in cytoplasm and plasma membrane was retarded by a factor of 2.4 and ca. 200, respectively, compared to the diffusion in solution, due to the higher local viscosity. No restricted diffusion (see Chapter 4) has been observed. The highest molecular brightness, η , detected at the saturation intensity, was ca. 15 kHz per molecule for both EGFP and EYFP and 7 kHz per molecule for ECFP. ECFP is most sensitive to photobleaching, having a bleaching quantum yield of $2.5 \cdot 10^{-4}$ which is more than 20 times higher than for EGFP. Experiments performed in the cytoplasm or plasmamembrane of transfected cowpea protoplasts yield a similar photobleaching quantum yield (Table 5.1) but the molecular brightness was ca. 30% lower. Cell lysates of the transfected protoplasts showed a relatively fast diffusion and a molecular brightness value close to the value found in buffer. Hence, the removal of scattering sources such as the large intracellular structures and the newly formed cell wall resulted in a significant increase of the signal intensity.

FRET in the CA_nY constructs

To study the applicability of FRET-FCM in living cells using FP's as fluorescent label, fusion proteins have been tested which had been designed for FCCM analysis. The fusion constructs consist of an ECFP moiety coupled to EYFP by a linker of 8 alanine residues (CA₈Y).

Table 5.1: Photophysical and diffusion properties of the fluorescent proteins *in vitro* and in transfected cowpea protoplasts (n=40).

dye	λ_{exc} (nm)	location	D_{tran} ($\times 10^{12} \text{m}^2 \cdot \text{s}^{-1}$)	η_{sat} (kHz)	I_{sat} ($\text{kW} \cdot \text{cm}^{-2}$)	Φ_b ($\times 10^5$)
ECFP	458	buffer ^{a)}	87 ± 4	9 ± 1	20 ± 6	25 ± 4
		cytoplasm	37 ± 8	6 ± 1	18 ± 4	21 ± 7
		membrane ^{b)}	0.4 ± 0.2	6 ± 1	23 ± 3	-
		cell lysates	78 ± 7	8 ± 1	20 ± 5	-
EGFP	488	buffer ^{a)}	88 ± 3	14 ± 2	18 ± 3	0.8 ± 0.3
		cytoplasm	41 ± 3	9 ± 2	17 ± 3	1.0 ± 0.4
		membrane ^{b)}	0.5 ± 0.1	8 ± 3	21 ± 5	-
		cell lysates	67 ± 5	12 ± 1	20 ± 6	-
EYFP	514	buffer ^{a)}	90 ± 2	19 ± 3	9 ± 2	5.0 ± 1.2
		cytoplasm	37 ± 3	13 ± 2	6 ± 1	6.3 ± 1.5
		membrane ^{b)}	0.4 ± 0.2	13 ± 2	4 ± 1	-
		cell lysates	62 ± 6	17 ± 1	8 ± 2	-

a) 50 nM Fluorescent protein in 50 mM PBS pH 7.5 and 10% sucrose

b) Fluorescent protein linked to CAAX membrane targeting sequence

Elongating this linker to 25 residues (CA₂₅Y) would reduce the FRET-efficiency due to the increased distance between the fluorophores. The FRET-efficiency of the constructs has been estimated by monitoring the ECFP fluorescence lifetime using time-correlated single photon counting (TCSPC). The fluorescence lifetime distribution of free diffusing ECFP, consists of three peaks at 0.48 ± 0.07 ns (with a relative amplitude of 21 %), 1.75 ± 0.20 ns (22 %) and 3.78 ± 0.05 ns (57 %), resulting in an average fluorescence lifetime of 2.5 ± 0.1 ns. The lifetimes are identical for CA₂₅Y, yielding an average lifetime of 2.3 ± 0.1 ns. For CA₈Y the average ECFP lifetime is 1.9 ± 0.2 ns. The FRET-efficiency can be calculated according to equation 5.6 (see Gadella et al., 1999):

$$E = 1 - \frac{\tau_{D,+A}}{\tau_{D,-A}} \quad (\text{Eq. 5.6})$$

where $\tau_{D,+A}$ and $\tau_{D,-A}$ are the fluorescence lifetimes of the donor in the presence and absence, respectively, of acceptor molecules. The FRET-efficiency of CA₈Y is 25 %. Analysis according equation 5.1, using the Förster radius of 5.0 nm for the CFP-YFP pair (Tsien et al., 1998), yields a distance of 2.2 nm between both dyes. A low FRET-efficiency has been calculated for the CA₂₅Y protein (8 %) and no FRET was observed for the control sample, an equimolar mixture of ECFP and EYFP.

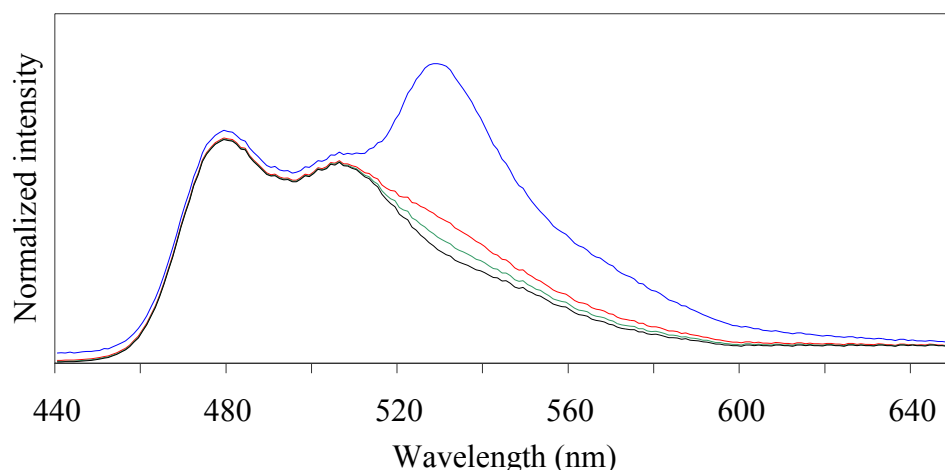


Figure 5.4: FRET characterization of ECFP (black line), CA₈Y (blue line), CA₂₅Y (red line) and equimolar mixture of ECFP + EYFP (green line) in the cytoplasm of transfected cowpea protoplasts using spectral imaging microscopy. The spectra were normalized with respect to the ECFP emission peak at 480 nm.

To test whether FRET was taking place in the CA_nY constructs *in vivo*, 12 hours after transfecting the cowpea protoplasts, fluorescence spectral imaging microscopy (FSPIM) measurements were carried out in 1x1 μm sections of the cytoplasm. The proteins were expressed homogeneously throughout the cytoplasm and the nucleus of the protoplast. In case the protein pair is present in constant stoichiometry, as is the case for the CA_nY fusion proteins, FRET can be determined by directly measuring the ratio of intensities of acceptor and donor emissions. The spectrum of intracellular ECFP (Fig. 5.4) shows a large emission peak around 476 nm and a small shoulder around 505 nm, which is characteristic for ECFP. The ratio of intensities at 527 nm and 458 nm was found to be $(0.51 \pm 0.05, n=20)$ for control cells, transfected with ECFP only. The spectra and emission ratio of the co-transfected ECFP and EYFP proteins ($0.55 \pm 0.05, n=25$) and the CA₂₅Y constructs ($0.58 \pm 0.04, n=25$) were similar. However the emission spectrum of CA₈Y has been shifted towards 525 nm and the emission ratio was 2.1 ± 0.8 ($n=25$) clearly indicating the presence of FRET. Similar experiments have been carried out *in vitro*. Measurements in microslides filled with purified protein yielded similar results.

FRET-FCM

Since FRET results in the sensitised emission of the acceptor molecule it might be possible to detect acceptor-specific fluctuations upon energy transfer. Therefore, ECFP was excited at 458 nm and the detected fluorescence was filtered by a 525DF35 bandpass filter, optimised for YFP detection. However, a major drawback in using the CFP-YFP pair in FCM is the relatively high cross-talk. In the experimental set-up used here, emission of ECFP in the YFP detection channel accounts for approximately 25-30% of the intensity detected in the CFP channel, using a 470-500 bandpass filter. Hence, careful calibration experiments are required

to correct for bleed-through of the donor. Direct excitation of EYFP using the 458 nm excitation line was very inefficient resulting in a fluorescence intensity indistinguishable to that of the background and thus acceptor cross-talk could be neglected. The FRET-FCM experiments for the CA_nY proteins suffered from low donor fluorescence intensities. Therefore measurement times of 10 minutes were required to acquire a curve for CA₈Y as is presented in figure 5.5. The diffusion coefficient retrieved is identical to the value found for EYFP excited at 514 nm. However, to validate that the observed fluctuation is not caused by an inadequate bleed-through correction, negative controls of binary mixtures of ECFP and EYFP were tested. The retrieved curves had no autocorrelation amplitude after bleed-through correction, ensuring that the observed fluctuation is related to FRET. Measurements of the CA₂₅Y protein required sampling times of several hours to achieve curves of similar quality to those of CA₈Y. The molecular brightness can be determined from FCS measurements by dividing the average intensity by the retrieved number of molecules. Since the excitation intensities were kept below 5 kW.cm⁻², no significant non-linear response due to saturation of triplet state build-up could be observed either in the donor or in the acceptor channels. However, the low quality of the FCS-curves did not allow a good determination of the molecular brightness of the acceptor molecule. Therefore it was not possible to estimate the absolute value for the FRET efficiency, according equation 5.2. Moreover, the high donor emission crosstalk and the complex photophysics of both acceptor and donor molecules severely complicates this type of FRET-analysis. Additional problems arose when the FRET-FCM measurements were acquired in the living protoplast. Due to the low number of detected photons relative to the background (SNR < 2), no autocorrelation curve was build. Since ECFP is relative sensitive to photobleaching increasing the laser power is a tempting but not effective method to increase the SNR. Moreover, the photon statistics were too low for PCH analysis.

Time-resolved fluorescence anisotropy measurements yielded a rotational correlation time $\phi_R = 16.8 \pm 0.3$ ns and 17.0 ± 0.3 ns for CA₈Y and CA₂₅Y, respectively. The correlation times are significantly smaller than expected for a protein twice the size of a single ECFP molecule ($\phi_R = 13$ ns). Similar observations have been observed for a single chain antibody domain fused to EGFP via a linker of 3 alanine residues (Hink et al., 1999). A hinge motion through the linker peptide could explain the relatively fast anisotropy decay.

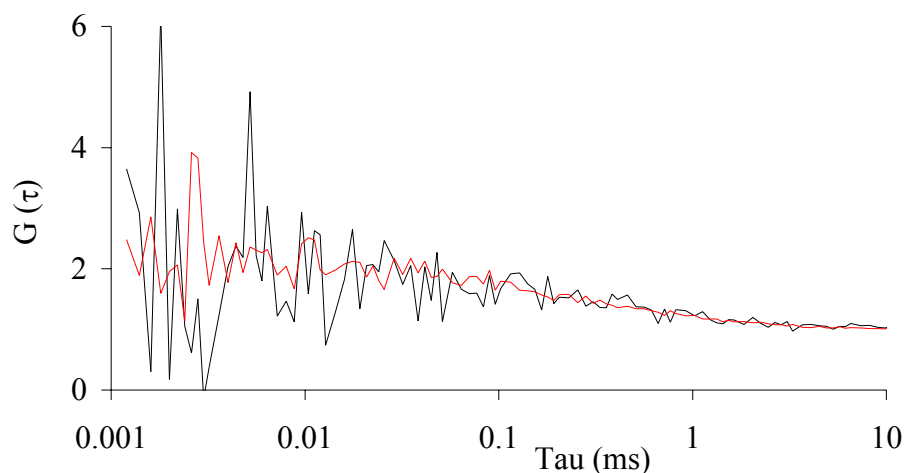


Figure 5.5: Typical FRET-autocorrelation curves for samples of 50 nM purified CA₈Y (red line) and CA₂₅Y (black line) in 50 mM PBS pH 7.5, at excited using the 458 nm laser line at 10 kW.cm⁻². The fluorescence has been detected using a 525DF35 bandpass filter. The curves were corrected for ECFP cross-talk. Measurement time was 12 and 45 minutes for CA₈Y and CA₈Y, respectively.

Dual-color FCCM

Dual-color FCCM is a technique based upon analysing the coincidence of two fluorophores (Fig 1.2) and so FRET is not a prerequisite to monitor molecular interactions here. Hence, it is possible to monitor large complexes where the fluorophores are separated by distances much larger than the Förster radius. *In vitro* measurements of ECFP resulted in autocorrelation curves in both detection channels giving rise to a cross-correlation curve as well, due to the crosstalk of the ECFP emission into the YFP detection channel. The amplitudes and decay times of the three curves were used to determine the size of the CFP, YFP and cross-correlation detection volumes (V_C , V_Y & V_{CY}) (Schwille et al., 1997; Rigler et al., 1999).

In the experimental configuration used, the ratio of the YFP and CFP detection volumes was $V_Y/V_C = 1.4$ and the amount of cross-talk of ECFP was 30%. In order to determine the number of dual colored fusion proteins (N_{CAY}), the cross-correlation curve was fitted to equation 5.7:

Table 5.2: Fluorescence detection efficiencies of ECFP and EYFP expressed as molecular brightness. Values were obtained by PCH analysis of the measurements ($t_s=60$ sec, $I=2.5$ kW.cm⁻²) in the cytoplasm of transfected cowpea protoplasts ($n=40$). Values were corrected for background contributions.

Dye	Molecular brightness η (kHz/molecule)			
	CFP Detector	YFP Detector	CFP Detector	YFP Detector
	λ_{exc} 458 nm	λ_{exc} 514 nm	λ_{exc} 458 nm	λ_{exc} 458 nm
ECFP	5.9 ± 0.3	0.0 ± 0.0	1.8 ± 0.1	0.1 ± 0.0
EYFP	0.0 ± 0.0	0.0 ± 0.0	0.3 ± 0.0	4.9 ± 0.2

$$G_{CY}(0) = 1 + \frac{N_{CAY} + \left(\frac{1}{G_{CFP}(0) - 1} \right) \left(\frac{\eta_{YCC}}{\eta_{YYY}} \right)}{\left(\frac{1}{G_{CFP}(0) - 1} \right) \left(\frac{1}{G_{YFP}(0) - 1} \right)} \quad (\text{Eq. 5.7})$$

where $G_{CFP}(0)$ and $G_{YFP}(0)$ are the amplitudes of the autocorrelation curves for the CFP and YFP detection channels after correction for non-correlated background and $\eta_{\text{detection, dye, excitation}}$ represents the molecular brightness of the dye at a given excitation wavelength and detection channel (see Table 5.2 for an overview). The FCCM measurements of the CA_nY in cowpea protoplasts were successful (Fig 5.6) since cross-correlating particles were observed after background and cross-talk correction.

The accuracy and sensitivity of the system to detect the cross-correlated product was tested by measuring CA_8Y samples in a concentration range of 10 pM-10 μM . The CA_8Y could be detected (within a measurement time of 5 minutes) between 0.8 nM and 2.5 μM . The selectivity has been tested by a titration of CA_nY with free ECFP or EYFP (Fig. 5.7), where the total amount of fluorescent particles remained 80 nM. The cross-correlated product could be detected accurately (confidence interval of 98%) down to a molar fraction of 4 mol% for the EYFP titration and 7 mol% for the ECFP titration. Analysis of the autocorrelation curves according to a two-component diffusion model was less precise and accurate below 30 mol%.

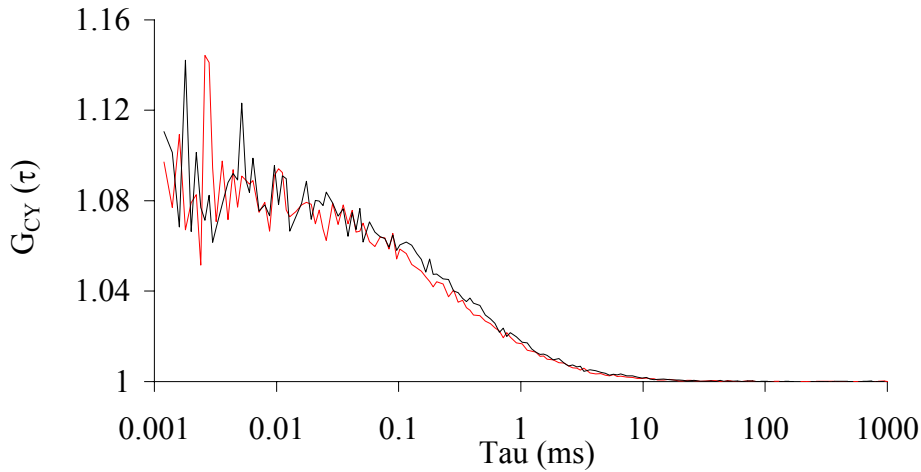


Figure 5.6: Cross-correlation curves of CA_8Y (gray) and $CA_{25}Y$ (black) expressed in the cytoplasm of transfected cowpea protoplasts. The curves have been calculated from the intensity traces acquired during 2 minutes in the CFP and YFP detection channels and were corrected for donor crosstalk and the non-correlated background fluorescence.

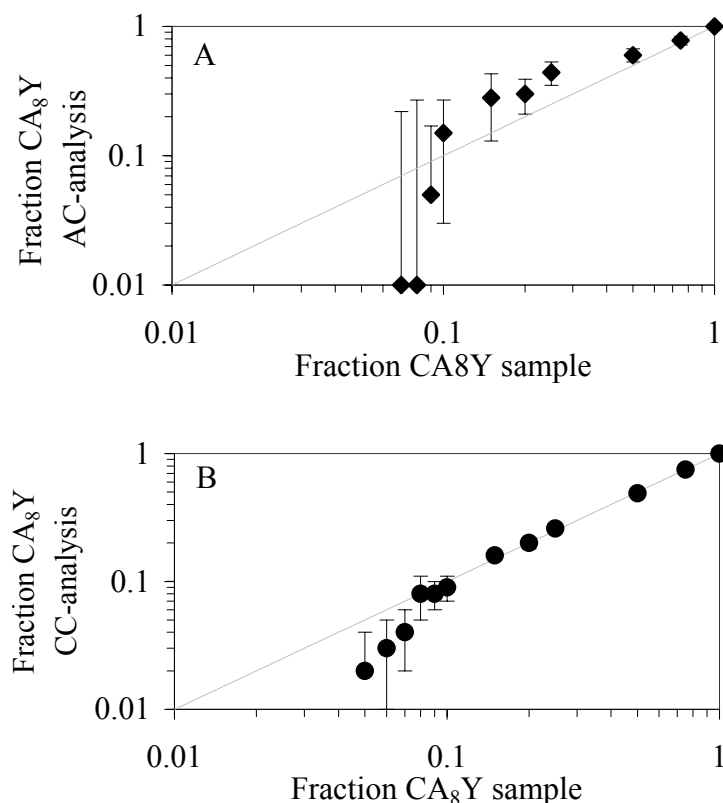


Figure 5.7: Titration of CA₈Y with purified ECFP. The total amount of protein was held constant at 80 nM. The amount of fusion protein was calculated via autocorrelation analysis of the CFP channel according to a two-species diffusion model (A) (Eq. 1.10) using a fixed value for the CFP diffusion time, or by cross-correlation analysis (B) (Eq. 1.21). The gray line represents the ideal situation that all added fusion proteins are retrieved from analysis. Bars indicate the 98% confidence interval.

Conclusion

The fluorescent proteins have changed plant cell biology completely since the difficulties associated with protein labelling, purification and cellular uptake of the protein into the plant cell can now be circumvented by fusing the FP genetically to the protein of interest. From the range of spectral variants, EBFP and DsRed are not suitable for use in fluctuation spectroscopy in living cowpea cells due to the relatively low quantum yield (EBFP), sensitivity to photobleaching and high level of autofluorescence at the emission wavelength. Although EGFP is the best variant for single color applications due to its high yield and relatively low sensitivity to photobleaching, ECFP-EYFP is the best pair to monitor molecular interactions. The low photon rate of sensitised YFP emission required measurement times above 10 minutes. FRET-FCS in cowpea protoplasts using the CFP-YFP pair was not successful since hardly any signal above background was detected due to the severe light-scattering. Although the FRET efficiency of the CA₂₅Y protein was too low to be detected via FRET-FCM, FCCM could clearly detect the fusion protein both *in vitro* and *in vivo*.

Materials and Methods

Constructs

The open reading frame of enhanced EBFP (F64L, Y66H, Y145F), ECFP (F64L, S65T, Y66W, N146I, M153T, V163A), EGFP (F64L, S65T), EYFP-Citrine (S65G, V68L, Q69K, S72A, T203Y) cDNA was amplified by the polymerase chain reaction from the full length cDNA and cloned into the pTYB11 vector (New England Biolabs, USA) using the following primers: FPfor (5'GGTGGTTGCTCTTCCAACATGGTGAGCAAGGGCG3') and FPrev (5'GGTGGTGGATTCTTACTTGTACAGCTCG3'). The ECFP-(Alanine)_n-EYFP constructs were created by PCR of EYFP cDNA using an elongated FPfor primer with a 5' alanine sequence of 24 or 75 bp long and an additional 5' *Dra*I cleavage site. ECFP was amplified using an elongated FPrev primer with a 5' *Dra*I cleavage site. His-tag was introduced into the DsRed by PCR of the DsRed construct (Clontech, USA) using the primers:

DsRedfor (5' CATGCCTGCAGGTCGACTCTAGA 3') and DsRedrev (5' GCGGCCGCTAATGGTGATGGTGATGGTGAAGGAACAGATGGTGGCGTCCCT 3') and cloned into PCR2.1 (Invitrogen, USA) and back ligated into the DsRed construct using *Pst*I and *Not*I cleavage sites. The sequence of the GFP gene has been optimised for plant codon usage and in this way a cryptic splice site has been eliminated (Haselhoff et al., 1997). However, in the experiments described here, this sequence has not been used. The pTYB11-FP and DsRed-His constructs were transformed via heatshock into BL21 DE3 and XL1Blue *E. coli* bacteria strains, respectively, for high expression levels. The expression was induced after 3 hours of incubation at 37°C by adding 0.3 mM IPTG. The bacteria were grown overnight at 20°C to obtain soluble protein.

Cell culture and handling

Tobacco BY2 (*Nicotiana tabacum* L. cv. Bright Yellow 2) and cowpea protoplasts were cultured as have been described in Chapter 4.

Transfection

Ten microgram purified plasmid in 30 µl water was added to $0.5-1 \cdot 10^6$ protoplasts in 75-150 µl solution of 0.6 M mannitol, 10 mM CaCl₂ pH 5.5. After gentle mixing 3 ml solution containing 40% (w/v) PEG Mw 6000, 0.6 M mannitol, 0.1 M Ca(NO₃)₂ was added. The protoplast suspension was incubated for 10 seconds under gentle shaking followed by addition of 4.5 ml washing solution consisting of 0.5 M mannitol, 15 mM MgCl₂ and 0.1% MES, pH 5.5 in order to stop the transfection. After incubation at room temperature for 20 minutes the cells were washed three times and incubated for 24 hours in petridishes at room temperature under constant illumination.

Purification of FP's

The fluorescent proteins, except for DsRed, were purified using the IMPACT™ (New England Biolabs, USA) system, which utilizes the inducible self-cleavage activity of an intein splicing element to separate the target protein from the affinity tag. Transformed bacteria were collected by centrifugation and resuspended in 50 mM Tris pH 8.0, 120 mM KCl, 1 mM EDTA. Cells were lysed by passage through a French pressure cell. Soluble protein was obtained after centrifugation at 20000*g for 30 minutes. Using an affinity column matrix of chitin beads purified the fusion protein. The fusion protein bound to the chitin and after extensive wash, the FP's were eluted from the column by incubating the beads overnight in 50 mM DTT. The DsRed protein carried a His-tag and isolation of the protein was performed according to the standard Ni-NTA procedures. The purity of the protein was checked on SDS-PAGE and was estimated to be at least 95% pure. Protein concentrations were determined from absorbance measurements.

Fluorescence spectral imaging microscopy

Fluorescence spectral imaging microscopy (FSPIM) (Goedhart et al., 2000) experiments were executed as have been described in chapter 4. Fluorescent spectral images were acquired using, a bandpass excitation filter (Omega), a 430DCLP dichroic mirror (Omega) and a 455 longpass emission filter (Schott). Microslides filled with 1 μ M purified protein or single protoplasts placed on object glasses were aligned across the entrance slit of the spectrograph. The cytoplasmic regions within the cell were selected for spectral analysis.

Fluorescence excitation and emission spectra

The steady-state fluorescence spectra were obtained with a Spex-Fluorolog 3.2.2 spectrofluorometer. Both excitation and emission spectra were corrected for (slit widths 1 nm in excitation and 2 nm in emission). Only for GFP at pH 5 and lower the background arising from buffer had to be subtracted from the GFP fluorescence. Buffer solutions of desired pH were prepared by adding predetermined aliquots of 1 N HCl. The GFP concentration in all these experiments was 50 nM.

Fluorescence lifetime measurements

Fluorescence lifetime experiments were carried out using a picosecond laser system and time-correlated single photon counting as described in detail in chapter 3. The excitation wavelength was 432 nm (coumarin 150 dye as laser medium, pumped by a mode-locked Nd-YLF laser) and the fluorescence was selected by using a Balzers bandpass filter (K50) in conjunction with a GG448 cut off filter (both filters were from Schott, Mainz, Germany).

Microscopy

The fluorescence fluctuation experiments were carried out with a Confocor2/LSM510 microscope (Carl Zeiss, Germany) as have been described in detail in Chapter 1. CFP and/or YFP were excited with the 458 nm or 514 nm line of an Argon-ion laser. The fluorescence was separated from excitation light by both a dual dichroic filter, reflecting both the 458 and 514 nm lines, and a secondary dichroic filter, LP510, to separate the emission into two different detection channels. The fluorescence emission was selected by bandpass filters (BP470-500 for CFP and BP527-562 for YFP, respectively) passed the size adjustable pinholes, set at a diameter of 30 μm (CFP-channel) and 40 μm (YFP-channel) before detection on avalanche photodiodes (Perkin Elmer, USA). The system was calibrated using purified YCam3.1 protein (Miyawaki et al., 1999) in PBS buffer pH 7.5, containing 1 mM EGTA.

Fluorescence fluctuation data acquisition

Measurements were performed in protoplasts 5-9 hours after transfection. Since only 60% of the cells were successfully transfected, those cells were selected which have a fluorescence intensity higher than 20 kHz, well above the highest intensity (12 kHz) observed for the autofluorescence in cytoplasm and cell membrane. The observation volume element was positioned in the cytoplasm or cell membrane that was localized by making a fluorescence intensity scan along the optical (z-) axis. The laser power was set at 3.1 $\text{kW}\cdot\text{cm}^{-2}$ for the 458 nm laser line (CFP) and 2.5 $\text{kW}\cdot\text{cm}^{-2}$ for the 514 nm laser line (YFP) to limit photobleaching, cellular damage and photophysical effects. Typical measurement times were 40-120 seconds.

Data analysis

The photon counting histogram files containing the experimental intensity traces were stored, reformatted and imported into the ISS software package, version 2.55 (ISS, USA). The PCH curves were analysed by a one- or two-species model (Eq. 1.25) to obtain the number of particles (N) and molecular brightness (η). The obtained intensity traces were stored, correlated and analysed in a home-developed software package which allows global fitting with several types of fitting models. Auto- and cross correlation curves were corrected for non-correlating background, according to equation 4.1, in the case of measurements within Cowpea protoplasts. Fitting parameters were averaged over 15-30 different FCS-curves, each obtained in another plant cell.

Acknowledgments

This research was supported by an investment grant from The Netherlands Organization for Scientific Research (NWO) and by a grant from the Earth and Life Sciences Foundation of NWO (ALW-NWO).

6

Fluorescence Fluctuation Analysis of AtSERK1 Oligomerization

Mark A. Hink, Khalid Shah, Sacco C. de Vries and Antonie J.W.G. Visser

Receptor kinases have been shown to play a key role in developmental processes such as cell proliferation, migration and differentiation. The classical model for receptor kinase-activation involves ligand binding-induced dimerization of the receptor. To study the oligomerization state and mobility of *Arabidopsis thaliana* somatic embryogenesis receptor kinase 1 (AtSERK1), a transmembrane protein involved in the embryogenesis of plant cells, AtSERK1-cDNA was fused to that of the enhanced cyan (ECFP) or yellow (EYFP) variant of green fluorescent protein (GFP) and transiently expressed in cowpea protoplasts. Photon counting histogram (PCH) analysis showed that 13% of the total number of labeled AtSERK1 molecules in the plasma membrane is present in dimerized form, while no evidence was found for higher oligomeric complexes. Using dual-color fluorescence cross-correlation spectroscopy (FCCS) it has been shown that both the monomeric as the dimerized form of fluorescent AtSERK1 diffuse in the plasma membrane according to a two dimensional Brownian diffusion model. Although fluorescent lipid molecules can be restricted in their motion along the plasma membrane of cowpea protoplasts, no indication for anomalous diffusion was found for the AtSERK1 fusion proteins.

Introduction

Receptor kinases have been shown to play a key role in developmental processes such as cell proliferation, migration and differentiation. The classical model for receptor kinase activation involves ligand binding induced dimerization of the receptor, resulting in autophosphorylation of both partners in the dimer (Lemon et al., 1994; Schlessinger, 1988). The mechanisms by which plant receptors transduce signals across the cell surface are largely unknown but plant receptors may also dimerize (Williams et al., 1997). Here the oligomerization of the somatic embryogenesis receptor kinase, isolated from *Arabidopsis thaliana* (AtSERK1), is studied. AtSERK1 is expressed during somatic embryogenesis, the process whereby somatic cells can develop into plants via characteristic morphological stages. (Schmidt et al., 1997; Hecht et al., 2001). The predicted primary structure of the AtSERK1 protein (69 kDa) consists of a N-terminal signal peptide followed by a leucine zipper (LZ) domain, 5 LRR units, a proline rich domain, a single transmembrane domain, and the 12 conserved domains of a serine-threonine kinase.

To study AtSERK1 by fluorescence techniques, cDNA has been fused to the cyan (CFP) or yellow (YFP) variant of enhanced green fluorescent protein (GFP) (Tsien, 1998; Conn, 1998) and transiently expressed in cowpea protoplasts. Shah et al. (2001) have shown by confocal imaging that the labeled AtSERK1 fusion protein is localized in the plasma membrane of the transfected protoplasts. These authors showed the potential for oligomerization of the AtSERK1 protein by yeast two-hybrid experiments and measurements of the YFP/CFP fluorescence emission ratio at the membrane of protoplasts, co-transfected with both the CFP- and the YFP-fusion construct. In 15% of the cells this ratio was enhanced due to the interaction of AtSERK1-CFP with AtSERK1-YFP, resulting in fluorescence resonance energy transfer (FRET) (Förster, 1948; Stryer, 1978; Tsien, 1993) (also see Chapter 5). Elimination of the extracellular LZ domain reduced the YFP/CFP emission ratio to control levels indicating that without the LZ Domain AtSERK1 is monomeric. Threonine residue 463 may play a key role in oligomerization and therefore point mutations were introduced to elucidate its effect. Although FRET provides a molecular proximity assay with nanometer-scale resolution, techniques to visualize FRET with high spatial resolution such as confocal imaging (Gordon et al., 1998; Xia et al., 2001) and fluorescence lifetime imaging microscopy (FLIM) (Gadella et al., 1999; Bastiaens and Squire, 1999) require a large amount of fluorescently tagged molecules ($> 1\mu\text{M}$) which may be well above physiologically relevant concentrations. In addition, it is difficult to retrieve information about the number of monomers found in the oligomeric complexes. However, techniques like photon counting histogram (PCH) (Chen et al., 1999) and fluorescence correlation spectroscopy (FCS) (Hess et al., 2002) can provide this information at a single-molecule detection level. Both techniques have been described extensively in Chapter 1. Briefly, the fluorescence intensity is monitored in a small observation volume that is continuously illuminated. A particle with a given

molecular brightness produces an intensity fluctuation as it passes the observation volume. Particles with a higher molecular brightness will result in stronger intensity fluctuations. Since small particles will diffuse more rapidly through the observation volume than large molecules, the duration of the fluorescence bursts contain information on the diffusion speed of the particles. Both PCH and FCS analysis use the same experimental data, but each technique focuses on a different property of the signal. While FCS is a measure of the time-dependent decay of the fluorescence fluctuations, PCH calculates the amplitude distribution of these fluctuations. Müller *et al.* (2000) showed that PCH analysis is capable of resolving particles with a brightness ratio of two. Therefore PCH should have the sensitivity to resolve the number of AtSERK1 proteins present in the oligomeric complexes, since oligomers consisting of n monomers are expected to be n times as bright as the monomer. In recent years FCS has been applied successfully to distinguish molecular species based on their diffusion coefficients (for a review see Hess *et al.*, 2002). Meseth *et al.* (1999) examined the resolving power of FCS to distinguish between different molecular sizes. In case of an unchanged molecular brightness upon interaction, the diffusion coefficients of the particles have to differ at least a factor of 1.6. This corresponds to a molecular weight difference of approximately four, which is required to distinguish the species without prior knowledge of the system. To overcome these limitations Schwille *et al.* (1997) have developed dual-color fluorescence cross-correlation spectroscopy (FCCS). Here two spectrally different fluorescent groups, e.g. green and red emitting dyes, are used, which are each excited and detected by separate light sources and detectors. Molecular interactions can be studied by following the coincidence of the fluorescence fluctuations in the two detectors (Fig. 1.2). The amplitude and decay of the cross-correlation curves correspond directly to the number and dynamics of the complexed particles, that carry both fluorescent dyes. To study the presence and diffusion behaviour of oligomerized AtSERK1, the interaction of AtSERK1-CFP with AtSERK1-YFP, co-transfected in cowpea protoplasts, was monitored by FCCS.

Results

Expression of AtSERK protein

To study AtSERK1 in living plant cells, the cDNA of AtSERK1 has been fused to the DNA sequences of the fluorescent proteins ECFP and EYFP and transfected into cowpea protoplasts. Starting from twelve hours after transfection, the expression levels in 60 ± 12 % of the cells were sufficiently high for imaging by a confocal microscope. The confocal images, acquired in the middle of the spherically shaped protoplast, showed the localization of AtSERK1-CFP (Fig. 6.1A), AtSERK1^{ΔLZ}-CFP and AtSERK1^{T463L}-CFP at the plasma membrane. A lateral intensity scan through the equatorial plane of the protoplast displays two strong fluorescent peaks separated approximately 50 μm from each other, which corresponds

to the average diameter of a protoplast. The fluorescence intensity in the cytoplasm, vacuole and nucleus was similar to the values obtained in non-transfected cells. The labeling pattern is similar to a protoplast loaded with the membrane marker BODIPY FL-HPC and it is therefore concluded that the two peaks represent the plasma membrane at the left and right border of the protoplast. *AtSERK1^{kin}*-CFP, lacking the transmembrane and extracellular domains, is localised in the cytoplasm (Fig. 6.1B). The expression pattern is similar to that found in protoplasts expressing (non-targeted) CFP. However, in contrast to *AtSERK1^{kin}*-CFP, the small cytosolic CFP is able to enter the protoplast nucleus. The level of expression and the localisation of the proteins was found to be independent on the type of fluorescent protein used for labeling.

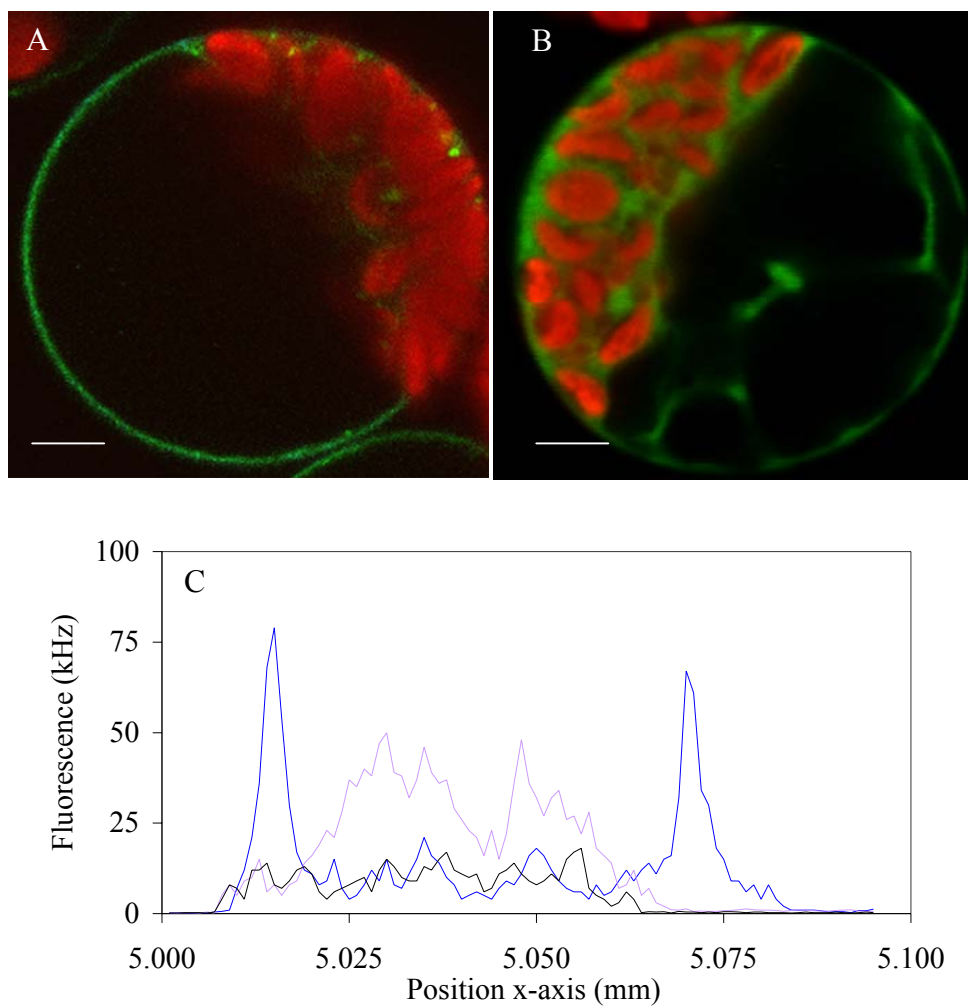


Figure 6.1: Fluorescent confocal images of CFP-labeled *AtSERK1* protein expressed in cowpea protoplasts, 16 hours after transfection. (A) *AtSERK1*, (B) *AtSERK1^{kin}*. The confocal images were acquired in the equator of the protoplast, by accumulating four sub-images (512*512 pixels, 1.3 seconds per sub-image) with a focused laser beam set at 2.5 kW.cm⁻². The bar represents 10 μ m. (C) Lateral intensity scans in the equator of cowpea protoplasts expressing *AtSERK1*-CFP (blue line) or *AtSERK1^{kin}*-CFP (cyan line). The intensity profile of non-transfected cells is indicated by the black line.

Photon counting histogram analysis of labeled AtSERK1 proteins

AtSERK1 forms oligomeric structures in the plasma membrane (Shah et al., 2001) but the exact composition of these aggregates was not known. Photon counting histogram analysis can retrieve this composition on basis of differences in molecular brightness between singly labeled monomers and multiply labeled complexes. To detect the fluorescence fluctuations of the AtSERK proteins, the observation volume was positioned in the upper plasma membrane of the transfected protoplasts, after checking the fluorescence intensity profile along the optical (z-) axis. Measurements of free fluorescent protein and AtSERK^{kin} were performed in the cytoplasm. Since PCH, like FCCS, is a technique analysing the relative fluorescence fluctuations an upper concentration limit exists above which no information can be retrieved. The lower concentration limit is set by the number and relative brightness of background components like endogenous autofluorescent molecules. The concentration fluorescent dye used in fluctuation spectroscopy is typically 100 pM-1 μ M *in vitro*, but in cowpea protoplasts a lower concentration of 5 nM is required to detect CFP or YFP in the cytoplasm. Here, the fusion constructs were expressed under control of the strong 35S promoter that leads to high levels of expressed protein (>1 μ M). Although this is sufficient for standard fluorescence imaging techniques like confocal imaging, the concentration fluorescent label is too high for fluctuation analysis. An alternative possibility to control the level of expressed protein, besides photobleaching of the excess of fluorescent protein, is the use of inducible promoters such as the tetracycline or ethanol promoters. The expression level of the gene can then be manipulated by varying the concentration of the inducer, which may even allow to perform an *in vivo* 'titration' of one type of molecule to another type (*i.e.* titration of AtSERK1-CFP to a constant amount of AtSERK1-YFP). To identify the time-window where the expression level of fluorescent AtSERK1 is optimal for fluctuation analysis, the molecular brightness and autocorrelation amplitude, $G(0)$, have been monitored over time. $G(0)$ minus one is related to the inverted number of fluorescent particles in the observation volume and thus a measure for the concentration of fluorescent particles. In the first five hours after transfection the acquired autocorrelation curves have very low signal to noise ratios (SNR) and low correlation amplitudes. PCH analysis of these data traces according to a single species model identified a high number of molecules with a low molecular brightness as source for the intensity fluctuations. The fluctuations observed are caused by the presence of a large number of dim, autofluorescent molecules. No indication for the presence of the relatively bright AtSERK1-CFP was found. However, after 5 hours the quality of the autocorrelation and PCH curves improved significantly. After 9 hours the normalized autocorrelation amplitude was approximately equal to 1 and the PCH histogram approached Poissonian behaviour. This indicates that at the expression levels of fluorescent AtSERK1 protein were so high that no information could be retrieved from the fluctuation analysis. Therefore, fluctuation experiments in transfected protoplasts were performed between 5-9 hours after transfection.

The intensity of CFP, YFP and the fluorescently labeled AtSERK1 proteins remained stable over time and no intensity drift was observed as have been reported for EGFP in HeLa cells (Chen et al., 2001). The photon counting histograms were analysed according to a model assuming the presence of a single species (Eq. 1.23). The reduced $\chi_{\delta n}^2$ (Eq. 6.2) indicates the quality of the fit model used. Values of $\chi_{\delta n}^2$ lower than one indicate that the data statistics are not sufficient to resolve the species completely, whereas a $\chi_{\delta n}^2$ larger than one indicates that more species than assumed in the fitting model are present (Müller et al., 2000). The single-species fits led to a good description of the experimental histograms for CFP, YFP and the fluorescently labeled AtSERK1 (Fig. 6.2), AtSERK1^{ΔLZ}, AtSERK1^{kin} and AtSERK1^{T463L}. The normalized residuals produced by the fits are close to one and distributed randomly and the fits yield a $\chi_{\delta n}^2$ around 0.9 indicating the proper choice of fitting model. Since the contribution of background in the plasma membrane and cytoplasm (in the regions lacking chloroplasts) was low, no background correction was required (Table 6.1).

Table 6.1: Photon counting histogram analysis of the AtSERK1 proteins labeled with CFP or YFP, expressed in cowpea protoplasts. The molecular brightness, η , and number of molecules, N , were retrieved by PCH analysis from the data acquired in the CFP and YFP detection channels. All PCH curves were fitted according to a single-species model, except for the data of AtSERK1 that had to be fitted by a two-species model to obtain a satisfactory fit. The standard deviations represent the variation of the parameter over different experiments (n=40).

Construct	$\eta_{\text{CFP chan}}$ (kHz/mol)	$N_{\text{CFP chan}} (-)$	$\eta_{\text{YFP chan}}$ (kHz/mol)	$N_{\text{YFP chan}} (-)$
no FP ^{a)}	0.3 ± 0.2	4.0 ± 1.6	0.2 ± 0.0	2.6 ± 0.9
no FP ^{b)}	0.4 ± 0.1	22 ± 16	0.3 ± 0.1	24 ± 12
CFP ^{b)}	6.1 ± 0.6	3.1 ± 0.3		
YFP ^{b)}			5.7 ± 0.5	2.5 ± 0.3
AtSERK1 ^{a)}	5.8 ± 0.3	2.8 ± 0.3	6.1 ± 0.4	2.6 ± 0.4
(2 nd component)	12.3 ± 0.5	0.39 ± 0.05	11.2 ± 0.8	0.36 ± 0.07
AtSERK1 ^{ΔLZ a)}	6.3 ± 0.2	3.5 ± 0.6	6.0 ± 0.2	3.0 ± 0.4
AtSERK1 ^{kin b)}	6.0 ± 0.5	2.7 ± 0.3	6.1 ± 0.6	2.7 ± 0.3
AtSERK1 ^{T463L a)}	6.1 ± 0.6	3.0 ± 0.2	5.7 ± 0.6	2.6 ± 0.3
CAAX ^{a)}	6.0 ± 0.6	4.0 ± 0.3	5.5 ± 0.4	2.5 ± 0.3

^{a)} Experiments in the plasma membrane.

^{b)} Experiments in cytoplasmic regions lacking chloroplasts.

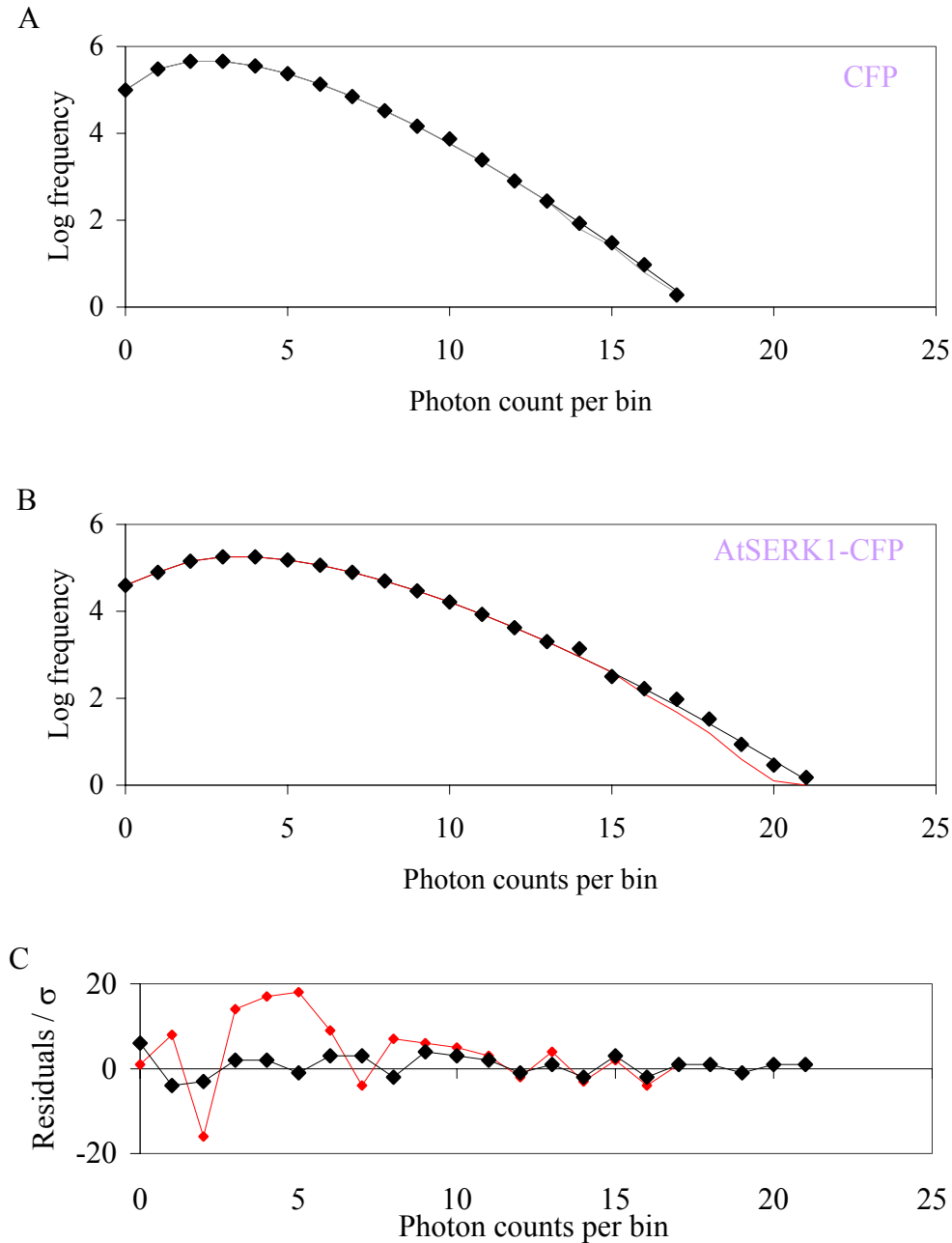


Figure 6.2: Representative photon counting histogram derived from the CFP fluorescence trajectory that has been measured in the cytoplasm of a protoplast expressing CFP (A) and in the upper plasma membrane of a protoplast expressing AtSERK1-CFP (B). The lines represent the fits to a single-species model (red line) or a two-species model (black line). (C) The normalized residuals between fitted and experimental data in panel B indicate the quality of the fit for both models.

The molecular brightness of CFP measured in the cytoplasm yields 6.1 ± 0.6 kHz per molecule and is similar for all the CFP-fusion proteins used in this study. However, the PCH of fluorescent AtSERK1-CFP required a multi-component model to fit the data, since the reduced standard deviation for the single-species model was 16. The two-species fit resulted in a χ^2_{red} of 0.8 with randomly distributed residuals (Fig. 6.2C).

Expansion of the fitting model by a third species did not result in an improvement of χ^2 ($\chi^2_{83}=0.8$). The fitting identified a large fraction of molecules (87%) with a molecular brightness of 5.8 ± 0.3 kHz per molecule. This value corresponds well to the value obtained from free CFP in the cytoplasm and therefore this fraction represents the AtSERK1 monomers. The second fraction of molecules (13%) had a brightness value of approximately twice the value of the large fraction, representing the dimerized form of AtSERK1-CFP molecules (12.3 ± 0.5 kHz.molecule⁻¹). In addition, similar results have been observed for the AtSERK1-YFP proteins: $\eta_1 = 6.1 \pm 0.4$ (88%) and $\eta_2 = 11.2 \pm 0.8$ kHz per molecule (12%). The other fusion proteins gave rise to photon count distributions that could be fitted by single-species models with a brightness value corresponding to the one found for free CFP. Therefore it was concluded that the mutations or deletions in AtSERK1^{ΔLZ}, AtSERK1^{kin} and AtSERK1^{T463L} prevent the receptor to dimerize.

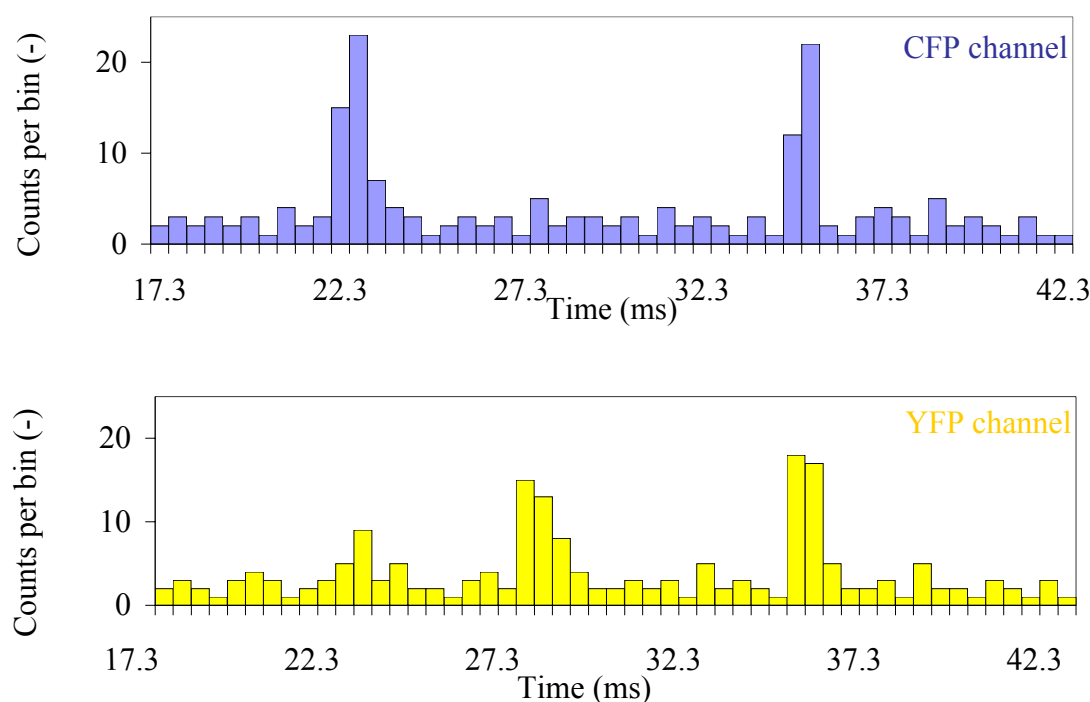


Figure 6.3: Real-time observation of molecular interaction of AtSERK1-CFP with AtSERK1-YFP in the upper plasma membrane of cowpea protoplasts, 6 hours after co-transfection. Both panels of the CFP channel (A) and YFP channel (B) show a portion of the detected fluorescence intensity trajectory binned to 500 μ sec per channel. The curves were not corrected for background fluorescence and cross-talk of the CFP fluorescence.

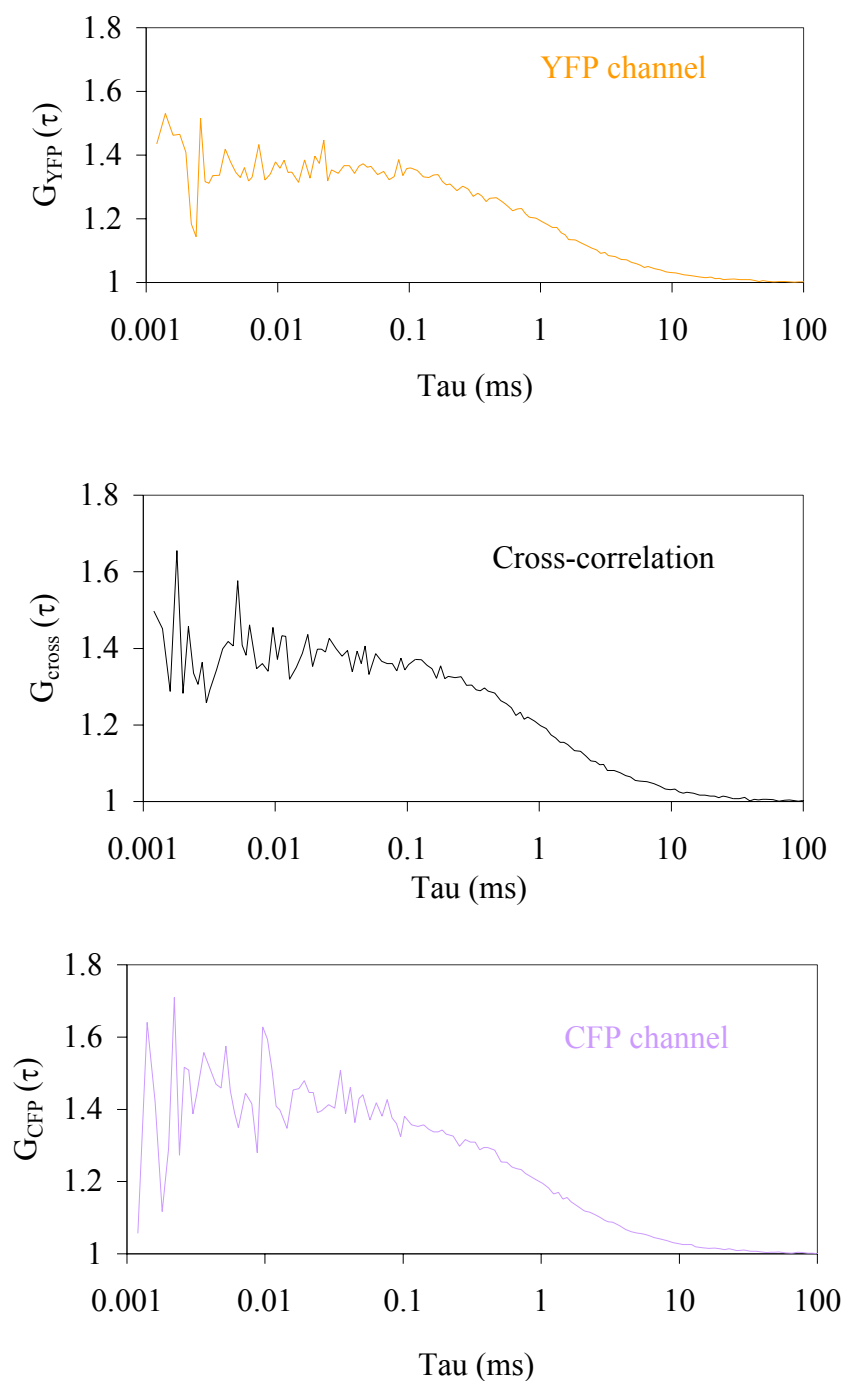


Figure 6.4: Auto- and cross-correlation curves of AtSERK1- CFP and -YFP in the membrane of co-transfected cowpea protoplasts. The curves have been corrected for non-correlating background, cross-talk and differences in the size of the observation volume. The measurement time for these curves was 2 minutes. The curves were analysed according models describing 2D Brownian motion (Eq. 5.5).

Fluorescence (cross-) correlation microscopy of CFP and YFP labeled AtSERK1 proteins

To confirm the presence and monitor the diffusion properties of the oligomeric structures, dual-color fluorescence cross-correlation microscopy was applied to the protoplasts expressing both CFP and YFP fusion proteins. Figure 6.3 displays a representative part of the non-corrected intensity traces of protoplasts co-transfected with AtSERK1-CFP and AtSERK1-YFP. Clearly visible are the intense fluorescent bursts corresponding to the passage of fluorescently labeled AtSERK1 protein molecules through the observation volume. It has been noted that all burst detected in the CFP-channel were accompanied by a simultaneous burst in the YFP channel. This phenomenon is caused by the ‘cross-talk’, the emission of the CFP-fluorophore in the YFP detector due to its long emission tail (Fig. 5.2). The fluorescence intensity ratio in the bursts, F_{YFP}/F_{CFP} , was found to be 0.30 ± 0.12 .

The experimental autocorrelation curves of AtSERK1-CFP and AtSERK1-YFP at the plasma membrane (Fig. 6.4) fitted well to the 2D diffusion model and no multi-component or restricted anomalous diffusion models were required to analyse the data, as have been the case for membrane proteins in other cell types (*i.e.* Harms et al., 2001) and lipid molecules in the cowpea membrane (see chapter 4 of this thesis). When labeled proteins can only form

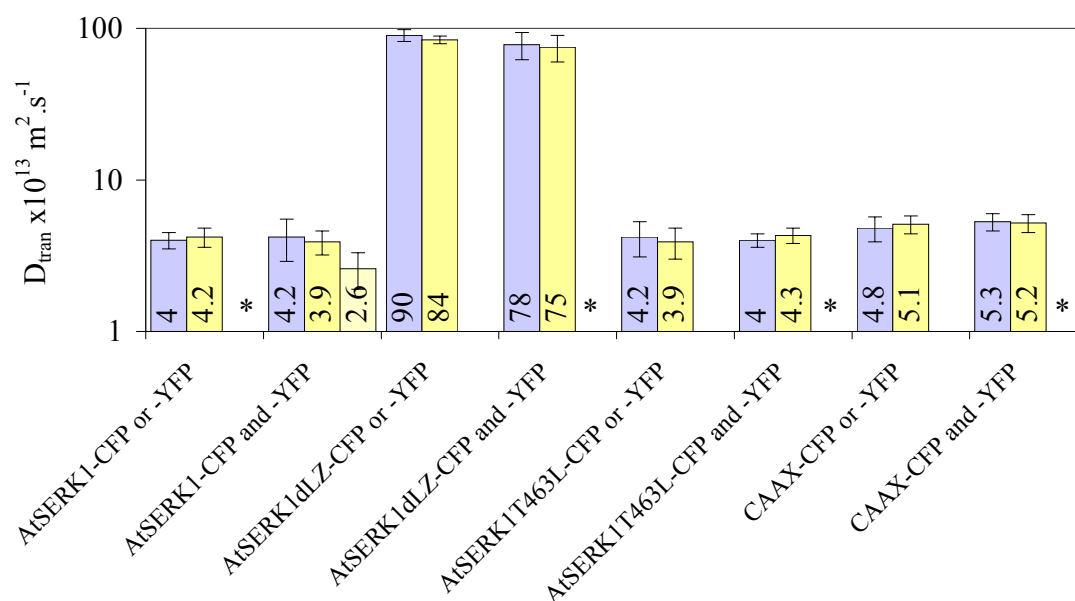


Figure 6.5: Diffusion coefficients of the various AtSERK1 and the membrane-targeted CAAX fusion proteins. The histogram displays three coefficients per construct: the first and second bar are the diffusion coefficients retrieved from fitting the autocorrelation curves of the CFP and YFP detection channels. The third bar presents the diffusion coefficient of the cross-correlation curve when both the CFP and YFP fusion proteins have been co-transfected. An asterisk (*) indicates that in the co-transfected cells no cross-correlating particles have been observed. The values were obtained by fitting the autocorrelation curves of the CFP and YFP traces to equation 5.4 for cytoplasm localized and 5.5 for membrane-localized proteins. The auto- and cross-correlation curves for the co-expressed AtSERK1-CFP and AtSERK1-YFP were fitted according to equation 1.14.

complexes with the molecules labeled with an other fluorophore, the number of complexed proteins can be retrieved from the FCCM-curve according to equation 1.21.

However, in our experimental system the oligomers do not only consist of particles carrying both the CFP and the YFP label, but also multiple CFP or multiple YFP labels can be present. From PCH analysis of singly FP-labeled AtSERK1 it is evident that the observed oligomeric structures of AtSERK1 consist of dimers. Therefore equation 1.21 has to be modified to take into account the presence of CFP-CFP or YFP-YFP labeled dimers. The molecular brightness of these dimers is approximately twice the value of the monomeric form, as has been determined by PCH. Hence, since the contribution of each species to the correlation curve scales with the square root of the brightness the cross-correlation curve reads:

$$G(0) = 1 + \frac{(N_C + N_{CAY} + 4N_{CC}) \left(\frac{\eta_{YCC}}{\eta_{YYY}} \right) + N_{CAY} \left(1 + \frac{\eta_{YCC}}{\eta_{YYY}} \right)}{(N_C + N_{CAY} + 4N_{CC}) \left(N_Y + 4N_{YY} + \left((N_C + 4N_{CC}) \left(\frac{\eta_{CCC}}{\eta_{YYY}} \right) \right) + N_{CAY} \left(1 + \frac{\eta_{YCC}}{\eta_{YYY}} \right) \right)} \quad (\text{Eq. 6.1})$$

Analysis of the AtSERK1 cross-correlation curves yielded $N_{CAY} = 1.0 \pm 0.3$, which corresponds to 7% of the total amount of AtSERK1 protein. Fitting the autocorrelation curves with a two-component 2D Brownian motion model, taking into account the differences in molecular brightness, yielded $N_{CC} = 0.5 \pm 0.1$ and $N_{YY} = 0.4 \pm 0.1$ complexed particles for the CFP and YFP channels, respectively. The sum of these complexed molecules ($N_{CC} + N_{YY} + N_{CAY}$) corresponds to $16 \pm 5\%$ of the total amount of protein, which agrees well with the values obtained from PCH. Therefore it was concluded that 15% of AtSERK1 is present in a dimerized form in the plasma membrane. Spectral imaging of AtSERK1-CFP/YFP fusion proteins at the protoplast membrane have showed that a small percentage of the AtSERK1 protein might exist as oligomers (Shah et al., 2001). It also appeared that there are only certain regions in the plasma membrane where AtSERK1 proteins are not monomeric. This indicates that a minority of the AtSERK1 receptor molecules on the plasma membrane is in a pre-dimerized state. This observation is in line with EGF receptor dimerization in mammalian cells where high affinity EGF receptors (12%) dimerize highly in some regions of the plasma membrane. Based on the quantitative determination of FRET on the EGF receptor in mammalian cells, it was suggested that the high-affinity subclass of receptors is present in a pre-dimerized state in the absence of the ligand. Since it is not known whether ligands that bind to AtSERK1 are present in the growth medium, it is not possible to assign the presence of AtSERK1 dimers to ligand induced dimerization or to pre-associated

receptor molecules. Therefore, identification of the ligand will be essential for determining the exact functioning of AtSERK1. The mutated forms of AtSERK1, AtSERK1^{ΔLZ}, lacking the leucine zipper domain, AtSERK1^{kin}, lacking the transmembrane and extracellular domain and AtSERK1^{T463L} did not result in a cross-correlating complex and therefore it is concluded that these domains and amino acids are essential in dimerization of the AtSERK1 receptor.

The photodynamics of the fluorescent proteins can complicate the analysis. Four processes have been identified that can contribute to the correlation curves besides the diffusion: Triplet state kinetics, pH- and intensity dependent flicker and blinking. The triplet state kinetics can be neglected since at the moderate excitation intensity used in this study only a small fraction of fluorophores will reside in the triplet state. The contribution of the pH-dependent flickering is only small since the fluorescent protein has been attached to the cytosolic C-terminus of AtSERK1. The pH of the cytoplasm lies around 7.3 which implicates that less than 7 % of the molecules is in the protonated dark state. It has been shown (Heikal et al., 2000) that EYFP-Citrine under 488 nm excitation, has a reversible proton binding time of approximately 100 μs at pH 7.3. The relaxation time is a factor of 10 smaller than the diffusion rate observed in our experiments. Therefore, molecules traversing the observation volume will change several times from the bright, deprotonated state to the dark, protonated state. Although this process reduces the number of detected photons, the molecules will be detected. The same holds true for the light-induced dependent flickering, that generates a large dark fraction of 37%. Therefore its contribution can not be neglected. The characteristic flicker rate ($\tau_{\text{photoconv}}^{-1}$) increases linearly with the excitation rate (k_{exc}) at a photoconversion quantum yield $\Phi_{\text{photoconv}} = \Delta(\tau_{\text{photoconv}}^{-1}) / \Delta k_{\text{exc}} = 3.5 \pm 0.6 \cdot 10^{-3}$ at 488 nm excitation (Heikal et al., 2000). Dickson et al. (1997) reported on the blinking of two YFP variants, T203F and T203Y, immobilized in polyacrylamide gels, with a characteristic relaxation time in the order of several seconds. If this behaviour is also present in ECFP and YFP-Citrine, which has been used in this study, this would implicate that it is possible that fluorescent protein are in the dark state when traversing the observation volume. If a dark fluorophore is part of a dimer this would mean that one of the fluorophores is not emitting photons and the doubly labeled dimer can therefore not be recognized as a cross-correlating species that would lead to an underestimation of the number of dimers.

The FRET-process between the CFP and YFP fluorophores is expected to take place on the sub-nanosecond timescale thus the fluctuation of FRET itself cannot be time-resolved with the FCS equipment. However, FRET can be studied by observing the sensitised emission of the acceptor molecule. Single-molecule studies, observing the fluorescence from single immobilized molecules, have reported on the combination of FRET and FCS applied to molecular systems labeled with ECFP and EYFP (Brasselet et al., 2000). However, we were not successful in monitoring FRET-FCS in cowpea protoplast (see chapter 5).

Numerous studies have reported on the capability of FCS to resolve kinetic parameters of the intramolecular dynamics of small biomolecules (i.e. Bonnet et al., 1998). However, many intermolecular processes like association and dissociation of membrane receptors take place on a time scale much longer than the residence time of the complex in the observation volume. A technique related to FCS that has been used to monitor slow processes is image correlation spectroscopy (ICS) (Petersen et al., 1993). ICS uses a confocal laser scanning microscope to collect fluorescence images. Spatial autocorrelation analysis of these images yields the concentration and aggregation state of the molecules. Time-series experiments can provide information on molecular dynamics (Srivastava and Petersen, 1996), but the resolution has been limited to the minimum acquisition time required for collecting the images.

Conclusion

Dual-color FCCM and PCH were successfully applied to study the oligomerization state and mobility of *Arabidopsis thaliana* somatic embryogenesis receptor kinase 1 (AtSERK1) in the plasma membrane of cowpea protoplasts. AtSERK1, a transmembrane protein involved in the embryogenesis of plant cells, has been fused with ECFP or EYFP and transiently expressed in cowpea protoplasts. PCH analysis showed that 13% of the total amount of AtSERK1 fusion protein in the plasma membrane is present in dimerized form, while no indication was found for higher oligomeric complexes. Both the monomeric as the dimerized form of the AtSERK1 fusion proteins diffuse in the plasma membrane according to normal two dimensional Brownian motion, although the diffusion of fluorescent lipid analogues was found to be restricted.

Materials and Methods

Constructs

The AtSERK1 construct was amplified by PCR from AtSERK1 full length cDNA (acc. no: A67827) and cloned downstream of the 35S promoter into the NcoI site of PMON999-YFP (Van Bokhoven et al., 1993) using primers NcoI215f (5' CATGCCATGGTGGAGTCGAGTT ATGTGG 3') and NcoI2068r (5' CATGCCATGGACCTTGGACCAGATAACTC 3') (Shah et al., 2001). The AtSERK1 intracellular kinase domain (AtSERK1^{kin}) was similarly cloned into the NcoI site of pMON999-CFP and pMON999-YFP using primers nAtSERKC 5' CCATCCGATGGGCCCACTAGATATT TTCTT 3' and NcoI2068r. A 60 bp NcoI-KpnI fragment corresponding to the signal sequence of AtSERK1 cDNA and a 1420 bp KpnI-NcoI fragment corresponding to the coding sequence of the AtSERK1 cDNA without the leucine zipper were prepared by PCR using primer pair NcoI215 and KpnI260 5' CAAA TTAGCAGAAGCAAGCCAC 3' and primer pair KpnI420 5' TGGGGAATGCAGAG TTATCTGGC 3' and NcoI2068 respectively. Both were ligated into the NcoI site of

PMON999-CFP/YFP plasmids to create truncated AtSERK1 fusion constructs without the leucine zipper domain (AtSERK1^{ΔLZ}). The fusion constructs AtSERK1-YFP and AtSERK1-CFP were used for replacing tyrosine-230 with single unpaired cysteine-230 in the extracellular domain immediately adjacent to the transmembrane domain. Site directed mutagenesis was performed according to manufacturer's instructions (Stratagene). This resulted in the AtSERK1^{Y230C} constructs. All constructs have been checked by sequence analysis. Control experiments were performed using pMon999, lacking the sequence encoding for a fluorescent protein.

Protoplast isolation

Cowpea mesophyll protoplasts were prepared by peeling off the lower epidermis of the primary leaves of ten days old *Vigna unguiculata*, using forceps. Three leaves were floated on a 15 ml enzyme solution (0.1% cellulase, 0.05% pectinase, 10 mM CaCl₂ and 0.5 M mannitol, pH 5.5) for 3.5 hours at room temperature with gentle shaking. The cells were washed twice by adding 2 ml solution containing 10 mM CaCl₂ and 0.5 M mannitol followed by centrifugation for 5 min at 600 rpm.

Transfection

Ten microgram purified plasmid in 30 μl water was added to $0.5-1 \cdot 10^6$ protoplasts in 75-150 μl solution of 0.6 M mannitol, 10 mM CaCl₂ pH 5.5. After gentle mixing 3 ml solution containing 40% (w/v) PEG Mw 6000, 0.6 M mannitol, 0.1 M Ca(NO₃)₂ was added. The protoplast suspension was incubated for 10 seconds under gentle shaking followed by addition of 4.5 ml washing solution consisting of 0.5 M mannitol, 15 mM MgCl₂ and 0.1% MES, pH 5.5 in order to stop the transfection. After incubation at room temperature for 20 minutes the cells were washed three times and incubated in petri-dishes at room temperature under constant illumination.

Microscopy

The fluorescence fluctuation experiments were carried out with a Confocor2/LSM510 microscope (Carl Zeiss, Germany) as have been described in detail in Chapter 1. The specific adjustments to monitor ECFP and EYFP was described in chapter 5.

Fluorescence fluctuation data acquisition

Measurements were performed in protoplasts 5-9 hours after transfection. Since only 60% of the cells were successfully transfected, those cells were selected that have a fluorescence intensity higher than 12 or 20 kHz in the cell membrane or cytoplasm, respectively, which is above the highest intensity (6 and 12 kHz, respectively) observed for the local autofluorescence. The observation volume element was positioned in the cytoplasm or cell

membrane that was identified by acquiring a fluorescence intensity scan along the optical (z-) axis. The laser power was set at 2.5 kW.cm^{-2} for the 458 nm laser line (CFP) and 3.1 kW.cm^{-2} for the 514 nm laser line (YFP) to prevent photobleaching, cellular damage and photophysical effects. These excitation intensities were still sufficient to achieve reasonable signal to noise ratios (5-10). Typical measurement times were 60-180 seconds.

Photon counting histogram analysis

The files containing the experimental intensity traces were stored, reformatted and imported into the ISS software package, version 2.55 (ISS, USA). The PCH curves were analysed by a one- or two-species model (Eq. 1.25) to obtain the number of particles (N) and molecular brightness (η). To validate the number of species included in the PCH fitting model, PCH traces and fits were exported to Igor Pro (Wavemetrics Inc., USA). Here the algorithm developed by Müller et al. (2000) was used to calculate the quality of the fitting model. The reduced χ_{on}^2 gives a measure of the ability to distinguish between the PCH curves of n and (n-1) species systems:

$$\chi_{\text{on}}^2 = \underset{\{N, \eta\}}{\text{Min}} \frac{\sum_{k=k_{\min}}^{k_{\max}} \left(M \frac{\Pi(k; \overline{N}_1, \overline{N}_2, \dots, \overline{N}_n, \eta_1, \eta_2, \dots, \eta_n) - \Pi(k; \overline{N}_1, \dots, \overline{N}_{n-1}, \eta_1, \dots, \eta_{n-1})}{\sigma_k} \right)^2}{k_{\max} - k_{\min} - d} \quad (\text{Eq. 6.2})$$

Here M is the number of data points, d the number of fitting parameters and k_{\min} and k_{\max} are the minimal and maximal number of photon counts per bin. N_n and η_n represent the number of particles and molecular brightness of the n-th species. σ_k is the standard deviation of finding k counts r times out of M trials and $\Pi(k; N_1, \dots, N_n, \eta_1, \dots, \eta_n)$ are the theoretical nth-species PCH functions. For a complete description see chapter 1.

FCCS analysis

The obtained intensity traces were stored, correlated and analysed in a home-developed software package which allows global fitting with several types of fitting models, using Marquardt least square fitting algorithms (see chapter 1). The quality of the fitting was checked using the minimal value of χ^2 and by visual inspection of the fitted trace and the residuals. Auto- and cross-correlation curves were corrected for uncorrelated background and light-driven photoconversions dynamics according to equations 4.1 and 1.13. The dynamical processes of triplet state conversions and pH-dependent flickering were omitted since experiments have been carried out at moderate excitation levels (Excitation intensity of 2.5 and 3.5 kW.cm^{-2} for and at an intracellular pH between 7 and 8. Fitting parameters were averaged over 25-35 different FCS-curves, each curve obtained in another plant cell.

Acknowledgments

We are grateful to Eugenia Russinova (Laboratory for Molecular Biology, Wageningen University, The Netherlands) for purification of the AtSERK-constructs, Jeroen Pouwels (Laboratory for Molecular Biology, Wageningen University, The Netherlands) for assistance with the protoplast transfections and Jan Willem Borst (MicroSpectroscopy Centre Wageningen, Wageningen University, The Netherlands) for valuable discussions. This work was supported by the Netherlands Council of Earth and Life Sciences (ALW-NWO).

Summarizing Discussion

One of the most intriguing challenges in life sciences is to understand how a complex mixture of molecular particles and structures can make up a living cell. Despite the immense number of studies devoted to unraveling the mysteries of the biological cell, many unanswered questions are left. In recent years a concerted research effort has led to the complete genomic sequence of several organisms. So far, only a fraction of these genes has been related with the biological function of the associated proteins. Moreover, much is unknown about the molecular basis of numerous biological processes such as cell proliferation, differentiation, intra- and extra-cellular communication and apoptosis. To increase our understanding about the complexity of these processes in living cells, experimental data on the spatial-temporal organization of the biomolecules is required.

Microspectroscopic techniques, which rely on fluorescence for detection, are a valuable tool to answer part of these questions. Not only are the methods sensitive, selective and non-invasive, but also they can be used to study living cells. Moreover, some of these techniques provide quantitative information on dynamic processes like molecular interactions at the single-molecule level with a temporal resolution ranging from sub-nanoseconds to days and a spatial resolution of a few hundred nanometers. With regard to the latter, light microscopy is inferior to other techniques such as electron microscopy (Joy and Pawley, 1992) or X-ray microscopy (Jacobson, 1999) which can attain resolutions down to 0.1 nm. However, rigorous sample preparation is required, thereby excluding these techniques for live cell imaging. Applications of scanning force microscopy (SFM) (Engel et al., 1999) and scanning near-field optical microscopy (SNOM) (Lewis et al., 1999), with resolving powers in the order of a few nanometers, are restricted to surfaces which limits their use for measurements in living cells. Therefore, microscopic techniques, and especially those based on fluorescence, are still the most widely used methods for obtaining information on living cells.

The research described in this thesis is devoted to the application of one of these fluorescence techniques, fluorescence correlation spectroscopy (FCS), to intracellular plant research. FCS retrieves information from the fluctuations in the fluorescence intensity that can be observed in a small volume element. The high sensitivity allows measurements under equilibrium conditions at the single-molecule detection level. Moreover, FCS-analysis can

retrieve a large number of parameters, describing the time-dependent decay of the fluctuations, such as the local particle concentration, mobility of the fluorescent particles and rate constants of fast reversible reactions like triplet kinetics and protonation of the chromophore. Hence, it has been recognized that FCS has a high potential to monitor the behaviour of fluorescently labeled biomolecules in living cells at physiological relevant concentrations. Therefore, FCS could be a valuable tool in cell biology, especially in the study of molecular interactions.

The behaviour of fluorescently labeled molecules was first studied in model biochemical systems, before applying FCS to the complex intracellular environment. The binding of an enhanced GFP labeled single chain antibody fragment (scFv-GFP) to its antigen, lipopolysaccharide, present in the outer cell membrane of *Ralstonia solanacearum* bacteria clearly demonstrates the ability of FCS to distinguish particles on basis of the difference in diffusion coefficient. The large number of binding sites on the bacterial wall makes it almost impossible to determine the binding affinity of the scFv-GFP to the LPS, but in simpler experimental systems binding affinity studies have been performed (*i.e.* Rauer et al., 1996; Van Craenenbroek et al., 2000; Chen et al., 2000). Nowadays, pharmaceutical companies utilize this property of FCS to discriminate between unbound ligand and complexed molecules, combined with other modalities of fluorescence in high-throughput screening facilities to identify and test potent drug molecules (Auer et al., 1998; Rudiger et al., 2001; Meyer-Almes, 2001). Although most of these applications concern measurements *in vitro*, cellular screening assays have been developed as well.

Although the characteristic intramolecular hinge motion observed for scFv-GFP by time-resolved fluorescence anisotropy (TRFA) has not been studied in detail, the fusion protein might serve as a simple model system in studying the kinetics of conformational fluctuations in proteins. Other groups have reported on the application of FCS to study conformational changes in fluorescently labeled DNA molecules. By selecting a fluorophore which is sensitive to the local environment (Edman et al., 1996; Wennmalm et al., 1997) or by attaching a quenching moiety to the DNA in the neighbourhood of the fluorophore (Bonnet et al., 1998) temporal changes in the fluorescence intensity might be observed since reversible changes in the conformation lead to a fluctuation of the fluorescence yield of the fluorophore. This dynamic process is visualized in the autocorrelation curve as an additional decay, superimposed on the diffusion decay as long as the characteristic relaxation time of the process is smaller than the residence time of the molecule in the observation volume.

The diffusion coefficients of micelles loaded with a fluorescent phospholipid have been determined by FCS as well as by dynamic light scattering (DLS). The measurements of the micelle hydrodynamic volume using both techniques have been demonstrated to be equivalent. However, the concentration sensitivity of FCS is orders of magnitude higher than that of DLS and is, moreover, able to determine the extremely low critical micelle concentration by measuring the diffusion time as function of detergent concentration.

Intracellular experiments may be complicated by the presence of autofluorescent molecules (Brock et al., 1998). Endogenous molecules like NAD(P)H, flavins and flavoproteins, mainly localized in the mitochondria, fluoresce in the blue and green spectral regions. Although the fluorescence intensity of the autofluorescence is sufficient for digital imaging, as has been demonstrated in biomedical research (Dellinger et al., 1998), in most cell types no FCS analysis could be performed due to the low quantum yield and the high sensitivity to photobleaching of these molecules. Therefore, endogenous autofluorescent molecules are easy to separate as a fraction of dim fluorescent species in PCH analysis. However, plant cells may contain additional molecules like chlorophyll, localized in the chloroplast, and pigment molecules in the vacuole that will not only fluoresce rather strongly but have broad absorption bands as well, able to absorb the fluorescence light emitted by other fluorophores. Hence, either experiments have been carried out in intracellular regions of cowpea protoplasts lacking these compartments or cell types were selected that originate from root tissue and therefore lack many pigment molecules that are responsible for intense autofluorescence. In order to achieve high signal to noise ratios (SNR) without disturbance of autofluorescence, dye depletion or cellular damage, the optimum emission wavelength of the fluorophores should lie between 560 and 610 nm and the excitation intensities in the visible range (458-514 nm) should not exceed 10 kW.cm^{-2} . The diffusion rate of synthetic fluorophores in the cytoplasm and nucleus of the plant cells was retarded by a factor 2 to 4 as compared to buffer due to the viscous intracellular environment. Moreover, FCS was able to distinguish between different types of motion: The diffusion of dyes such as rhodamine green and Cy5 did show a clear deviation from normal Brownian motion in the cytoplasm and the curves could only be fitted according to a multi-component diffusion model or an anomalous diffusion model, indicating the restricted movement of the fluorophores. One reason for this behaviour is the non-specific interactions with (large) cellular structures. As have been shown by Dittrich et al. (2000) labeling molecules with these fluorophores may result that the affinity of the fluorophore to cellular components, influences the dynamics of the labeled molecule as a whole. This may cause non-specific interactions which can lead to non-physiological behaviour. The diffusion of fluorescent lipid analogues in the plant plasma membrane showed a clear deviation from Brownian motion as well, most likely caused by the presence of inhomogeneities in the plasma membrane such as microdomains.

Green fluorescent protein and the large number of variants available have changed microscopic research in (plant) cell biology completely. The possibility to genetically fuse the FP moiety to the protein of interest have replaced the laborious and sometimes inefficient methods of protein labeling, purification and microinjection. On basis of their photophysical characteristics EGFP is the best fluorophore to select for single channel fluctuation spectroscopy experiments and ECFP-EYFP is the best pair to be used in dual-color based methods such as fluorescence resonance energy transfer (FRET) or dual-color fluorescence

cross-correlation microscopy (FCCM). To test the applicability of FRET-FCM using ECFP and EYFP as donor-acceptor pair, fusion proteins of ECFP and EYFP having a linker of 8 or 25 alanine residues (CA₈Y and CA₂₅Y, respectively) were created. Fluorescence lifetime measurements and spectral imaging microscopy yielded FRET-efficiencies of 25% for CA₈Y and only 8% for CA₂₅Y both *in vitro* and *in vivo*. FRET-FCS measurements by autocorrelating the sensitised emission of EYFP suffered from very low fluorescence count rates. Prolonged measurement times and precise bleed-through correction were required to visualize the presence of FRET in the CA₈Y protein. FRET measurements within the plant cells were not successful most likely due to severe scattering of the fluorescence in the plant cells, which further reduced the detected fluorescence intensity.

In order to detect molecular interactions FRET can be used but this technique requires that the acceptor and donor molecules are in close proximity of each other. However, dual-color cross-correlation microscopy (FCCM) does not require a small distance between two fluorophores since the technique has been based upon the coincidence of intensity fluctuations in two different detection channels. This difference can be illustrated with CA₂₅Y. Although some FRET occurred ($E = 8\%$) as have been retrieved from fluorescence lifetime and spectral analysis, autocorrelation of the sensitised acceptor intensity traces did yield a FRET-FCM curve. However, using FCCM the cross-correlation curve for the CA₂₅Y protein was clearly present within 2 minutes. This implies that in studies involving interactions between molecules within large complexes or across the plasma-membrane, where FRET studies might not be possible due to the relatively long distances between the molecules, dual-color FCCM is an attractive alternative.

To study the oligomerization state and mobility of *Arabidopsis thaliana* somatic embryogenesis receptor kinase 1 (AtSERK1), a transmembrane protein involved in the embryogenesis of plant cells, AtSERK1-cDNA was fused to that of ECFP or EYFP and transiently expressed in cowpea protoplasts. Photon counting histogram (PCH) analysis showed that 16% of the total amount of AtSERK1 fusion protein in the plasma membrane is present in dimerised form, while no evidence was found for higher oligomeric complexes. By FCCM measurements it was shown that both the monomeric as the dimerised form of fluorescent AtSERK1 diffuse in the plasma membrane according to a two-dimensional Brownian diffusion model. Although it has been shown that fluorescent lipid molecules can be restricted in their motion along the plasma membrane of cowpea protoplasts, no indication for anomalous diffusion was found for the AtSERK1 fusion proteins.

Prospects

The potential of FCS to monitor molecular interactions between biomolecules at physiologically relevant concentrations has been demonstrated. However, in order to further develop the application of fluctuation techniques in plant research many aspects are still subject of improvement. An important issue is the development of high-quality fluorescent

dyes which preferably have a small absorbance band with a large extinction coefficient and a small emission band combined with a high fluorescence quantum yield. Moreover, the dyes should be less sensitive for photobleaching, do not transfer to dim or dark states and are small in size. However, working with plant systems implies almost always that the extracellular dye has to be introduced into the cell crossing the physical barrier of the cell wall, thus methods that can label the protein via genetic methods, like for FP's, are preferred. To reduce background fluorescence and follow dynamical processes more specifically, caged fluorophores may be used. These probes are non-fluorescent until the caging group is released by photoactivation, usually with a short pulse of ultraviolet light at the desired subcellular location of the cell (Politz et al., 1999). Moreover, Griffin et al. (1998) synthesized a membrane permeant non-fluorescent trivalent arsenic compound which binds to a specific domain of only 6 amino acids long, containing 4 cysteine residues. Upon binding to the domain a fluorescent group is formed. This is a very promising approach to label since it is probable that insertion of 6 amino acids in a helix will have less effect on the activity of the host protein than a fusion with GFP.

In recent years much progress has been made to increase the amount of information that can be retrieved from the collected intensity trace, using approaches used for single-molecule studies. Upon a small extension of the FCS equipment additional parameters such as molecular brightness, fluorescence lifetime, spectral characteristics and anisotropy could be retrieved (Chen et al., 1999; Kask et al., 2000; Palo et al., 2000; Fries et al., 1998; Schaffer et al., 1999, Böhmer et al., 2002). To describe the complicated environmental properties and dynamical processes occurring within the living cell more advanced fit models are required to analyse the experimental data (*i.e.* Gennerich and Schild, 2000).

The ultimate goal in plant science would be to monitor molecular dynamics not only in single living cells but in whole plants. However, scattering of the light, due to the presence of optically dense structures such as the plant cell wall, will drastically reduce the signal to noise ratio, as have been shown in this thesis. The use of a multi-photon excitation (MPE) source could significantly reduce this scattering. Moreover, the higher penetration depth and lower photobleaching of fluorophores in out-of-focus regions could improve the signal quality sufficiently enabling to perform FCS measurements in plant tissues (Schwille et al., 1999b) or even whole plants. Dual-color cross-correlation experiments using two-photon excitation has been developed as well (Heinze et al., 2000). The experimental set-up is much easier to use compared to its one-photon counterpart since the alignment of excitation and detection volumes is much less critical since the fluorescence originates only from the same focal spot (hence, no pinholes are required). Moreover, two-photon absorption bands of fluorophores are in most cases much broader than for one-photon excitation (Xu et al., 1996), which makes it possible to accomplish simultaneous excitation of spectrally distinct dyes using only one excitation wavelength. Hence, it might even be possible to use multicolor

detection in order to study for example the dynamics of biological complexes that consists of several different molecules.

Besides the diffusion characteristics and concentration, the aggregation state of a molecule is an important parameter in biological systems since many biochemical reactions such as signal transduction across the membrane or immune recognition processes are believed to involve protein oligomerization. However, application to slow moving molecules, such as membrane proteins proved to be difficult. Small diffusion coefficients ($<10^{-13} \text{ m}^2 \cdot \text{s}^{-1}$) of these molecules lead to a relatively long residence time in the excitation volume, where the continuous illumination of the fluorophore results in an increased chance of photobleaching. Moreover, this type of experiments requires long measurement times in order to retrieve good quality data, due to the square root dependence of the SNR on the number of sampled fluctuations (Koppel, 1974; Qian, 1990). However, biological samples could change dynamics or position during prolonged measurement sessions. Therefore, Petersen et al. (1993) introduced image correlation spectroscopy (ICS) using a confocal laser scanning microscope. Spatial autocorrelation analysis of the images yields the concentration and aggregation state of the molecules. Time-series of ICS can provide information on molecular dynamics (Srivastava and Petersen, 1996) but the resolution has been limited to the minimum acquisition time required for collecting the images. In recent years the technique has been extended by including options for dual-color cross correlation (Brown et al., 1999), two-photon excitation and video-rate detection (Wiseman et al., 2000).

The spatial resolution of a standard confocal microscope, that is being used for FCS, is limited to several hundred nanometers. The observation volume in the microscope can be approximated by a cylinder with a diameter of $0.5 \text{ } \mu\text{m}$ and a height of ca. $1.5 \text{ } \mu\text{m}$. This implicates that it is not possible to exclusively monitor small or thin subcellular compartments, like the cell membrane, which is ca. 5 nm thick. However, recent developments in optical microscopy have pushed the resolution below the diffraction-limited spot size to approximately 100 nm (Hell et al., 1997) and much progress is obtained in this field. Moreover, smaller observation volumes would allow analysing more concentrated dye solutions as would be the case for the expression of GFP-fusion proteins under control of a 35S promoter.

References

- Akashi, K., H. Miyata, H. Itoh and K. Kinoshita Jr.. Preparation of giant liposomes in physiological conditions and their characterization under an optical microscope. *Biophys. J.* **71**, 3242 (1996).
- Akcakir, O., J. Therrien, G. Belomoin, N. Barry, J.D. Müller, E. Gratton and M. Nayfeh. Detection of luminescent single ultra-small silicon nanoparticles using fluorescence fluctuation spectroscopy. *Appl. Phys. Lett.* **76**, 1857 (2000).
- Ambrose, W.P., P.M. Goodwin, J.H. Jett, A. van Orden, J.H. Werner and R.A. Keller. Single molecule fluorescence spectroscopy at ambient temperature. *Chem. Rev.* **99**, 2929 (1999).
- Aragón, S.R. and R. Pecora. Fluorescence correlation spectroscopy and Brownian rotational diffusion. *Biopolymers* **14**, 119 (1975).
- Aragón, S.R. and R. Pecora. Fluorescence correlation spectroscopy as a probe of molecular dynamics. *J. Chem. Phys.* **64**, 1791 (1976).
- Auer, M., K.J. Moore, F.J. Meyer-Almes, R. Guenther, A.J. Pope and K. Stoeckli. Fluorescence correlation spectroscopy: lead discovery by miniaturized HTS. *DDT* **3**, 457 (1998).
- Axelrod, D., D.E. Koppel, J. Schlessinger, E.L. Elson and W.W. Webb. Mobility measurement by analysis of fluorescence photobleaching recovery kinetics. *Biophys. J.* **16**, 1055 (1976).
- Baird, G.S., D.A. Zacharias and R.Y. Tsien. Biochemistry, mutagenesis and oligomerization of DsRed, a red fluorescent protein from coral. *Proc. Natl. Acad. Sci. USA.* **97**, 11984 (2000).
- Balaban, R.S., I. Kurz, H.E. Cascio and P.D. Smith. Microscopic spectral imaging using a video camera. *J. Micros.* **141**, 31 (1986).
- Bastiaens, P.I.H. and A. Squire. Fluorescence lifetime imaging microscopy: spatial resolution of biochemical processes in the cell, *Trends Cell Biol.* **9**, 48 (1999).
- Beechem, J.M., E. Gratton, M. Ameloot, J.R. Knutson and L. Brand. The global analysis of fluorescence intensity and anisotropy decay data: second-generation theory and programs. *In Topics in Fluorescence Spectroscopy*, Vol. 2, J.R. Lakowicz (ed.), Plenum Press, New York, 241 (1992).
- Benjamin, L. Partial molal volume changes during micellization and solution of nonionic surfactants and perfluorocarboxylates using a magnetic density balance. *J. Phys. Chem.* **70**, 3790 (1966).
- Berland, K.M., P.T.C. So and E. Gratton. Two-photon fluorescence correlation spectroscopy: method and application to the cellular environment. *Biophys. J.* **68**, 694 (1995).
- Berne, B.J. and R. Pecora. Dynamic light scattering, with applications to chemistry, biology and physics. Wiley, New York (1975).
- Böhmer, M., M. Wahl, H.J. Rahn, R. Erdmann and J. Enderlein. Time-resolved fluorescence spectroscopy. *Chem. Phys. Chem Phys.* **353**, 439 (2002).
- Bonnet, G., O. Krichevsky and A. Libchaber. Kinetics of conformational fluctuations in DNA hairpin-loops. *Proc. Natl. Acad. Sci. USA* **95**, 8602 (1998).
- Boonen, G., A. Pramanik, R. Rigler and H. Häberlein. Evidence for specific interactions between a kavain derivative and human cortical neurons measured by fluorescence correlation spectroscopy. *Planta Med.* **66**, 7 (2000).
- Brasselet, S., E.J.G. Peterman, A. Miyawaki, W.E. Moerner. Single-molecule fluorescence resonant energy transfer in calcium concentration dependent cameleon *J. Phys. Chem. A.* **104**, 3676 (2000).
- Brejce, K., T.K. Sixma, P.A. Kitts, S.R. Kain, R.Y. Tsien, M. Ormö and S.J. Remington. Structural basis for dual excitation and photoisomerization of the *Aequorea victoria* green fluorescent protein. *Proc. Natl. Acad. Sci. USA* **94**, 2306 (1997).
- Brochon, J.C. Maximum entropy method of data-analysis in time-resolved spectroscopy. *Methods Enzym.* **240**, 262 (1994).

-
- Brock, R., G. Vamosi, G. Vereb and T.M. Jovin. Rapid characterization of green fluorescent protein fusion proteins on the molecular and cellular level by fluorescence correlation microscopy. *Proc. Natl Acad. Sci. USA* **96**, 10123 (1999).
- Brock, R., M. Hink and T. Jovin. Fluorescence correlation microscopy of cells in the presence of autofluorescence. *Biophys. J.* **75**, 2547 (1998).
- Brown, C.M., M.G. Roth, N.Y. Henis and N.O. Petersen. An internalization-component influenza hemagglutinin mutant causes the redistribution of AP-2 in clathrin free clusters. *Biochemistry* **38**, 15166 (1999).
- Brünger, A.T., D.J. Leahy, T.R. Hynes and R.O. Fox. 2.9 Å resolution structure of an anti-dinitrophenyl-spin-label monoclonal antibody Fab fragment with bound hapten. *J. Mol. Biol.* **221**, 239 (1991).
- Brünger, A.T.. *X-plor, Version 3.1, a system for the X-ray crystallography and NMR*, Yale University Press, New Haven (1992).
- Carson, M.C.. Ribbons 2.0. *J. Appl. Crystallog.* **24**, 958 (1991).
- Chalfie, M., Y. Tu, G. Euskirchen, W. Ward and D. Prasher. Green fluorescent protein as a marker for gene expression. *Science* **263**, 802 (1994).
- Chattoraj, M., B.A. King, G.U. Bublitz and S.G. Boxer. Ultra-fast excited state dynamics in green fluorescent protein: Multiple states and proton transfer. *Proc. Natl. Acad. Sci. USA* **93**, 8362 (1996).
- Chen, Y., J.D. Müller, P.T.C. So and E. Gratton. The photon counting histogram in fluorescence fluctuation spectroscopy. *Biophys. J.* **77**, 553 (1999).
- Chen, Y., J.D. Müller, S.Y. Tetin, J.D. Tyner and E. Gratton. Probing ligand protein binding equilibria with fluorescence fluctuation spectroscopy. *Biophys. J.* **79**, 1074 (2000).
- Chen, Y., J.D. Müller, Q. Ruan and E. Gratton. Molecular brightness characterization of EGFP *in vivo* by fluorescence fluctuation spectroscopy. *Biophys. J.* **82**, 133 (2002).
- Clontech, Living colors fluorescent proteins. www.clontech.com (2002).
- Cluzel, P., M. Surette and S. Leibler. An ultrasensitive bacterial motor revealed by monitoring signaling proteins in single cells. *Science* **287**, 1652 (2000).
- Cody, C.W., D.C. Prasher, W.M. Westler, F.G. Prendergast and W.W. Ward. Chemical structure of the hexapeptide chromophore of the Aequorea green-fluorescent protein. *Biochemistry* **32**, 1212 (1993).
- Conn, P.M. (ed.). Green fluorescent protein. *Methods Enzymol.* **302**, Academic Press, New York (1998).
- Dahan, M., A.A. Deniz, T. Ha, D.S. Chemla, P.G. Schultz and S. Weiss. Ratiometric measurement and identification of single diffusing molecules. *Chem. Phys.* **247**, 85 (1999).
- Delagrave, S., R.E. Hawtin, C.M. Silva, M.M. Yang and D.C. Youvan. Red-shifted excitation mutants of the green fluorescent protein. *Biotechnology* **13**, 151 (1995).
- Dellinger, M., M. Geze, R. Santus, E. Kohen, C. Kohen, J.G. Hirschberg and M. Moniti. Imaging of cells by autofluorescence: a new tool in the probing of biopharmaceutical effects at the intracellular level. *Biotechnol. Appl. Biochem.* **28**, 25 (1998).
- Denk, W., J. H. Strickler and W. W. Webb. Two-photon laser scanning fluorescence microscopy. *Science* **248**, 73 (1990).
- Dickson, R.M., A.B. Cubitt, R.Y. Tsien and W.E. Moerner. On/off blinking and switching behaviour of single molecules of green fluorescent protein. *Nature* **388**, 355 (1997).
- Dittrich, P. and P. Schwille. Photobleaching and stabilization of fluorophores used for single-molecule analysis with one- and two-photon excitation. *Appl. Phys. B* **73**, 829 (2001).
- Dittrich, P., F. Malvezzi-Campeggi, M. Jahnz and P. Schwille. Accessing molecular dynamics in cells by fluorescence correlation spectroscopy. *Biol. Chem.* **383**, 491 (2001).
- Edidin, M.. Lipid microdomains in cell surface membranes. *Cur. Opin. Struct. Biol.* **7**, 528 (1997).
- Edman, L., Ü. Mets and R. Rigler. Conformational transitions monitored for single molecules in solution. *Proc. Natl. Acad. Sci. USA* **93**, 6710 (1996).

- Edward, J.T.. Molecular volumes and the Stokes-Einstein equation. *J. Chem. Educ.* **47**, 261 (1970).
- Eggeling, C., J. Widengren, R. Rigler and C.A.M. Seidel. Photobleaching of fluorescent dyes under conditions used for single-molecule detection: Evidence of two-step photolysis. *Anal. Chem.* **70**, 2651, (1998).
- Eggeling, C., S. Berger, L. Brand, J.R. Fries, J. Schaffer, A. Volkmer and C.A.M. Seidel. Data registration and selective single-molecule analysis using multi-parameter fluorescence detection. *J. Biotechnol.* **86**, 163 (2001).
- Ehrenberg, M. and R. Rigler. Rotational Brownian motion and fluorescence intensity fluctuations. *Chem. Phys.* **4**, 390 (1974).
- Eid, J.S., J.D. Müller and E. Gratton. Data acquisition card for fluctuation correlation spectroscopy allowing full access to the detected photon sequence. *Rev. Sci. Instrum.* **71**, 361 (2000).
- Eigen, M. and R. Rigler. Sorting single molecules: application to diagnostics and evolutionary biotechnology. *Proc. Natl. Acad. Sci. USA.* **91**, 5740 (1994).
- Eigenbrot, C., M. Randal, A.A. Kossiakoff and L. Presta. X-ray structures of the antigen-binding domains from three variants of humanized anti-p185-HER2 antibody 4D5 and comparison with molecular modeling. *J. Mol. Biol.* **229**, 969 (1993).
- Elson, E.L. and D. Magde. Fluorescence correlation spectroscopy. I. Conceptual basis and theory. *Biopolymers* **13**, 1 (1974).
- Elson, E.L. and R. Rigler (eds.). Fluorescence correlation spectroscopy. Theory and applications, Springer, Berlin (2001).
- Engel, A., Y. Lyubchenko and D. Müller. Atomic force microscopy: a powerful tool to observe biomolecules at work. *Trends Cell. Biol.* **9**, 77 (1999).
- Engh, R.A. and R. Huber. Accurate bond and angle parameters for X-ray protein structure refinement. *Acta Crystallogr. A* **47**, 392 (1991).
- Fahey, P.F., D.E. Koppel, L.S. Barak, D.E. Wolf, E.L. Elson and W.W. Webb. Lateral diffusion in planar lipid bilayers *Science* **195**, 305 (1977).
- Fahey, P.F. and W.W. Webb. Lateral diffusion in phospholipid bilayer membranes and multilamellar liquid crystals. *Biochemistry* **17**, 3046 (1978).
- Feder, T.J., I. Brust-Mascher, J.P. Slattery, B. Baird and W.W. Webb. Constrained diffusion or immobile fraction on cell surfaces: A new interpretation. *Biophys. J.* **70**, 2767 (1996).
- Feher, G. and M. Weissman. Fluctuation spectroscopy: determination of chemical reaction kinetics from the frequency spectrum of fluctuations. *Proc. Natl. Acad. Sci. USA* **70**, 870 (1973).
- Fendler, J.H. Membrane mimetic chemistry. Wiley-Interscience, New York (1982).
- Földes-Papp, Z., B. Angerer, P. Thyberg, M. Hinz, S. Wennmalm, W. Ankenbauer, H. Seliger, A. Holmgren and R. Rigler. Fluorescent high-density labeling of DNA: error-free substitution for a normal nucleotide. *J. Biotech.* **86**, 237 (2001a).
- Földes-Papp, Z., U. Demel and G.P. Tilz. Ultrasensitive detection and identification of fluorescent molecules by FCS: Impact for immunobiology. *Proc. Natl. Acad. Sci. USA* **98**, 11509 (2001b).
- Földes-Papp, Z. and R. Rigler. Quantitative two-color fluorescence cross-correlation spectroscopy in the analysis of polymerase chain reaction. *Biol. Chem.* **382**, 473 (2001c).
- Förster, T. Zwischenmolekulare Energiewanderung und Fluoreszenz. *Ann. Phys.* **2**, 55 (1948).
- Fradkov, A.F., Y. Chen, L. Ding, E.V. Barsova, M.V. Matz and S.A. Lukyanov. Novel fluorescent proteins from *Discosoma* coral and its mutants possesses a unique far-red fluorescence. *FEBS Lett.* **479**, 127 (2000).
- Fries, J.R., L. Brand, C. Eggeling, M. Köllner and C.A.M. Seidel. Quantitative identification of different single molecules by selective time-resolved confocal fluorescence spectroscopy *J. Chem. Phys.* **102**, 6601 (1998).

-
- Gadella, T.W.J., Jr. and T.M. Jovin. Oligomerization of epidermal growth factor receptors (EGFR) on A431 cells studied with time-resolved fluorescence imaging microscopy. A stereochemical model for tyrosine kinase receptor activation. *J. Cell. Biol.* **129**, 1543 (1995).
- Gadella, T.W.J., Jr. Fluorescence lifetime imaging microscopy (FLIM): Instrumentation and applications. In *Fluorescent and luminescent probes for biological activity. A practical guide to technology for quantitative real-time analysis. Biological Techniques Series 2*, W.T. Mason (ed.), Academic Press, New York, 467 (1999).
- Gadella, T.W.J., Jr., G.N.M. van der Krogt and T. Bisseling. GFP-based FRET microscopy in living plant cells. *Trends Plant Sci.* **4**, 287 (1999).
- Gennerich, A. and D. Schild. Fluorescence correlation spectroscopy in small cytosolic compartments depends critically on the diffusion model used. *Biophys. J.* **79**, 3294 (2000).
- Goedhart, J., H. Röhrig, M.A. Hink, A. van Hoek, A.J.W.G. Visser, T. Bisseling and T.W.J. Gadella Jr.. Nod factors vintegrate spontaneously in biomembranes and tansfer rapidly between membranes and to root hairs, but transbilayer flip-flop does not occur. *Biochemistry* **38**, 10898 (1999).
- Goedhart, J., M.A. Hink, A.J.W.G. Visser, T. Bisseling and T.W.J. Gadella. *In vivo* fluorescence correlation microscopy (FCM) reveals accumulation and immobilization of Nod factors in root hair cell walls. *Plant J.* **21**, 109 (2000).
- Gordon, G.W., G. Berry, X.H. Liang, B. Levine and B. Herman. Quantitative fluorescence resonance energy transfer measurements using fluorescence microscopy. *Biophys. J.* **74**, 2702 (1998).
- Griep, R.A., C. van Twisk, J.K.C.M. van Beckhoven, J.M. van der Wolf and A. Schots. Fluobodies: green fluorescent single-chain Fv fusion protein. *Phytopathology* **88**, 795 (1998).
- Griffin, B.A., S.R. Adams and R.Y. Tsien. Specific covalent labeling of recombinant protein molecules inside living cells. *Science* **281**, 269 (1998).
- Ha, T., A.Y. Ting, J. Liang, W.B. Caldwell, A.A. Deniz and D.S. Chemla, P.G. Schultz, and S. Weiss. Single-molecule fluorescence spectroscopy of enzyme conformational dynamics and cleavage mechanism. *Proc. Natl. Acad. Sci. USA.* **96**, 893 (1999).
- Ha, T.. Single-molecule fluorescence resonance energy transfer. *Methods* **25**, 78 (2001).
- Harms, G.S., L. Cognet, P.H.M. Lommerse, G.A. Blab and T. Schmidt. Autofluorescent proteins in single-molecules research: Applications to live cell imaging microscopy. *Biophys. J.* **80**, 2396 (2001a).
- Harms, G.S., L. Cognet, P.H.M. Lommerse, G.A. Blab, H. Kahr, R. Gamsjäger, H.P. Spaink, N.M. Soldatov, C. Romanin and T. Schmidt. Single-molecule imaging of L-type Ca²⁺ channels in live cells. *Biophys. J.* **80**, 2396 (2001b).
- Harvey, S.C.. Transport properties of particles with segmental flexibility. I. Hydrodynamic resistance and diffusion coefficients of a freely hinged particle. *Biopolymers* **18**, 1081 (1979).
- Harvey, S.C. and H.C. Cheung. Transport properties of particles with segmental flexibility. II. Decay of fluorescence polarization anisotropy from hinged macromolecules. *Biopolymers* **19**, 913 (1980).
- Haselhoff, J., K.R. Siemering, D.C. Prasher and S. Hodge. Removal of a cryptic intron and subcellular localization of green fluorescent protein are required to mark transgenic *Arabidopsis* plants brightly. *Proc. Natl. Acad. Sci. U.S.A.* **94**, 2122 (1997).
- Haugland, R.P.. Handbook of fluorescent probes and research chemicals. Molecular Probes Inc. (1996).
- Haupts, U., S. Maiti, P. Schwille and W.W. Webb. Dynamics of fluorescence fluctuations in green fluorescent protein observed by fluorescence correlation spectroscopy. *Proc. Natl. Acad. Sci. USA* **95**, 573 (1998).
- Hayward, A.C.. Biology and epidemiology of bacterial wilt, caused by *Ralstonia solanacearum*. *Annu. Rev. Phytopathol.* **29**, 65 (1991).
- Hecht, V., J-P. Vielle-Calzada, M.V. Hartog, E.D.L. Schmidt, K. Boutilier, U. Grossniklaus and S.C. de Vries. The *Arabidopsis* somatic embryogenesis receptor kinase 1 gene is expressed in developing ovules and embryos and enhances embryogenic competence in culture, *Plant Physiology* **127**, 803 (2001).

- Heikal, A.A. S.T. Hess, G.S. Baird, R.Y. Tsien and W.W. Webb. Molecular spectroscopy and dynamics of intrinsically fluorescent proteins: Coral red (dsRed) and yellow (Citrine) *Proc. Natl. Acad. Sci. USA* **97**, 11996 (2000).
- Heim, R., D.C. Prasher and R.Y. Tsien. Wavelength mutations and posttranslational auto-oxidation of green fluorescent protein. *Proc. Natl. Acad. Sci. USA* **91**, 12501 (1994).
- Heim, R., A. Cubitt and R.Y. Tsien. Improved green fluorescence. (1995) *Nature* **373**, 663 (1995).
- Heim, R. and R.Y. Tsien. Engineering green fluorescent protein for improved brightness, longer wavelengths and fluorescence resonance energy transfer. *Cur. Biol.* **6**, 178 (1996).
- Heinze, K.G., A. Koltermann and P. Schwille. Simultaneous two-photon excitation of distinct labels for dual-color fluorescence crosscorrelation analysis. *Proc. Natl. Acad. Sci. USA* **97**, 10377 (2000).
- Hell, S.W. M. Schrader and H.T.M. van der Voort. Far-field fluorescence microscopy with resolution in the 100 nm range. *J. Microsc.* **187**, 1 (1997).
- Henriksson, M., A. Pramanik, J. Shafqat, Z. Zhong, M. Tally, K. Ekberg, J. Wahren, R. Rigler, J. Johansson and H. Jörnvall. Specific binding of proinsulin C-peptide to intact and to detergent-solubilized human skin fibroblasts. *Bioch. Bioph. Res. Com.* **280**, 423 (2001).
- Hess, S.T., S. Huang, A.A. Heikal and W.W. Webb. Biological and chemical applications of fluorescence correlation spectroscopy: A review. *Biochemistry* **41**, 697 (2002).
- Hink, M. and A.J.W.G. Visser. Characterization of membrane mimetic systems. In *Applied fluorescence in chemistry, biology and medicine*. W. Rettig, B. Strehmel and S. Schrader (eds.), Springer Verlag, Berlin, 101 (1998).
- Hink, M.A., A. van Hoek and A.J.W.G. Visser. Dynamics of phospholipid molecules in micelles: characterization with fluorescence correlation spectroscopy and time-resolved fluorescence anisotropy. *Langmuir* **15**, 992 (1999).
- Huang, N., K. Florine-Kasteel, G.W. Feigenson and C. Spink. Effect of fluorophore linkage position of n-(9-anthroyloxy) fatty acids on probe distribution between coexisting gel and fluid phospholipid phases. *Biochim. Biophys. Acta* **939**, 124 (1988).
- Jacobson, C.. Soft X-ray microscopy. *Trends Cell Biol.* **9**, 44 (1999).
- Jankowski, T. and R. Janka. Confocor 2. The second generation of fluorescence correlation microscopes. In *Fluorescence correlation spectroscopy. Theory and applications*, E.L. Elson, and R. Rigler (eds.), Springer, Berlin, 410 (2001).
- Joy, D.C. and J.B. Pawley. High-resolution scanning electron microscopy. *Ultramicroscopy* **47**, 80 (1992).
- Kamiuchi, T., E. Abe, M. Imanishi, T. Kaji, M. Nagaoka and Y. Sugiura. Artificial nine zinc-finger peptide with 30 base pair binding sites. *Biochemistry* **37**, 13827 (1998).
- Kask, P., R. Günther and P. Axhausen. Statistical accuracy in fluorescence fluctuation experiments. *Eur. Biophys. J.* **25**, 163 (1997).
- Kask, P., K. Palo, D. Ullmann and K. Gall. Fluorescence-intensity distribution analysis and its application in biomolecular detection technology. *Proc. Natl. Acad. Sci. USA* **96**, 13756 (1999).
- Kask, P., K. Palo, N. Fay, L. Brand, Ü. Mets, D. Ullmann, J. Jungmann, J. Pschorr and K. Gall. Two-dimensional fluorescence intensity distribution analysis: Theory and applications. *Biophys. J.* **78**, 1703 (2000).
- Kettling, U., A. Koltermann, P. Schwille and M. Eigen. Real-time enzyme kinetics monitored by dual-color fluorescence cross-correlation spectroscopy. *Proc. Natl. Acad. Sci. USA* **95**, 1416 (1998).
- Kim, H.D., G.U. Nienhaus, T. Ha, J.W. Orr, J.R. Williamson and S. Chu. Mg^{2+} -dependent conformational change of RNA studied by fluorescence correlation and FRET on immobilized single molecules. *Proc. Natl. Acad. Sci. USA* **99**, 4284 (2002).
- Kleywegt, G.J. and T.A. Jones. Databases in protein crystallography. *Acta Crystallogr. D* **54**, 1119 (1998).

-
- Kneen, M., J. Farinas, Y. Li and A.S. Verkman. Green fluorescent protein as a noninvasive intracellular pH indicator *Biophys. J.* **74**, 1591 (1998).
- Köhler, R.H., P. Schwill, W.W. Webb and M.R. Hanson. Active protein transport through plastid tubules: velocity quantified by fluorescence correlation spectroscopy. *J. Cell Sci.* **113**, 3921 (2000).
- Koltermann, A., U. Kettling, J. Bieschke, T. Winkler and M. Eigen. Rapid assay processing by integration of dual-color fluorescence cross-correlation spectroscopy: High-throughput screening for enzyme activity. *Proc. Natl. Acad. Sci. USA.* **95**, 1421 (1998).
- Koopman W.J.H., M.A. Hink, A.J.W.G. Visser, E.W. Roubos and B.G. Jenks. Evidence that Ca^{2+} -waves in *Xenopus* melanotropes depend on calcium-induced calcium release: a fluorescence correlation microscopy and linescanning study. *Cell Calcium* **26**, 59 (1999).
- Koppel, D.E. Statistical accuracy in fluorescence correlation spectroscopy. *Phys. Rev. A.* **10**, 1938 (1974).
- Korlach, J., P. Schwill, W.W. Webb and G.W. Feigenson. Characterization of lipid bilayer phases by confocal microscopy and fluorescence correlation spectroscopy. *Proc. Natl Acad. Sci. USA* **96**, 8461 (1999).
- Kretschmann, E. and H. Raether. Surface plasmon resonance. *Z. Naturforsch. A* **23**, 2135 (1968).
- LaClair, J.J. Selective detection of the carbohydrate-bound state of concanavalin A at the single molecule level. *J. Amer. Chem. Soc.* **119**, 7676 (1997).
- Lakowicz, J.R. Principles of fluorescence spectroscopy. Kluwer, New York (1999).
- Lamb, D. C., A. Schenk, C. Rocker, C. Scalfi Happ and G.U. Nienhaus. Sensitivity enhancement in fluorescence correlation spectroscopy of multiple species using time-gated detection. *Biophys. J.* **79**, 1129 (2000).
- Laskowski, R.A., M.W. MacArthur, D.S. Moss and J.M. Thornton. *PROCHECK*: a program to check the stereochemical quality of protein structures. *J. Appl. Crystallogr.* **26**, 283 (1993).
- Lee, J., I.B.C. Matheson, F. Müller, D.J. O'Kane, J. Vervoort and A.J.W.G. Visser. The mechanism of bacterial bioluminescence. In *Chemistry and biochemistry of flavoenzymes*. F. Müller (ed.), Vol. 2, CRC Press, Boca Raton, 109 (1991).
- Lemon, M.A. and J. Schlessinger. Regulation of signal transduction and signal diversity by receptor oligomerization. *Trends Biochem. Sci.* **19**, 459 (1994).
- Lewis, A., A. Radko, N. Ben Ami, D. Palankar and K. Lieberman. Near-field scanning optical microscopy in cell biology. *Trends. Cell. Biol.* **9**, 70 (1999).
- Llopis, J., J.M. McCaffery, A. Miyawaki, M.G. Farquhar and R.Y. Tsien. Measurement of cytosolic, mitochondrial, and Golgi pH in single living cells with green fluorescent proteins. *Proc. Natl. Acad. Sci. USA* **95**, 6803 (1998).
- Lossau, H., A. Kummer, R. Heinecke, F. Pöllinger-Dammer, C. Kompa, G. Bieser, T. Jonsson, C.M. Silva, M.M. Yang, D.C. Youvan and M.E. Michel-Beyerle. Time-resolved spectroscopy of wild-type and mutant Green Fluorescent Proteins reveals excited state deprotonation consistent with fluorophore-protein interactions. *Chem. Phys.* **213**, 1 (1996).
- Magde, D., E.L. Elson and W.W. Webb. Thermodynamic fluctuations in a reacting system: Measurement by fluorescence correlation spectroscopy. *Phys. Rev. Lett.* **29**, 705 (1972).
- Magde, D., E.L. Elson and W.W. Webb. Fluorescence correlation spectroscopy. II. An experimental realization. *Biopolymers* **13**, 29 (1974).
- Maiti, N.C., S. Mazumdar and N. Periasamy. Dynamics of porphyrin molecules in micelle. Picosecond time-resolved fluorescence anisotropy studies. *J. Phys. Chem.* **99**, 10708 (1995).
- Mandel, L. Fluctuations of photon beams and their correlations. *Proc. Phys. Soc.* **72**, 1037 (1958).
- Margeat, E., N. Poujol, A. Boulahtouf, Y. Chen, J.D. Müller, E. Gratton, V. Cavailles and C.A. Royer. The human estrogen receptor alpha dimer binds a single SRC-1 coactivator molecule with an affinity dictated by agonist structure. *J. Mol. Biol.* **306**, 433 (2001).
- Marquardt, D.W. An algorithm for least squares estimation of nonlinear parameters. *J. Soc. Indust. Appl. Math.* **11**, 431 (1963).

- Martínez-Zaguilán, R., M.W. Gurulé and R.M. Lynch. Simultaneous measurement of intracellular pH and Ca^{2+} in insulin-secreting cells by spectral imaging microscopy. *Am. J. Physiol.* **270**, 1438 (1996).
- Matz, M.V., A.F. Fradkov, Y.A. Labas, A.P. Savitsky, A.G. Zaraisky, M.L. Markelov and S.A. Lukyanov. Fluorescent protein from nonbioluminescent Anthozoa species. *Nature Biotechnol.* **17**, 969, (1999).
- McCafferty, J., A.D. Griffiths, G. Winter and D.J. Chiswell. Phage-antibodies: filamentous phage displaying antibody variable domains. *Nature* **348**, 552 (1990).
- Meseth, U., T. Wohland, R. Rigler and H. Vogel. Resolution of fluorescence correlation measurements. *Biophys. J.* **76**, 1619 (1999).
- Meyer, T. and H. Schindler. Particle counting by fluorescence correlation spectroscopy: simultaneous measurement of aggregation and diffusion of molecules in solutions and on membranes. *Biophys. J.* **54**, 983 (1998).
- Meyer-Almes, F.J. Nanoparticle immunoassays: A new method for use in molecular diagnostics and high throughput pharmaceutical screening based on fluorescence correlation spectroscopy. In *Fluorescence correlation spectroscopy. Theory and applications*. E.L. Elson and R. Rigler (eds.) Springer, Berlin, 204 (2001).
- Miyawaki, A., O. Griesbeck, R. Heim and R.Y. Tsien. Dynamic and quantitative Ca^{2+} measurements using improved cameleons. *Proc. Natl. Acad. Sci. U.S.A.* **96**, 2135 (1999).
- Müller, J.D., Y. Chen and E. Gratton. Photon counting histogram statistics. In *Fluorescence correlation spectroscopy. Theory and applications*, E.L. Elson and R. Rigler (eds.), Springer, Berlin, 410 (2001).
- Müller, J.D., Y. Chen and E. Gratton. Resolving heterogeneity on the single molecular level with the photon-counting histogram. *Biophys. J.* **78**, 474 (2000).
- Nagata, T., Y. Nemoto and S. Hasezawa. tobacco BY-2 cell line as the "HeLa" cell in the cell biology of higher plants. *Int. Rev. Cytology* **132**, 1 (1992).
- Neugebauer, J. A guide to the properties and uses of detergents in biology and biochemistry. Calbiochem-Novabiochem International (1994).
- Nomura, Y., H. Takana, L. Poellinger, F. Higashino and M. Kinjo. Monitoring of in vitro and in vivo translation of green fluorescent protein and its fusion proteins by fluorescence correlation spectroscopy. *Cytometry* **44**, 1 (2001).
- Novikov, E.G., A. van Hoek, A.J.W.G. Visser and J.W. Hofstraat. Linear algorithms for stretched exponential decay analysis. *Opt. Commun.* **166**, 189 (1999).
- O'Connor, D.V. and D. Phillips. Time-correlated photon counting. Academic Press, London (1984).
- Oehlschläger, F., P. Schuille and M. Eigen. Detection of HIV-1 RNA by nucleic acid sequence-based amplification combined with fluorescence correlation spectroscopy. *Proc. Natl. Acad. Sci. USA* **93**, 12811 (1996).
- Ormö, M., A.B. Cubitt, K. Kallio, L.A. Gross, R.Y. Tsien and S.J. Remington. Crystal structure of the *Aequorea victoria* green fluorescent protein. *Science* **273**, 1392 (1996).
- Overbeck, E., C. Sinn, I. Flammer, J. Rička. Silicon avalanche photodiodes as detectors for photon correlation experiments. *Rev. Sci. Instrum.* **69**, 3515 (1998).
- Palmer, A.G. and N.L. Thompson. Molecular aggregation characterized by high order autocorrelation in fluorescence correlation spectroscopy. *Biophys. J.* **52**, 257 (1987).
- Palmer, A.G. and N.L. Thompson. High-order fluorescence fluctuation analysis of model protein clusters. *Proc. Natl. Acad. Sci. USA* **86**, 6148 (1989).
- Palo, K., Ü. Mets, S. Jäger, P. Kask and K. Gall. Fluorescence intensity multiple distributions analysis: Concurrent determination of diffusion times and molecular brightness. *Biophys. J.* **79**, 2858 (2000).
- Pap, E.H.W., M. Ketelaars, J.W. Borst, A. van Hoek and A.J.W.G. Visser. Reorientational properties of fluorescent analogues of the protein kinase C cofactors diacylglycerol and phorbol ester. *Biophys. Chem.* **58**, 255 (1996).

-
- Patterson G.H., S.M. Knobel, W.D. Sharif, S.R. Kain and D.W. Piston. Use of green fluorescent protein and its mutants in quantitative fluorescence microscopy. *Biophys. J.* **73**, 2782 (1997).
- Pecora, R. Dynamic light scattering. Plenum Press: New York (1985).
- Petersen, N.O. and E.L. Elson. Measurements of diffusion and chemical kinetics by fluorescence photobleaching recovery and fluorescence correlation spectroscopy. *Methods Enzymol.* **130**, 454 (1986).
- Petersen, N.O., P.L. Höddelius, P.W. Wiseman, O. Seger and K.E. Magnusson. Quantitation of membrane receptor distributions by image correlation spectroscopy: concept and application. *Biophys. J.* **65**, 1135 (1993).
- Politz, J.C., E.S. Brown, D.E. Wolf and T. Pederson. Intranuclear diffusion and hybridisation state of oligonucleotides measured by fluorescence correlation spectroscopy in living cells. *Proc. Natl. Acad. Sci. USA* **95**, 6043 (1998).
- Politz, J.C.. Use of caged fluorochromes to track macromolecular movement in living cells. *Trends Cell Biol.* **9**, 284 (1999).
- Pollok, B.A. and R. Heim. Using GFP in FRET-based applications. *Trends Cell Biol.* **9**, 57 (1999).
- Pramanik, A., A. Juréus, Ü. Langel, T. Bartfai and R. Rigler. Galanin receptor binding studies in the membranes of cultured cells measured by fluorescence correlation spectroscopy. *Biomed. Chromatogr.* **13**, 119 (1999).
- Prasher, D.C, V.K. Eckenrode, W.W. Ward, F.G. Prendergast and M.J. Cormier. Primary structure of the *Aequorea victoria* green-fluorescent protein. *Gene* **111**, 229 (1992).
- Qian, H.. On the statistics of fluorescence correlation spectroscopy. *Biophys. Chem.* **38**, 49 (1990).
- Qian, H and E.L. Elson. Distribution of molecular aggregation by analysis of fluctuation moments. *Proc. Natl. Acad. Sci. USA* **87**, 5479 (1990a).
- Qian, H and E.L. Elson. On the analysis of high order moments of fluorescence fluctuations. *Biophys. J.* **57**, 375 (1990b).
- Qian, H and E.L. Elson. Analysis of confocal laser-microscope optics for 3-D fluorescence correlation spectroscopy. *Appl. Opt.* **30**, 1185 (1991).
- Quitevis, E.L., A.H. Marcus and M.D. Fayer. Dynamics of ionic lipophilic probes in micelles: Picosecond fluorescence depolarisation measurements. *J. Phys. Chem.* **97**, 5762 (1993).
- Rarbach, M., U. Kettling, A. Koltermann and M. Eigen. Dual color fluorescence cross-correlation spectroscopy for monitoring the kinetics of enzyme-catalyzed reactions. *Methods* **24**, 104 (2001).
- Rauer, B., E. Neumann, J. Widengren and R. Rigler. Fluorescence correlation spectroscopy of the interaction kinetics of tetramethylrhodamin α -bungarotoxin with *Torpedo californica* acetylcholine receptor. *Biophys. Chem.* **58**, 3 (1996).
- Rigler, R., Ü. Mets, J. Widengren and P. Kask. Fluorescence correlation spectroscopy with high count rates and low background, analysis of translational diffusion *Eur. Biophys. J.* **22**, 169 (1993).
- Rigler, R.. Fluorescence correlations, single molecule detection and large number screening. Applications in biotechnology. *J. Biotechnol.* **41**, 177 (1995).
- Rigler, R., A. Pramanik, P. Jonasson, G. Kratz, O.T. Jansson, P.-Å. Nygren, S. Ståhl, K. Ekberg, B.-L. Johansson, S. Uhlén, M. Uhlén, H. Jörnvall, and J. Wahren. Specific binding of proinsulin C-peptide to human cell membranes. *Proc. Natl. Acad. Sci. USA* **96**, 13318 (1999).
- Rigler, R., Z. Földes-Papp, F.J. Meyer-Almes, C. Sammet, M. Volcker and A. Schnetz. Fluorescence cross-correlation: A new concept for polymerase chain reaction. *J. Biotechnol.* **63**, 97 (1999).
- Rippe, K.. Simultaneous binding of two DNA duplexes to the NtrC-enhancer complex studied by two-color fluorescence cross-correlation spectroscopy. *Biochemistry* **39**, 2131(2000).
- Robson, R.J. and E.A. Dennis. The size, shape and hydration of nonionic surfactant micelles. Triton X-100. *J. Phys. Chem.* **81**, 1075 (1977).

- Rosenholm, J.B., T. Drakenberg and B.J. Lindman. A carbon-13 NMR shielding study of the water-sodium octanoate-pentanol, and water-sodium-octanoate-decanol systems. *J. Colloid Interface Sci.* **63**, 538 (1978).
- Rudiger, M., U. Haupts, K.J. Moore and A.J. Pope. Single-molecule detection technologies in miniaturized high throughput screening: Binding assays for G protein-coupled receptors using fluorescence intensity distribution analysis and fluorescence anisotropy. *J. Biomol. Screen.* **6**, 29 (2001).
- Saleh, B.. Photonelectron statistics. With applications to spectroscopy and optical communication. Springer Verlag, Berlin (1978).
- Saxton, M.J.. Single particle tracking: The distribution of diffusion coefficients. *Biophys. J.* **72**, 1744 (1997).
- Schaffer, J., A. Volkmer, C. Eggeling, V. Subramaniam, G. Striker and C.A.M. Seidel. Identification of single molecules in aqueous solution by time-resolved fluorescence anisotropy. *J. Phys. Chem. A* **103**, 331 (1999).
- Schlessinger, J.. Signal transduction by allosteric receptor oligomerization. *Trends Biochem. Sci.* **13**, 443 (1988).
- Schmidt, E.D.L., F. Guzzo, M.A.J. Toonen and S.C. de Vries. A leucine rich repeat containing receptor-like kinase marks somatic plant cells competent to form embryos *Development* **124**, 2049 (1997).
- Schmidt, T., G.J. Schütz, W. Baumgartner, H.J. Gruber, H. Schindler. Imaging of single molecule diffusion. *Proc. Natl. Acad. Sci. USA* **93**, 2926 (1996).
- Schütz, G.J., H. Schindler and T. Schmidt. Single molecule microscopy on model membranes reveals anomalous diffusion. *Biophys. J.* **73**, 1073 (1997).
- Schwille, P., F.J. Meyer-Almes and R. Rigler. Dual-color fluorescence cross-correlation spectroscopy for multicomponent diffusional analysis in solution. *Biophys. J.* **72**, 1878 (1997).
- Schwille, P., J. Korch and W.W. Webb. Fluorescence correlation spectroscopy with single molecule sensitivity on cell and model membranes. *Cytometry* **36**, 176 (1999a).
- Schwille, P., U. Haupts, S. Maiti and W.W. Webb. Molecular dynamics in living cells observed by fluorescence correlation spectroscopy with one- and two-photon excitation. *Biophys. J.* **77**, 2251 (1999b).
- Schwille, P., S. Kummer, A.A. Heikal, W.E. Moerner and W.W. Webb. Fluorescence correlation spectroscopy reveals fast optical excitation-driven intramolecular dynamics of yellow fluorescent proteins. *Proc. Natl. Acad. Sci. USA* **97**, 151 (2000).
- Schwille, P.. Fluorescence correlation spectroscopy and its potential for intracellular applications. *Cell Bioch. Bioph.* **34**, 383 (2001a).
- Schwille, P.. Cross-correlation analysis in FCS. In *Fluorescence correlation spectroscopy. Theory and applications*. E.L. Elson and R. Rigler (eds.), Springer, Berlin, 360 (2001b).
- Shah, K., T.W.J. Gadella Jr., H. Van Erp, V. Hecht and S.C. de Vries. Subcellular localization and oligomerization of the *Arabidopsis thaliana* somatic embryogenesis receptor kinase 1 protein. *J. Mol. Biol.* **309**, 641 (2001).
- Siegel, R.M., J.K. Frederiksen, D.A. Zacharias, F. Ka-Ming Chan, M. Johnson, D. Lynch, R.Y. Tsien, and M.J. Lenardo. Fas preassociation required for apoptosis signaling and dominant inhibition by pathogenic mutations. *Science* **288**, 2354 (2000).
- Silvius, J.R., D. del Giudice and M. Lafleur. Cholesterol at different bilayer concentrations can promote or antagonize lateral segregation of phospholipids of differing acyl chain length. *Biochemistry* **35**, 15198 (1996).
- Sippl, M.J.. Recognition of errors in three-dimensional structures of proteins. *Proteins* **17**, 355 (1993).
- Srivastava, M. and N.O. Petersen. Image cross-correlation spectroscopy: A new experimental biophysical approach to measurement of slow diffusion of fluorescent molecules. *Methods Cell Sci.* **18**, 47 (1996).
- Starr, T. E. and N.L. Thompson. Total internal reflection with fluorescence correlation spectroscopy: Combined surface reaction and solution diffusion *Biophys. J.* **80**, 1575, (2001).

-
- Steiner, R.F. Fluorescence anisotropy: Theory and applications. *In* Topics in fluorescence spectroscopy. J.R. Lakowicz (ed.) Plenum Press, New York, Vol. 2, 1 (1991).
- Stryer, L. and R.P. Haugland. Energy transfer: a spectroscopic ruler. *Proc. Natl. Acad. Sci. U.S.A.* **58**, 719 (1967).
- Stryer, L.. Fluorescence energy transfer as a spectroscopic ruler. *Ann. Rev. Biochem.*, **47**, 819 (1978).
- Svedberg, T. and K. Inouye. Eine neue Methode zur Prüfung der Gültigkeit des Boyle-Gay-Lussacschen Gesetzes für Kolloide Lösungen. *Z. Phys. Chem.* **77**, 145 (1911).
- Swaminathan, R., C.P. Hoang and A.S. Verkman. Photobleaching recovery and anisotropy decay of green fluorescent protein GFP-S65T in solution and cells: Cytoplasmic viscosity probed by green fluorescent protein translational and rotational diffusion. *Biophys. J.* **72**, 1900 (1997).
- Szabo, A. J. Theory of fluorescence depolarization in macromolecules and membranes. *J. Chem. Phys.* **81**, 150 (1984).
- Teich, M.C. and B.E.A. Saleh. Photon bunching and antibunching. *In* Progress in optics. E. Wolf (ed.), North-Holland Publishing Company, Amsterdam, 1 (1988).
- Terry, B.R., E.K. Matthews and J.J. Haseloff. Molecular characterisation of recombinant green fluorescent protein by fluorescence correlation microscopy. *Biochem. Biophys. Res. Comm.* **217**, 21 (1995).
- Thompson, N.L.. Fluorescence correlation spectroscopy. *In* Topics in fluorescence spectroscopy. J.R. Lakowicz (ed.), Plenum Press, New York, 337 (1991).
- Tormo, J., E. Stadler, T. Skern, H. Auer, O. Kanzler, C. Betzel, D. Blaas and I. Fita. Three-dimensional structure of the Fab fragment of a neutralizing antibody to human rhinovirus serotype 2. *Protein Sci.* **1**, 1154 (1993).
- Tsien, R.Y., J. Backsai and R. Adams. FRET for studying intracellular signalling. *Trends Cell Biol.* **3**, **242** (1993).
- Tsien, R.Y.. The green fluorescent protein. *Annu. Rev. Biochem.* **67**, 509 (1998).
- Van Bokhoven, H., J. Verver, J. Wellink and A van Kammen. Protoplasts transiently expressing the 200 K coding sequence of cowpea mosaic virus B-RNA support replication of M-RNA. *J. Gen. Vir.* **74**, 2233 (1993).
- Van Craenenbroeck, E. and Y. Engelborghs. Quantitative characterization of the binding of fluorescently labeled colchicines to tubulin in vitro using fluorescence correlation spectroscopy. *Biochemistry* **38**, 5082 (1999).
- Van Craenenbroeck, E., G. Matthys, J. Beirlant and Y. Engelborghs. A statistical analysis of fluorescence correlation data. *J. Fluoresc.* **9**, 4 (1999).
- Van Craenenbroeck, E., J. Vercammen, G. Matthys, J. Beirlant, C. Marot, J. Hoebeke, R. Strobbe and Y. Engelborghs. Heuristic statistical analysis of fluorescence fluctuation data with bright spikes: Application to ligand binding to the human serotonin receptor expressed in *Escherichia coli* cells. *Biol. Chem.* **382**, 355 (2001).
- Van den Berg, P.A.W., J. Widengren, M.A. Hink, R. Rigler and A.J.W.G. Visser. Fluorescence correlation spectroscopy of flavins and flavoenzymes: Photochemical and photophysical aspects. *Spectrochim. Acta A* **57**, 2135 (2001).
- Van der Meer, W.B., M. Ameloot, H. Hendrickx and H. Schröder. Effect of orientational order on the decay of the fluorescence anisotropy in membrane suspensions. A new approximate solution of the rotational diffusion equation. *Biophys. J.* **46**, 515 (1984).
- Van Hoek, A., and A. J. W. G. Visser. Cw dye laser synchronously pumped by the third harmonic of a mode-locked cw Nd:YLF laser for tunable blue and green excitation and picosecond time-correlated photon counting detection. *Proc. SPIE* **1640**, 325 (1992).
- Van Rompaey, E., Y. Chen, J.D. Müller, E. Gratton, E. van Craenenbroeck, Y. Engelborghs, S. De Smedt and J. Demeester. Fluorescence fluctuation analysis for the study of interactions between oligonucleotides and polycationic polymers. *Biol. Chem.* **382**, 379 (2001).

- Vanden Broek, W., Z. Huang and N.L. Thompson. High-order autocorrelation with imaging fluorescence correlation spectroscopy: Application to IgE on supported planar membranes. *J. Fluoresc.* **9**, 313 (1999).
- Visser, A.J.W.G. and M.A. Hink. New perspectives of fluorescence correlation spectroscopy *J. Fluoresc.* **9**, 81 (1999).
- Visser, A.J.W.G., A. van Hoek, N.V. Visser, Y. Lee and S. Ghisla. Time-resolved fluorescence study of the dissociation of FMN from the yellow fluorescence protein from *Vibrio fischeri*. *Photochem. Photobiol.* **65**, 570 (1997).
- Visser, A.J.W.G., P.A.W. van den Berg, N.V. Visser, A. van Hoek, H.A. van den Burg, D. Parsonage and A. Claiborne. Time-resolved fluorescence of flavin adenine dinucleotide in wild-type and mutant NADH peroxidase. Elucidation of quenching sites and discovery of a new fluorescence depolarization mechanism. *J. Phys. Chem. B* **102**, 10431 (1998).
- Visser, A.J.W.G., P.A.W. van den Berg, M.A. Hink and V.N. Petushkov. Fluorescence correlation spectroscopy of flavins and flavoproteins *In* Fluorescence correlation spectroscopy. Theory and applications. E.L. Elson and R. Rigler (eds.), Springer, Berlin, 360 (2001).
- von Smoluchowski, M. Studien über Molekularstatistik von Emulsionen and deren Zusammenhang mit der Brownschen Bewegung. *Wien Berichte* **123**, 2381 (1914).
- Vos, K., A. van Hoek and A.J.W.G. Visser. Application of a reference deconvolution method to tryptophan fluorescence in proteins. A refined description of rotational dynamics. *Eur. J. Biochem.* **165**, 55 (1987).
- Wachsmuth, M., W. Waldeck and J. Langowski. Anomalous diffusion of fluorescent probes inside living cell nuclei investigated by spatially-resolved fluorescence correlation spectroscopy. *J. Mol. Biol.* **298**, 677 (2000).
- Wachter, R.M., M.-A. Elsliger, K. Kalio, G.T. Hanson and S.J. Remington. Structural basis of spectral shifts in the yellow-emission variants of green fluorescent protein. *Structure* **6** 1267 (1998).
- Waggoner, A.S., O.H. Griffith and C.P. Christensen. Magnetic resonance of nitroxide probes in micelle-containing solutions. *Proc. Natl. Acad. Sci. U.S.A* **57**, 1198 (1967).
- Waizenegger, T., R. Fischer and R. Brock. Intracellular concentration measurements in adherent cells: A comparison of import efficiencies of cell-permeable peptides. *Biol. Chem.* **383**, 291 (2002).
- Wall, M. A., M.Socolich and R. Ranganathan. The structural basis for red fluorescence in the tetrameric GFP homolog DsRed. *Nat. Struct. Biol.* **7**, 1133 (2000).
- Wallace, M.I., L. Ying, S. Balasubramanian and D. Klenerman. FRET fluctuation spectroscopy: Exploring the conformational dynamics of a DNA hairpin loop. *J. Phys. Chem.* **104**, 11551 (2000).
- Walter, N.S., P. Schwille and M. Eigen. Fluorescence correlation analysis of probe diffusion simplifies quantitative pathogen detection by PCR. *Proc. Natl. Acad. Sci. USA* **93**, 12805 (1996).
- Weiss, S. Fluorescence spectroscopy of single biomolecules. *Science* **283**, 1676 (1999).
- Wennmalm, S., L. Edman and R. Rigler. Conformational fluctuations in single DNA molecules. *Proc. Natl. Acad. Sci. USA* **94**, 10641 (1997).
- Widengren, J., Ü. Mets and R. Rigler. Fluorescence correlation spectroscopy of triplet states in solution: A theoretical and experimental study. *J. Phys. Chem.* **99**, 13368 (1995).
- Widengren, J. and R. Rigler. Mechanisms of photobleaching investigated by fluorescence correlation spectroscopy. *Bioimaging* **4**, 149 (1997).
- Widengren, J. and R. Rigler. Fluorescence correlation spectroscopy as a tool to investigate chemical reactions in solutions and on cell surfaces. *Cell. Mol. Biol.* **44**, 857 (1998).
- Widengren, J., B. Terry and R. Rigler. Protonation kinetics of GFP and FITC investigated by FCS. Aspects of the use of fluorescent indicators for measuring pH. *Chem. Phys.* **249**, 259 (1999).
- Widengren, J. Ü. Mets and R. Rigler. Photodynamic properties of green fluorescent proteins investigated by fluorescence correlation spectroscopy. *Chem. Phys.* **250**, 171 (1999).

-
- Widengren, J. and C.A.M. Seidel. Manipulation and characterization of photo-induced transient states of Merocyanine 540 by fluorescence correlation spectroscopy. *Phys. Chem. Chem. Phys.* **2**, 3435 (2000).
- Widengren, J. and P. Schwille. Characterization of photoinduced isomerization and back-isomerization of the cyanine dye Cy5 by fluorescence correlation spectroscopy. *J. Phys. Chem. A* **104**, 6416 (2000).
- Widengren, J., E. Schweinberger, S. Berger and C.A.M. Seidel. Two new concepts to measure fluorescence energy transfer via fluorescence correlation spectroscopy: Theory and experimental realizations. *J. Phys. Chem. A* **105**, 6851 (2001).
- Williams, R.M., D. Piston and W. W. Webb. Two-photon molecular excitation provides intrinsic 3-dimensional resolution for laser-based microscopy and microphotochemistry. *FASEB J.* **8**, 804 (1994).
- Williams, R.W., J.M. Wilson and E.M. Meyerowitz. A possible role of kinase-associated protein phosphatase in the *Arabidopsis* CLAVATA1 signaling pathway. *Proc. Natl Acad. Sci. USA* **94**, 10467 (1997).
- Wiseman, P.W., J.A. Squier, M.H. Ellisman and K.R. Wilson. Two-photon image correlation spectroscopy and image cross-correlation spectroscopy. *J. Microsc.* **200**, 14 (2000).
- Wouters, F.S., P.J. Verveer and P.I.H. Bastiaens. Imaging biochemistry in living cells. *Trends Cell Biol.* **11**, 203 (2001).
- Xia, Z. and Y. Liu. Reliable and global measurement of fluorescence resonance energy transfer using fluorescence microscopes. *Biophys. J.* **81**, 2395 (2001).
- Xie, X.S. and J.K. Trautman. Optical studies of single molecules at room temperature. *Ann. Rev. Phys. Chem.* **49**, 441 (1998).
- Xu, C, W. Zipfel, J.B. Shear, R.M. Williams and W.W. Webb. Multiphoton fluorescence excitation: New spectral windows for biological nonlinear microscopy. *Proc. Natl. Acad. Sci. USA* **93**, 10763 (1996).
- Yang, F., L.G. Moss and G.N. Phillips. The molecular structure of green fluorescent protein. *Nature Biotechnol.* **14**, 1246 (1996).
- Yoshida, N., M. Kinjo, and M. Tamura. Microenvironment of endosomal aqueous phase investigated by the mobility of microparticles using fluorescence correlation spectroscopy. *Biochem. Biophys. Res. Com.* **280**, 312 (2001).
- Zana, R., H. Levy, D. Danino, Y. Talmon and K. Kwetkat. Micellization of amphiphiles: selected aspects. *Langmuir* **13**, 402 (1997).

Samenvatting

Om te kunnen overleven zullen organismen in staat moeten zijn om zich aan te passen aan veranderingen in de leefomgeving. Cellen, de bouwstenen van het organisme, reageren op deze veranderingen door het versturen van signaalmoleculen (bv. hormonen). Belangrijke cellulaire processen als deling, groei, differentiatie en dood worden gestart na ontvangst van specifieke signaalmoleculen, die op hun beurt weer andere signaalmoleculen kunnen activeren. Op deze manier is in de loop van de evolutie een netwerk van signaalroutes ontstaan dat de cellulaire processen van een organisme reguleert. Fouten in dit netwerk kunnen leiden tot afwijkingen, ziektes of zelfs tot de dood. Eén van de meest fascinerende uitdagingen in celbiologisch onderzoek is om te achterhalen hoe deze netwerken precies werken. Om de signaalmoleculen te kunnen bestuderen zijn vele verschillende technieken beschikbaar. Microspectroscopische technieken hebben het voordeel dat naast het bestuderen van spectroscopische parameters tegelijkertijd ruimtelijke informatie wordt verkregen. Om moleculen bij zeer lage, fysiologisch relevante concentraties te kunnen observeren wordt gebruik gemaakt van een methode die zeer gevoelig en selectief is: fluorescentie. Door het aanstralen van een fluorescent molecuul met een specifieke kleur licht, zal het in de aangeslagen toestand terechtkomen. Wanneer het molecuul weer spontaan naar de grondtoestand terugkeert kan dit molecuul licht met een andere kleur uitzenden: fluorescentie. Aangezien de meeste moleculen zelf nauwelijks fluorescent zijn worden er speciale fluorescente groepen aan het molecuul gekoppeld waardoor de moleculen duidelijk herkenbaar zijn ten opzichte van de overige moleculen in de cel.

In hoofdstuk 1 worden de principes van twee fluorescentie methodes beschreven: Fluorescentie correlatie spectroscopie (FCS) en fotontelling histogram analyse (PCH). FCS en PCH extraheren informatie uit de fluctuaties in de fluorescentie intensiteit. De fluorescentie intensiteit wordt gemeten in een klein observatie volume met behulp van een microscoop. Dit volume is in de orde van grootte van een femtoliter wat overeenkomt met het volume van een *E. coli* bacterie. Bij een lage concentratie fluorescente moleculen kan de beweging van individuele moleculen door het observatie volume waargenomen worden. Daar waar FCS het tijds-afhankelijke verval van de fluctuaties analyseert, resulterend in waarden voor concentratie, diffusie en reactiesnelheids constanten, kan PCH moleculen met verschillende fluorescentie intensiteiten onderscheiden. Voordelen van deze methodes zijn de kleine hoeveelheden benodigde fluorescente moleculen per meting (pico- tot micromolair concentraties) en het meten in een evenwichtstoestand: er geen verstoring van het monster nodig om de meting te kunnen uitvoeren. Hoewel beide methodes al enkele jaren bestaan is het aantal toepassingen in (levende) cellen zeer beperkt.

De studies die in dit proefschrift worden beschreven hebben als doel om FCS en PCH metingen in een plantencel te optimaliseren zodat met deze technieken signaaltransductie processen in levende plantencellen kunnen worden gevolgd.

Voordat FCS en PCH met succes toegepast kunnen worden in levende plantencellen zijn eerst meer eenvoudige systemen bestudeerd. Daartoe zijn bindings studies uitgevoerd met het enkel-keten variabel antilichaam fragment (scFv), gekoppeld aan een groen fluorescent eiwit (GFP). ScFv-GFP bindt aan het antigeen lipopolysaccharide, dat zich in de celwand van Gram-negatieve bacteriën bevindt. Door de grote verschillen in massa en dus in de diffusieconstanten tussen scFv-GFP en het complex met *Ralstonia solanacearum* bacteriën, is het mogelijk om met FCS onderscheid tussen het ligand en het complex te maken.

Omdat de cel wordt afgescheiden door de plasmamembraan zullen signaalmolekulen deze membraan moeten passeren om binnenin de cel te geraken of een interactie moeten aangaan met andere molekulen die zich in of nabij de plasmamembraan bevinden. De samenstelling en dynamica van de plasmamembraan spelen daarom ook een grote rol in signaaltransductie. In hoofdstuk 3 wordt beschreven hoe micellen die op membranen lijken kunnen worden gekarakteriseerd. Met behulp van FCS zijn de diffusie-snelheid en hydrodynamische straal van micellen bepaald, die een fluorescent fosfolipide bevatten. De precisie en nauwkeurigheid van deze bepalingen werden bevestigd met behulp van dynamische lichtverstrooiing. De toevoeging van het relatief grote fosfolipide-molekuul aan de micel maakte de micel groter. De bewegelijkheid van de fosfolipide in de micel werd bestudeerd met tijdsopgeloste fluorescentiespectroscopie. Vergelijkbare studies werden uitgevoerd aan fosfolipiden in de membraan van levende plantencellen. In hoofdstuk 4 wordt beschreven welke factoren de FCS-metingen in levende cellen kunnen verstoren zoals is geïllustreerd met de metingen aan kousenband protoplasten en suspensie cellen van tabak. Bij FCS-metingen in levende cellen, fluorescentie correlatie microscopie (FCM) genoemd, wordt gebruik gemaakt van het ruimtelijk oplossend vermogen van de microscoop om bepaalde delen van de cel te identificeren. FCM metingen aan geïnjecteerde fluorescente molekulen in de kern en cytoplasma van de cellen wijzen erop dat veel kleurstoffen niet-specifieke interacties met cellulaire structuren kunnen aangaan. Een nauwgezette selectie van de fluorescente groep is daarom noodzakelijk om betrouwbare FCS-metingen te kunnen opzetten. De migratie van de fosfolipiden in de plasmamembraan van de cel kan niet worden verklaard met een model dat normale Brownse beweging beschrijft maar wel met een multi-component analyse of met een model welke rekening houdt met afwijkende, beperkte diffusie.

Mede door lichtverstrooiing en de aanwezigheid van autofluorescente moleculen in de cel is het noodzakelijk om sterk fluorescerende groepen te gebruiken om het te bestuderen molekuul zichtbaar te maken. Wanneer de koppeling van een fluorescente groep aan een molekuul

buiten de cel gebeurd (bv. d.m.v organische synthese) moet het fluorescente produkt de cel binnengebracht worden. Echter de aanwezigheid van de celwand maakt het bijzonder lastig om dit in plantencellen uit te voeren. Het gebruik van (auto-) fluorescente eiwitten (FP's) is dan een uitstekend alternatief. Deze eiwitten, die in verschillende kleuren beschikbaar zijn, kunnen via genetische procedures aan het eiwit van interesse gekoppeld worden. Na transfectie van het recombinante DNA wordt het fluorescente produkt door de cel zelf aangemaakt. De FP's vertonen bijzondere eigenschappen wanneer ze met licht aangestraald worden en zijn gevoelig voor de pH van de omgeving. In het onderzoek beschreven in hoofdstuk 5 zijn de verschillende FP-varianten gekarakteriseerd om te achterhalen welke FP het meest geschikt is voor intracellulaire studies en hoe ongewenste eigenschappen van de FP's de FCM-metingen in cellen kunnen verstoren.

Om interacties tussen verschillende signaalmolekulen aan te tonen kan elk molecuul aan een andere variant van de fluorescente eiwitten (bv. het cyaankleurig eiwit (CFP) en het geel gekleurde eiwit (YFP)) gekoppeld worden. Wanneer nu de cyaankleurige variant met licht aangeslagen wordt is het mogelijk dat de energie die daarbij geabsorbeerd wordt overspringt naar de geelgekleurde variant waardoor er ook gele fluorescentie ontstaat. Dit proces wordt fluorescentie resonantie energie overdracht (FRET) genoemd. FRET treedt alleen op wanneer beide moleculen zich op minder dan enkele nanometers afstand van elkaar bevinden ($1 \text{ nm} = 10^{-9} \text{ m}$). Echter, de hoeveelheid gele fluorescentie van de FRET-positieve controle eiwitten was te laag in plantencellen om er FRET-FCM mee uit te voeren. Een tweede methode om interactie tussen de hierboven beschreven eiwitten aan te tonen is met behulp van fluorescentie cross-correlatie microscopie (FCCM), waarbij twee detectoren gebruikt worden. Bij deze methode is FRET niet noodzakelijk maar wordt gebruikt gemaakt van het gelijktijdig passeren van een cyaangekleurd deeltje en een geel gekleurd deeltje. Dit komt voor wanneer een complex bestaande uit eiwitten met beide fluorescente groepen door het observatie volume diffundeert. In het geval van niet-interacterende eiwitten zullen de cyaan en geel gekleurde deeltjes onafhankelijk van elkaar het observatie volume passeren.

Op deze manier is de dimerisatie van de membraanreceptor betrokken bij de somatische embryogenese van de zandraket, AtSERK1, bestudeerd. PCH analyse toonde aan dat 15% van de receptoren als dimeer in de plasma membraan aanwezig is en dat er geen hogere oligomere structuren, zoals tri- of tetra-meren aantoonbaar zijn. FCCM-analyse toonde aan dat de migratie van het dimeer langzamer is dan die van het (kleinere) monomeer.

Samenvattend hebben de resultaten die beschreven zijn in dit proefschrift geleid tot nieuwe methodes om moleculen op fysiologisch relevante concentraties in levende plant systemen te bestuderen. Ons inzicht in de eigenschappen van cellulaire processen wordt hierdoor sterk vergroot.

List of Abbreviations

APD	Avalanche PhotoDiode
AtSERK	<i>Arabidopsis thaliana</i> somatic embryogenesis receptor kinase
BFP	Blue Fluorescent Protein
BLM	Black Lipid Membrane
BY2	Bright Yellow 2 tobacco cell
CA _n Y	Fusion protein of ECFP and EYFP with n-alanine residue linker
CFP	Cyan Fluorescent Protein
CMC	Critical Micelle Concentration
DLS	Dynamic Light Scattering
DsRed	Red fluorescent protein isolated from <i>Discosoma sp.</i>
FCCM	Fluorescence Cross-Correlation Microscopy
FCCS	Fluorescence Cross-Correlation Spectroscopy
FCM	Fluorescence Correlation Microscopy
FCS	Fluorescence Correlation Spectroscopy
FIDA	Fluorescence Intensity Distribution Analysis
FILDA	Fluorescence Intensity Lifetime Distribution Analysis
FIMDA	Fluorescence Intensity Multiple Distribution Analysis
FLIM	Fluorescence Lifetime Imaging Microscopy
FP	Fluorescent Protein
FRAP	Fluorescence Recovery After Photobleaching
FRET	Fluorescence Resonance Energy Transfer
FSPIM	Fluorescence SPECTral Imaging Microscopy
FWHM	Full Width Half Maximum
GFP	Green Fluorescent Protein
GUV	Giant Unilamellar Vesicle
HcRed	Red fluorescent protein isolated from <i>Heteractis crispa</i>
ICS	Image Correlation Spectroscopy
LPS	LipoPolySaccharide
MEM	Maximum Entropy Method
MPE	Multi Photon Excitation
NA	Numerical Aperture
PCH	Photon Counting Histogram
ScFv	Single Chain of Variable antibody Fragments
SFM	Scanning Force Microscopy
SNOM	Scanning Nearfield Optical Microscopy
SNR	Signal to Noise Ratio
SPT	Single Particle Tracking
SUV	Single Unilamellar Vesicle
TIR	Total Internal Reflection
TRFA	Time-Resolved Fluorescence Anisotropy
TCSPC	Time-Correlated Single Photon Counting
YFP	Yellow Fluorescent Protein

Dankwoord

Het was eind 1996 toen ik als student Moleculaire Wetenschappen de vakgroep Biochemie binnenwandelde om bij Ton Visser een afstudeervak te doen. Tijdens mijn afstudeervak werd mijn interesse gewekt voor het uitvoeren van microspectroscopisch onderzoek. Ik hoefde dan ook niet lang na te denken toen een OIO positie vrijkwam op een project waarbij microspectroscopie met celbiologie gecombineerd zou gaan worden. Nu, bij het afronden van dit promotieonderzoek is het leuk om even stil te staan bij degenen die hierbij betrokken zijn geweest. Ton, in de afgelopen jaren heb jij als begeleider en promotor van dit project, mij de gelegenheid gegeven om dit onderzoek in alle vrijheid te verrichten waarvoor alle dank. Middels je grote spectroscopische kennis, de goede discussies die we samen hebben gehad en je kritische blik op mijn schrijfstijl heb je een grote bijdrage geleverd aan dit promotieonderzoek. Ook Ton Bisseling wil ik bedanken voor het mogelijk maken van deze promotie. Je enthousiasme voor microspectroscopie heeft bijgedragen tot de toenemende samenwerking tussen Moleculaire Biologie en het MicroSpectroscopisch Centrum waardoor steeds duidelijker de kracht van integratie tussen biologische en biofysische groepen naar voren komt. In dit kader mag ik de dagelijkse lunchsessie met Dorus, Joachim en Joop niet vergeten. Voor jullie vertrek naar de UvA was dit de gelegenheid om naast de experimenten in de kelder ook de nieuwe klonerings- en synthese- strategieën te bespreken. Jullie interesse en enthousiasme heeft mijn plezier in het werk sterk vergroot.

Velen hebben een steentje bijgedragen aan het onderzoek zoals dat in dit boekje opgetekend staat: Wim Wolkers, Remko Fokkert, Frank Vergeldt en Eward Pap ben ik erkentelijk voor de hulp bij het meten en analyseren van de micel en vesicle samples. The collaboration with Eugene Novikov, Victor Skakun and Anatoli Digris from Belarussia resulted in two great software programs which have made the analysis of the FCS and TRFA data a lot easier. Michel Eppink, Remko Griep en Arjen Schots bedank ik voor hun bijdrage aan het onderzoek van de single-chain antilichaam fragmenten. De samenwerking met Sacco de Vries en Khalid Shah resulteerde in een project waarbij de toepasbaarheid van FCS en PCH in levende plantcellen duidelijk aangetoond kon worden. Daarnaast zijn er de talloze gasten geweest die de kelder van het Transitorium opzochten om eens te proberen of hun eigen systeem ook mooie FCS-resultaten op kon leveren. Al waren niet alle meetsessies even succesvol, ze zorgden voor verbreding van de horizon en daardoor ook voor vele nieuwe ideeën.

Petra, jij was mijn kamergenote gedurende de eerste jaren. Bedankt voor de gezelligheid, de gesprekken en de praktische hulp bij het afronden van dit boekje. Vooral de laatste paar jaren heb ik veel met Jan-Willem samen gewerkt. Naast het beheren van de microscopen, het mede opzetten van de FEBS cursus en webpagina's zijn we de laatste maanden intensief betrokken

geweest bij het opzetten van de multi-photon microspectroscopie. Met jouw praktische instelling en grote inzet hebben we al snel leuke resultaten kunnen boeken, hopenlijk zullen er nog vele volgen. De tijdsopgeloste fluorescentie experimenten zouden niet zo succesvol zijn zonder de hulp van Arie. Jouw vakmanschap en kennis waren onontbeerlijk in deze en ik heb net zoals bij de huidige opbouw van de multi-photon apparatuur veel van je geleerd. Verder bedank ik de collega's van het MSC en lab 7 Nina, Ruchira, Maarten, Niek, Olga, Marsha, Boudwijn, Hans, Annemie, Riet, Gideon, Ahmed, Mamoudou, Jan-Jaap en Martina voor de goede werksfeer zowel binnen als buiten het lab. Daarnaast wil ik alle medewerkers van Biochemie en Moleculaire Biologie bedanken voor de hulp en de prettige tijd in het Transitorium. Uiteraard een woord van dank aan mijn ouders voor de interesse en steun die zij mij de afgelopen jaren gegeven hebben. Onmisbaar was ook de support van overige familie, vrienden en bekenden en de broodnodige ontspanning (maar vooral inspanning) met de 'polderstoempers' en de 'TROLL'-ers.

Curriculum vitae

Markus Abraham Hink was born in Oudkarspel, The Netherlands on January 15th 1973. He graduated from grammar school at the Petrus Canisius College in Alkmaar and subsequently started to study Molecular Sciences at the Wageningen Agricultural University (WAU) in 1992. His undergraduate theses were in Cell Biology and Virology (Dr. R. Stet, WAU and Prof. J. Vlak, WAU; "Expression of rainbow trout MHC class II β proteins in the baculovirus expression system") and in Biochemistry (Prof. A.J.W.G. Visser, WAU; "Characterization of lipid membrane systems using Fluorescence Correlation Spectroscopy"). Thereafter, he spent four months at the Department of Molecular Biology at the Max-Planck Institute for Biophysical Chemistry in Göttingen, Germany (Dr. T.M. Jovin and Dr. R. Brock; "Fluorescence Correlation Microscopy: characterization of autofluorescence and injection of dextrans in live cells"). In June 1997 he graduated with distinction, where after he joined the MicroSpectroscopy Centre as a research assistant to study the application of fluorescence correlation spectroscopy in cell science, funded by Carl Zeiss Jena, Germany. In April 1998 he started the PhD project that is described in this thesis, in the Laboratory for Biochemistry at Wageningen University under supervision of Prof. A.J.W.G. Visser. This research was financially supported by the Netherlands Organization for Scientific Research (NWO) through the division of Earth and Life Sciences (ALW). From June 2002 he works as a post-doc on the EU project "Insight Inside: Signal transducing protein machines revealed by subcellular single molecule spectroscopy and imaging" at the Microspectroscopy Centre in Wageningen.

List of publications

Brock, R., M.A. Hink and T.M. Jovin. Fluorescence correlation microscopy of cells in the presence of autofluorescence. *Biophys. J.* **75**, 2547 (1998).

Hink, M.A. and A.J.W.G. Visser. Characterization of membrane mimetic systems with fluorescence correlation spectroscopy. In *Applied Fluorescence in Chemistry, Biology and Medicine*. W. Rettig, B. Strehmel, S. Schrader and H. Seifert (eds.) Springer-Verlag Berlin, 101 (1998).

Hink, M.A., A. van Hoek and A.J.W.G. Visser. Dynamics of phospholipid molecules in micelles: Characterization with fluorescence correlation spectroscopy and time-resolved fluorescence anisotropy. *Langmuir* **15**, 992 (1999).

Koopman, W.J.H., M.A. Hink, A.J.W.G. Visser, E.W. Roubos and B.G. Jenks. Evidence that Ca^{2+} -waves in *Xenopus* melanotropes depend on calcium-induced calcium release: a fluorescence correlation microscopy and linescanning study. *Cell Calcium* **26**, 59 (1999).

Goedhart, J., H. Rohrig, M.A. Hink, A. van Hoek, A.J.W.G. Visser, T. Bisseling and T.W.J. Gadella, Jr. Nod factors integrate spontaneously in biomembranes and transfer rapidly between membranes and to root hairs, but transbilayer flip-flop does not occur. *Biochemistry* **38**, 10898 (1999).

Visser, N.V., M.A. Hink, A. van Hoek and A.J.W.G. Visser. Comparison between fluorescence correlation spectroscopy and time-resolved fluorescence anisotropy as illustrated with a fluorescent dextran. *J. Fluoresc.* **9**, 251 (1999).

Visser, A.J.W.G. and M.A. Hink. New perspectives of fluorescence correlation spectroscopy. *J. Fluoresc.* **9**, 81 (1999).

Goedhart, J., M.A. Hink, A.J.W.G. Visser, T. Bisseling and T.W.J. Gadella. *In vivo* fluorescence correlation microscopy (FCM) reveals accumulation and immobilization of Nod factors in root hair cell walls. *Plant J.* **21**, 109 (2000).

Hink, M.A., R.A. Griep, J.W. Borst, A. van Hoek, M.H.M. Eppink, A. Schots and A.J.W.G. Visser. Structural dynamics of green fluorescent protein alone and fused with a single chain Fv protein. *J. Biol. Chem.* **275**, 17556 (2000).

Uskova, M.A., J.W. Borst, M.A. Hink, A. van Hoek, A. Schots, N.L. Klyachko and A.J.W.G. Visser. Fluorescence dynamics of green fluorescent protein in AOT reversed micelles. *Biophys. Chem.* **87**, 73 (2001).

Visser, A.J.W.G., P.A.W. van den Berg, M.A. Hink, V.N. Petushkov. Fluorescence correlation spectroscopy of flavins and flavoproteins. In *Fluorescence Correlation Spectroscopy. Theory and Applications*. E. Elson and R. Rigler (eds.) Springer-Verlag, Berlin, 9 (2001).

Van den Berg, P.A.W., J. Widengren, M.A. Hink, R. Rigler and A.J.W.G. Visser. Fluorescence correlation spectroscopy of flavins and flavoenzymes: photochemical and photophysical aspects. *Spectrochim. Acta A* **57**, 2135 (2001).

Visser, N.V., M.A. Hink, J.W. Borst, G.N.M. van der Krogt and A.J.W.G. Visser. Circular dichroism spectroscopy of fluorescent proteins. *FEBS Lett.* **521**, 31 (2002).

Hink, M.A., J.W. Borst and A.J.W.G. Visser. Fluorescence correlation spectroscopy of GFP fusion proteins in living plant cells. *Methods Enzymol.* **361** (2002). In press.

Hink, M.A., T. Bisseling and A.J.W.G. Visser. Imaging protein-protein interactions in living cells. *Plant Mol. Biol.* (2002). In press.